NOAA Technical Report NOS 136 NGS 48

A Refined M_2 Tide from Geosat Altimetry

Carl A. Wagner

June 1991

U.S. DEPARTMENT OF COMMERCE
National Oceanic and Atmospheric Administration
National Ocean Service

A REFINED M_2 TIDE FROM GEOSAT ALTIMETRY

Carl A. Wagner
National Geodetic Survey
Coast and Geodetic Survey
National Ocean Service, NOAA
Rockville, MD 20852

ABSTRACT. More than 4,000,000 global Geosat altimeter observations, taken mostly in 1986-87, have been analyzed for the M_2 tide at overlapping points in the satellite's exact repeat mission (ERM). The results are compatible with the Schwiderski (1983) tide model at a level of 5.5 cm (rms discrepancy). The principal features of that model (amphidromes and highs) are unchanged. The altimeter solutions use independent time series for more than 1,900 4° by 4° areas of the deep oceans. They have been calibrated through nine roughly equal and independent subset analyses employing different arcs of the ERM configuration. Results show that 1,652 of the full set M_2 solutions have calibrated errors of less than 5 cm. Fairly good agreement exists between the 4° altimeter solutions and the few (point) tide gage results reported by Schwiderski.

INTRODUCTION

With the launch of the U.S. Navy's GEOdetic SATellite (Geosat) in 1985 and initiation of its exact repeat mission (ERM) in late 1986, long-term monitoring of ocean dynamics from precise altimetry has come of age (e.g., Cheney *et al.* 1989). This report contains a refined analysis (see also Wagner 1990) determining the single largest component of ocean dynamics from this altimetry, namely the M_2 ocean tide.

The emphasis in this study is the deep ocean tide over the whole globe. Currently, the best information available on this dominant (semidiurnal) lunar tide is a combination of theory and scattered tide gage records with a claimed accuracy of better than 5 cm at all deep ocean points (Schwiderski 1983). Considering that the M_2 marine tide has a power of the order of 30 cm, rms (somewhat less in deep oceans), this seems a modest claim in spite of the well known discrepancies between tidal models in the past. [See Schwiderski (1980) for a thorough review.] Nevertheless, precise satellite altimetry should eventually establish a new standard. For example, with Geosat, 1-second averages of altimetric heights have a precision of about 10 cm. More than 30,000,000 such observations have been taken since the satellite was launched in 1985 (e.g., Cheney *et al.* 1987, 1988; Doyle *et al.* 1989). Indeed such altimetry from Seasat in the summer of 1978 has already proven to be compatible with the best of the tidal theory models for M_2 [e.g., Brown (1983) in one location, and Mazzega (1985) globally, but only at long wavelengths]. However, use of limited Seasat data has not permitted a completely independent and global test over a wide spectrum, which is now possible with long-term ERM altimetry from Geosat.

In a preliminary, brief study with ERM altimetry (Wagner 1990), I showed that such an independent evaluation of this tide at many deep ocean points was possible even without using all the (1-second) Geophysical Data Records (GDRs) in this mission.

In a complementary analysis of Geosat ERM altimetry, Cartwright and Ray (1990) used methods similar to those here but they were not aimed specifically at M_2. While resolving a broad spectrum of tides they also did not utilize the difference data as a continuous time series and thus sacrificed some of its power. Here I follow the ideas of

Brown (1983) for local determination and the elimination of orbit error. The concept of developing the ERM altimetry in time series as a close analog of an ordinary tide gage follows the work of Cheney *et al.* (1989). The basic idea behind the method is simple. I analyze the differences of altimetrically determined sea heights at nearly overlapping ocean points in the ERM to extract the tide signal there that should be beating at precisely known frequencies. The goal is to do this at as many independent ocean points as practical and with as little coupling of information between the tidal points as possible.

Motivation for Discrete Tide Solutions

In a single ERM cycle of 17.0505 days, using the 1-second GDRs, about 500,000 distinct deep ocean locations can be sampled directly. However, in a year these points could only be resampled about 21 times, which leaves a small margin in the two-parameter M_2 solution for the myriad of other tidal and other ocean effects of both long and short wavelengths that disturb the sea height. It is known that the various lunisolar tides are a long wavelength phenomenon with correlation lengths typically of the order of 20° to 30° (e.g., Mazzega and Jourdin 1988). Furthermore the satellite moves rapidly (6.6 km/sec) traversing wide areas of the ocean within a small fraction of a tidal period. Therefore, to simplify both the data handling problem and to increase the signal-to-noise ratio of the solutions, the difference data along-track have been averaged in passes within square area bins of a few degrees on a side. Such averaging also promises to reduce the bias effects of small scale (so-called mesoscale) ocean dynamics (eddies and rings) that can cause disturbances of up to 50 cm in ocean heights over the order of 100 km within the 17-day minimum resampling time. Note also that the bins have been chosen to be 5° or less to keep them well within the average correlation lengths for the tides.

The Geosat ERM yields a ground track that provides both an ascending and descending pass at different times through (roughly) every 1° by 1° ocean area. Thus averaging the point data along-track into these areas roughly doubles the power of the along-track data to discriminate the tides. But even 42 "observations" a year seems scanty for a "satellite tide gage." In the preliminary solution (Wagner 1990), I averaged in 5° by 5° areas and, with an average "sea bin" containing 45 pass observations, managed to achieve satisfactory results but only for a relatively small number of stations (<1000). With more than twice as many GDRs analyzed here, the new solutions have both a finer resolution and greater density.

The overall features of the method here remain the same. The altimetrically determined sea heights on the GDRs (Cheney *et al.* 1987) are first corrected for media and surface effects, including Schwiderski's (1980) 11 principal tide models, and a detailed geoid to yield sea topographic heights (STH). In contrast to others who use "collinear" altimetry techniques (e.g., Cheney *et al.* 1989), I chose to work with STH rather than straight sea height differences, recognizing that tracks in successive ERM cycles are never precisely overlapping and that both the ±1-km crosstrack error and the 7-km along-track gap between 1-second GDRs may introduce unacceptably large geoid gradient errors for sea height differences over rough sea height zones. [See Brenner *et al.* (1990).]

In the present work all the new heights were determined with the aid of the Gem T1 gravity model, which is able to define the Geosat radial position to within a few meters (Haines *et al.* 1990). The orbits so determined are valid for upwards of a complete ERM cycle, but because of the burden of preprocessing only selected 1- and 2-day arc segments (or windows) of these were used from all of the first year of ERM cycles in 1986-87.

Using the arc segments in cycle 1 as a reference, similar STHs in succeeding cycles were overlapped with those in cycle 1 and the (cycle n - cycle 1) point differences averaged into 2° by 2° (deep ocean) bins. Typically the data reduction involved in this averaging process was about 20:1, permitting a rapid evaluation of the "orbit error" in the arc differences. This was accomplished in the next step of the analysis.

Orbit Error Reduction

A principal justification for using the overlapping (or collinear) arc technique was to reduce the orbit error effect at the outset to as low a value as possible. It is well known that radial orbit error affects satellite positions mostly near 1 cycle per revolution (cpr) but with a further complex spectrum at lower and higher frequencies. The error spectrum diminishes rapidly above 2 cpr due to the attenuation of the geopotential with satellite altitude (e.g., Marsh and Williamson 1980, Wagner 1989). However in an ERM all the orbit error effects from the geopotential of period less than 1 ERM cycle (17 days here) are cancelled after such differencing. The only orbit effects remaining are discrepancies in the initial conditions of the trajectory (at exactly 1 cpr) and errors in non-conservative force modeling such as radiation pressure and drag. These errors may amount to 10 to 50 cm, but are also characteristically at or near 1 cpr (e.g., Tapley *et al.* 1982).

In spite of the power and complexity of the orbit error spectrum, Mazzega (1985) was still able to derive a reasonable broad scale global M_2 tide (up to wave number 4 to 6) from the limited Seasat altimetry treated directly (i.e., without differencing) and ignoring this disturbance completely! Mazzega also overcame the large static geoid error in his analysis of the direct STHs for Seasat (order of 2 m) by lumping it with other mean error sources in 1° by 1° ocean regions and removing it from his data prior to his limited global spherical harmonic M_2 solution.

While Mazzega's achievement was remarkable, it was gained from data dominated by highly "colored" and powerful noise. Thus Mazzega's solutions effected further residual reductions of the data in his small ocean regions of only 3 to 7 percent. Furthermore, these solutions were for the full M_2 tide. In my method, before deriving the tide solutions I reduced the STH differences (2° averages) in each orbit-arc window of a constant, a secular term, and two fixed frequencies near 1 cpr. Then I found that a large number of the 5° by 5° M_2 solutions reduced the resulting sea level differences by more than 40 percent.

On the other hand, there is a disadvantage to removing the "simple" orbit error signal (at and near 1 cpr) in the STH differences. If this is done without coupling with the tidal solution(s) (as in my 5° analysis and here also), there is danger that some global scale tide signal will be lost in the parameters of this orbit solution. The problem arises because the tide signal along-track has enough power at global wavelengths to cause systematic distortion of the signal from such a "high pass" filter. In this report I will show from simulations what the likely effects of such removal may be on the remaining tide signal.

This orbit-coupling, while serious, appears to be well within the calibrated errors I found for the current model-correction solutions. Indeed, one of the reasons I sought a thorough calibration of the results is just because of this orbit filter-induced distortion. In light of the extent of this problem it is fair to ask why a coupled solution was not attempted. The only real drawback is the mechanics of such coupling with the present technique of short arc (1 to 2 day) sampling. The refined solution here is made from 126 such arcs (their differences with cycle 1). With six "orbit" parameters for each independent arc and some 2,000 4° by 4° bins with two M_2 parameters each, the coupled system would involve about 5,000 parameters, although there would be considerable sparsity in the normal matrix for them. But even this system is not sufficient when considering the effects of many other tides (both lunisolar and ocean "weather") that affect the data.

Fortunately, the distorting effect of uncoupling the orbit from the tide solutions is mitigated here with the use of longer arcs. In any case the calibration should indicate how important <u>all</u> the systematic errors are in the M_2 solutions, including, of course, the neglect of other tide corrections as well as mismodelling of the media effects on the altimetric signal.

Inverse Barometer Effect

In regard to the media corrections, note that in this study as well as in Wagner (1990) the sea height was corrected for atmospheric pressure acting on the sea surface as a simple inverse-barometer. I show below that this

effect is clearly seen in the altimeter measurements at a level of about 10 cm (rms) over the 1- to 2-day arcs (but predominantly outside the tropics). While this correction minimizes distortion of the M_2 signal, it absorbs some of the ocean weather tides particularly at semiannual, annual, and longer irregular periods such as the El Nino. The result has been that the solutions for these periods cannot be compared directly with those of other investigators who have made more geographically limited determinations for these tides without such corrections from Geosat altimetry [e.g., Cheney *et al.* (1989)] or island gage records [e.g., Wyrtki and Leslie, 1980].

Harmonic Analysis of Tide Differences

The extraction of tidal information from overlap or crossing arc altimetry (for one small ocean area) was first reported by Brown (1983) from limited Seasat data. He used sub-revolution arcs to remove the orbit signal from altimetric sea heights before differencing (which appears both less efficient in removing the orbit error and more likely to remove some significant tide signal than the technique employed here). But otherwise I follow his method of harmonic least squares analysis of the differenced signal.

One of the intriguing questions in such an analysis of harmonic data is: given a constant level of "noise" in a sea height signal, are harmonic solutions from height differences "better" than direct solutions from the heights themselves? In appendix A, I attempt to answer this question for the simplest cases of ideal and discrete data distributions. For example, it might be thought that there would be no advantage to using differences since the gain of achieving a possible doubled sensitivity (differencing of highs and lows) would be offset by the increased noise level of the differenced solution (a factor of $\sqrt{2}$). Results show, however, that even in the case of ideal (continuous) data the difference solution has a lower theoretical error which does not seem to have been remarked on previously.

DATA WINDOWS ON GLOBAL SEA TOPOGRAPHY IN THE GEOSAT ERM

I have divided the 17-day ERM cycle into 11 data windows or arc segments, which are all processed independently to permit calibration of the solutions. (See fig. 1a.) The segments beginning with the 0th, 3rd, 5th, 9th, and 13th days are all 1 day in length (labeled L, B, D, A, and E) while those beginning with days 1, 6, 11, and 15 are all 2 (contiguous) days long (labeled I, G, F, and H). These segments contain the bulk of the analysis. A few scattered 2- and 3-day (noncontiguous) segments have also been used: J containing data in days 4 and 8, and K containing data in days 10 and 14. All the 2-day arc heights used orbits determined from a small number of U.S. Doppler stations with the Gem T1 gravity field (Haines *et al.* 1990). This field was also used with the 1-day arcs B and C and the noncontiguous arcs J and K. All the other 1-day arcs used the Gem 10 gravity field [see Wagner, 1990].

The 1-second sea heights on the GDRs are averages of finest resolution 10-per- second data. They were first screened of erratic signals by only holding those which "fit" the finer data to better than 10 cm (standard deviation). Then the passed averages were corrected for media effects on the altimeter height from retardation due to the wet and dry troposphere and the ionosphere, and electromagnetic bias due to nonsymmetrical reflection from waves. The inverse barometer (mentioned above) was also corrected for as well as a detailed geoid based on Geos 3 altimetry (Rapp 1978), an 11 component tide model (Schwiderski 1980, 1983), and finally a solid Earth tide (Cartwright and Edden 1973). Below I examine briefly some of these effects as seen in the Geosat difference altimetry.

But with regard to the ocean tide, no secondary or tide loading correction to the bottom (solid) tide was applied in Cheney *et al.* (1989) even though this was known to be as much as 6 cm in some parts of the deep ocean (combined tide effects). Recently a number of papers have been devoted to this topic [Ray and Sanchez (1989), Francis and Mazzega (1990)] which recommend various computational schemes to overcome this deficit. Here, I have used a fundamental algorithm due to Goad (1980) employing integrated Green's functions and the same Schwiderski (1983) M_2 ocean tide model as that on the GDRs to correct my M_2 solutions for ocean loading.

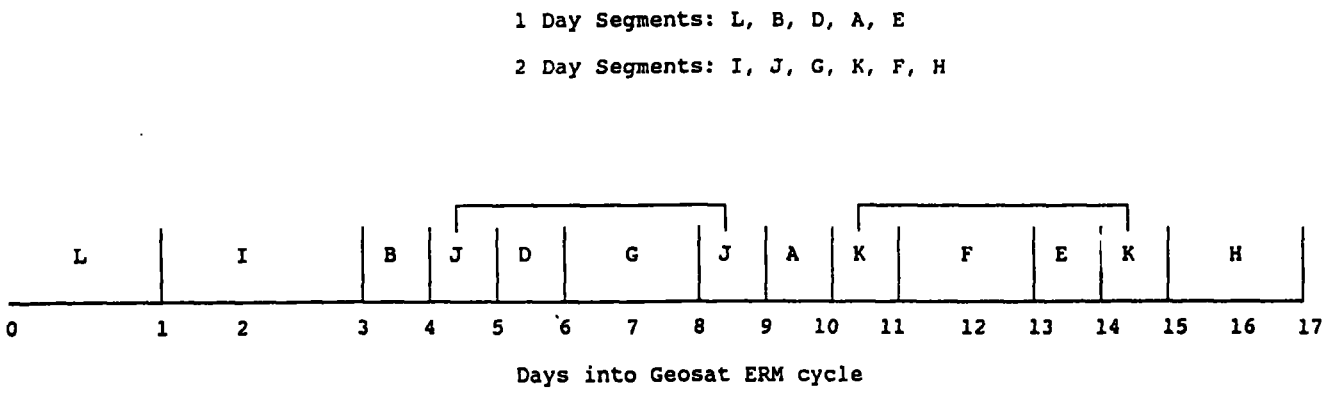

Figure 1a.–Arc segments (windows) used in Geosat tide analysis.

The resultant sea topographic heights (STH) were further edited of trench, seamount, and other anomalies by rejecting all STHs with absolute values greater than 10 m or followed by heights giving STH slopes greater than 1 m/10 km (absolute). Typical arcs with the Gem 10 ephemeris then had STH values of 4 m (rms) while those with the Gem T1 ephemeris were only about 2 m (rms). Both had spectra dominant at 1 cpr although many of the Gem T1 STH arcs showed strong indications of detailed geoid error.

For example, figs. 1b, c, and d show the first few revolutions of the corrected and edited STHs for the first two cycles of segment G (a Gem T1 arc). In figs. 1c and d the level of "orbit error" near 1 cpr appears to be not as strong as what seems to be geoid deficiencies (at extreme latitudes and over "rough" bottom topography) in the early 1978 model. This contrasts sharply with similar STHs computed with the Gem 10 radial ephemeris where strong consistent signals of near 1 cpr are seen in all Geosat arcs (e.g., for segments L, A, and E) at a level of 4 to 5 m (Wagner 1990).

Note that the time scale for fig. 1d is shifted by 1 ERM cycle with respect to fig. 1c, resulting in a close agreement between the two STH signals. I proceeded to difference these signals accordingly in the following way. Holding the data in cycle 1 as reference, I found the STHs in the following cycle(s) that came within 10 km of a reference track point and then interpolated (or extrapolated) successive reference heights to the point of closest approach of the later cycle data. I then took the difference of the later cycle with the (interpolated) cycle-1 heights, always finding that the distance from the later cycle positions to the closest point on the reference ground track was within 1.2 km. Figure 1e shows these differences for the first three cycles of segment G.

The differences in fig. 1e are dominated by a strong 1 cpr signal which probably arises from the difference of radial ephemeris error for the Gem T1 orbits computed for cycles 1 and 2. In theory, the so-called periodic gravitational errors on the orbit (with integer repeat periods in an ERM cycle) perfectly cancel in these differences. For nearly circular orbits of long repeat periods, the only sensible orbit errors that do not repeat exactly are those at exactly 1 cpr (due to errors in the initial orbit adjustment to the tracking information) and near 1 cpr (and other frequencies) due (presumably) to nonconservative mismodeled forces on the satellite (such as radiation pressure and atmospheric drag) and station position errors. According to Tapley *et al.* (1982) the likely error from nonconservative force mismodeling on the more complex Seasat spacecraft was 45 cm (one-way error). Another likely source of error near 1 cpr at a level of about 50 cm arises from poor station positions in the unadjusted operational Doppler network used in the Gem T1 orbit determinations (Haines *et al.* 1990).

In any case, the use of overlapping differences has reduced the discrepancies in STHs by about an order of magnitude but still shows a signal that is related to the orbit and not the tide or likely mismodeled media or surface corrections. With regard to the tide, for example, the total surface (ocean plus solid) signal is of the order of 50 cm

(rms). It is expected that the deep ocean tides have been modeled in the GDRs to about 20 percent of this figure, or 10 cm (one-way measure) according to Tapley *et al.* 1982. [See also Schwiderski 1980).]

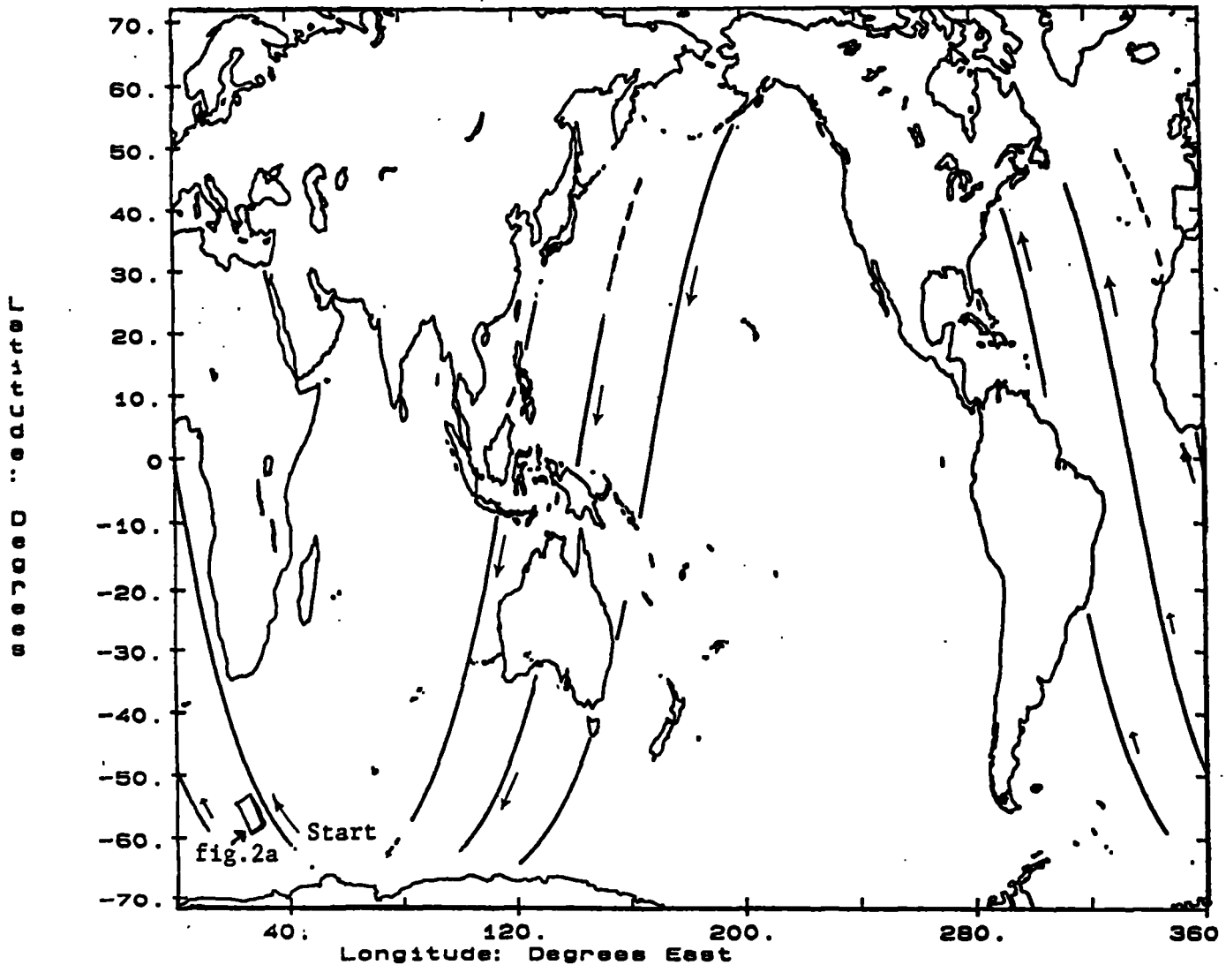

Figure 1b.–First three revolutions of Geosat ERM track: segment G (day windows 7 and 8). Solid portions of track contain altimetric sea height information for segment in first ERM cycle, dashed portions contain data for second cycle only.

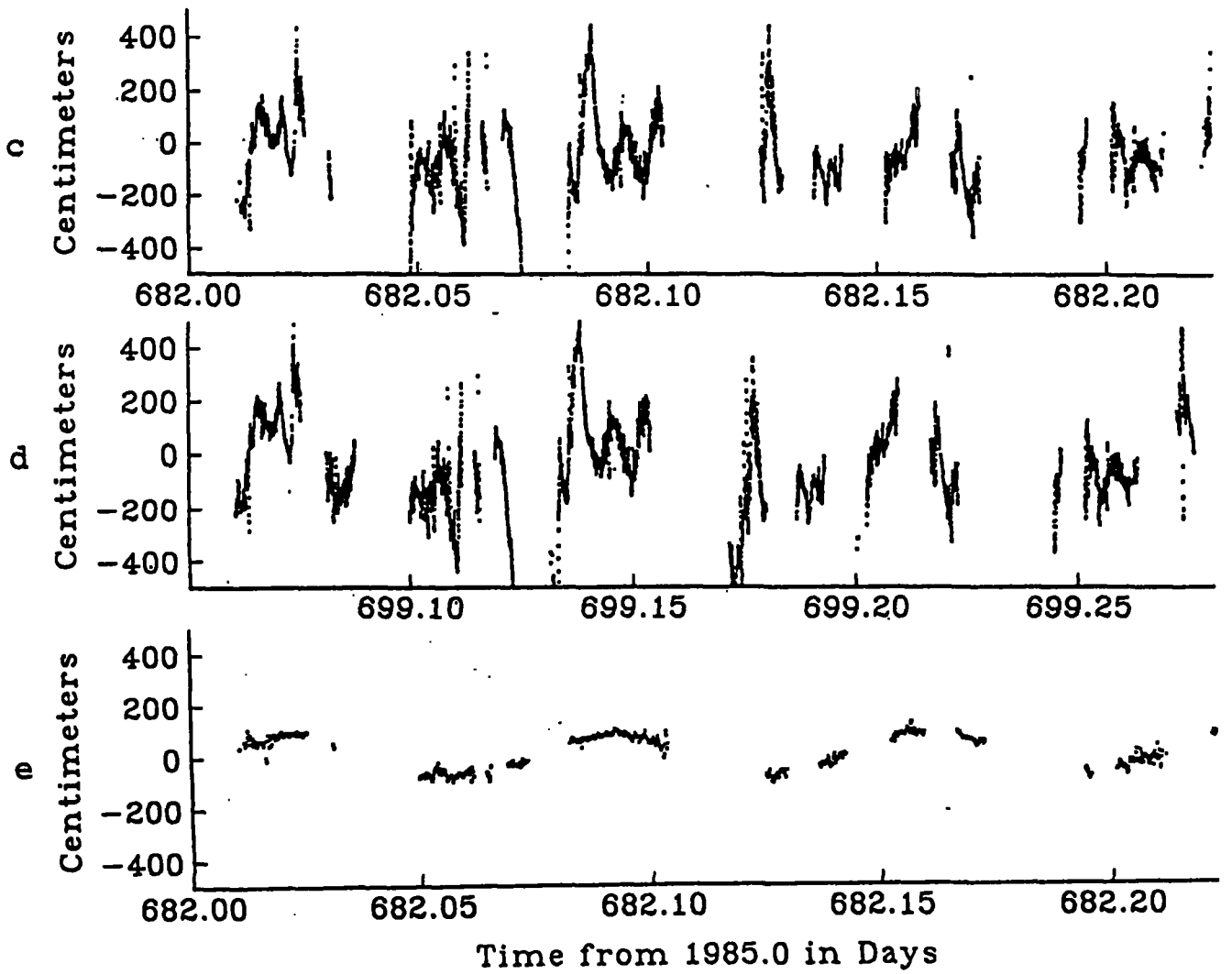

Figures 1c,d,e.–The first three revolutions of sea topographic height (STH) in the Geosat ERM, segment G: (c) cycle 1, (d) cycle 2, and (e) their differences. (c). The signal here (STH) is the altimetric sea height with all media and surface corrections applied and a detailed geoid subtracted. Large excursions of STH (greater than about 200 cm absolute) are probably due to error in the detailed geoid, a 1978 model based on surface gravimetry and Geos 3 altimetry which was weak in the southern oceans. (d)–Note close correspondence of this signal with that in first three revolutions of overlapping first cycle (fig.1c). Note parts of the track here are not represented in first cycle. Many of these missing parts of passes are due to a delay in attitude stablization of the spacecraft coming off a long land segment. (e)–The rms difference here is 52 cm dominated by a clear 1 cpr "orbit error" signal. These differences were computed by holding the following cycle (here cycle 2) heights fixed and interpolating base cycle height at point of closest approach with the following cycle (with this segment pair: 0.3 km,rms). Most of the large rapid variations here are due to mesoscale dynamics (or differences in dynamics over these 17 days) which are greatly reduced in size after taking 2° by 2° averages of these data.

Figure 1e shows that, once the 1 cpr signal is removed, the variation within the major blocks of these two-way difference data is of the order of 20 cm (amplitude), which is suggestive of anticipated tidal error. To see this variation in greater (time) detail we can examine how the first few 2° averages smooth these "point" differences.

Figure 2a shows the first substantial 1-second difference series near the beginning of the first overlap for segment G in the southwestern Indian Ocean. At the smallest scale (about 10 km) the "point" differences appear to be random with a noise level of 10 to 15 cm, compatible with the assumption above of 10 cm one- way precision. The data with error bars in fig. 2a show the average and standard deviation for this point data in the 2° by 2° area bins indicated above the time line. (See also fig. 1b). The formal errors of these averages are considerably less than 10 cm because, on average, 21 point differences are aggregated into them. However, I do not apply this formal value in the tide solutions directly since it is clear that in most of the bins the differences have at least a linear trend.

Figure 2b shows the complete set of averaged differences for this cycle pair of segment G with a detail of the first three revolutions in fig. 2c. In many areas there has been significant reduction of systematic variation between the point difference data (fig. 1e) and the 2° smoothed data (fig. 2c). Closer examination shows these to be too large (up to 40 cm) over too small a scale (200 to 300 km) to be lunisolar tidal discrepancies. They are undoubtedly the result of mesoscale ocean dynamics, but in any case the 2° smoothing has substantially removed their influence on the tidal determination. In some places, of course, where only a small corner of a 2° bin was sampled, an isolated "smoothed" point may remain in such active zones (fig. 2c). Many of these are further filtered by the orbit reduction process described below (which used a 3-sigma edit criteria to reject outliers which escaped the previous screening processes).

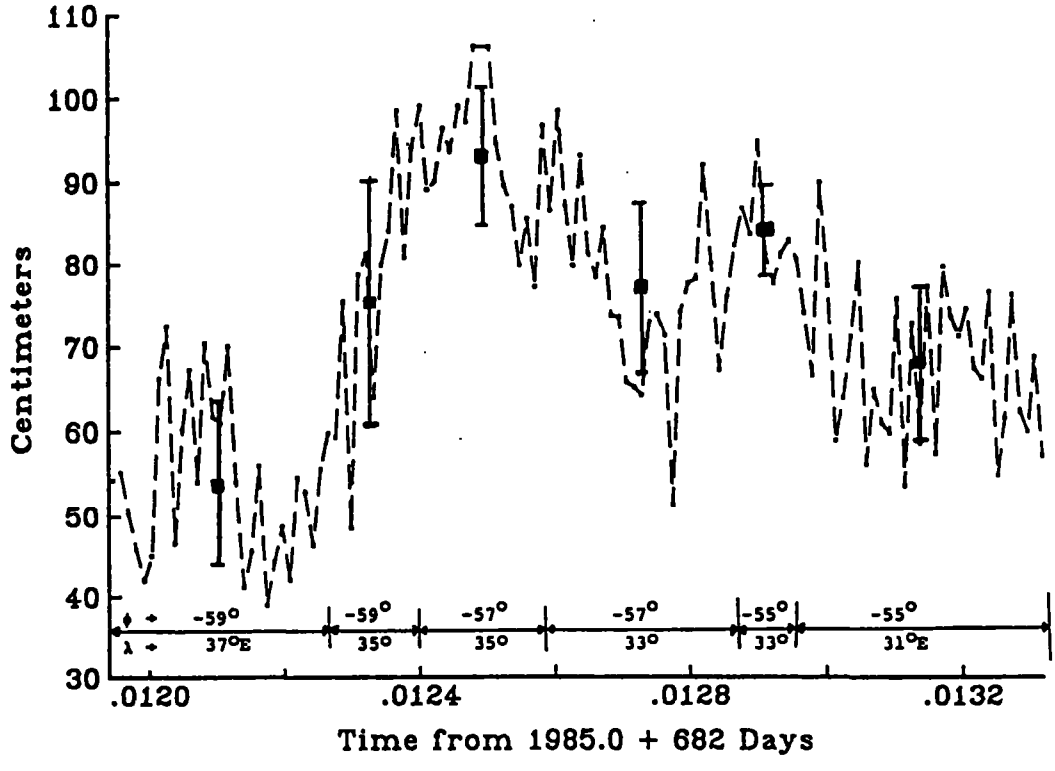

Figure 2a.--STH differences for segment G: Geosat cycle 2 minus 1. An expansion of the data in fig. 1e near the start of this segment (southwest Indian Ocean). Dashed line connects the 1-second point difference data. Solid vertical lines show 2° by 2° smoothed differences centered in their respective "bins." Error bars show standard deviations for 1-second data in these bins. Smoothed data were computed as simple average of 1-second differences. In normal regions where sampling is uniform and no outliers exist this minimum computation is acceptable. For abnormal zones it would be preferable to use a linear (or even quadratic) function to screen "bad" points and average the "good" data more accurately.

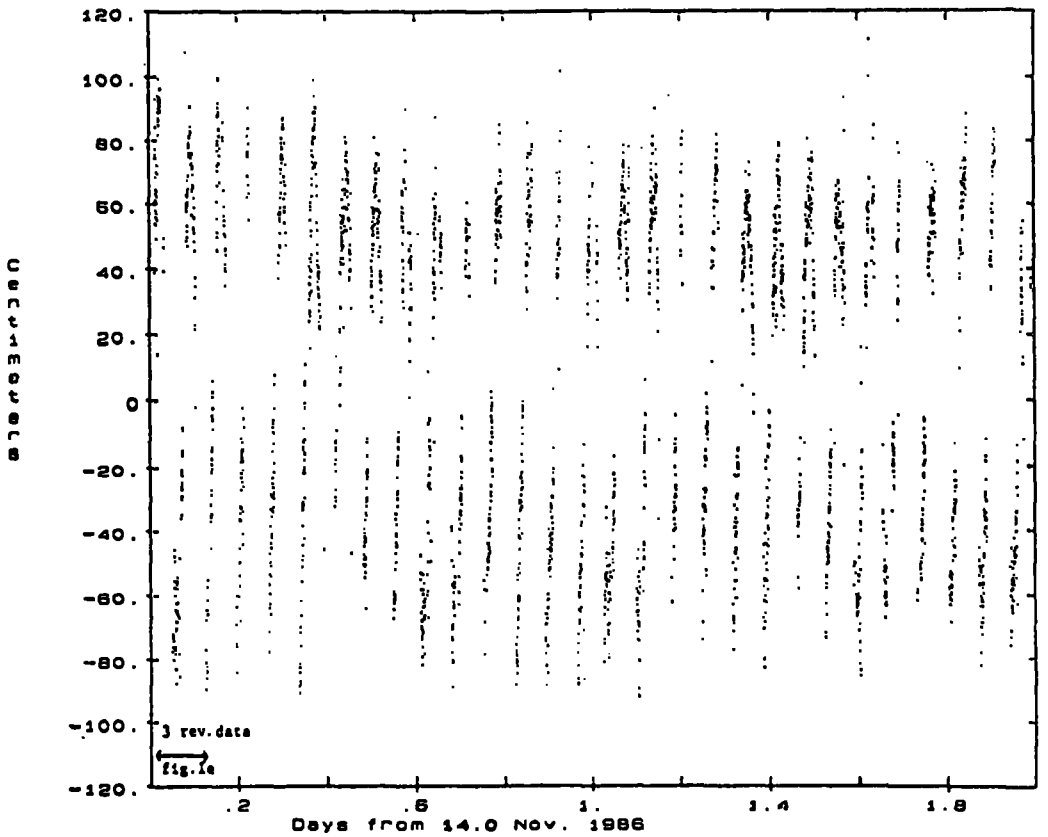

Figure 2b.–Complete 28 revolutions of 2° by 2° smoothed STH differences for segment G, Geosat ERM (cycle 2 minus 1). Again the 1 cpr (orbit) signal dominates these data. Its apparent strong modulation is mostly due to varying continental cutoffs of the track. However, there is a small orbit modulation near 1 cpr due probably to the different fundamental periods of the 1-cpr effects in the two cycles. These periods were established from separate 17-day orbital arcs with different initial conditions.

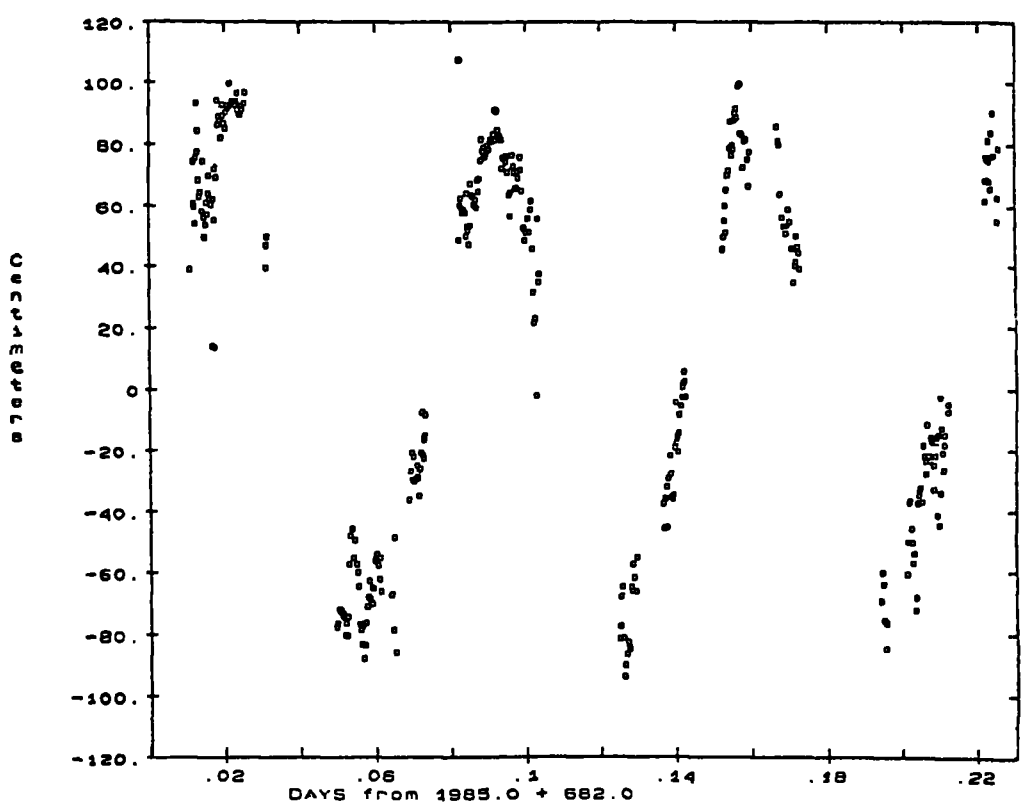

Figure 2c.–2° by 2° smoothed STH differences: first three revolutions of segment G referenced to first Geosat ERM overlap. Except for a few "outliers" to the "orbit" signal at near 1 cpr, the remaining variations appear to have the long range waviness expected of a tidal signal.

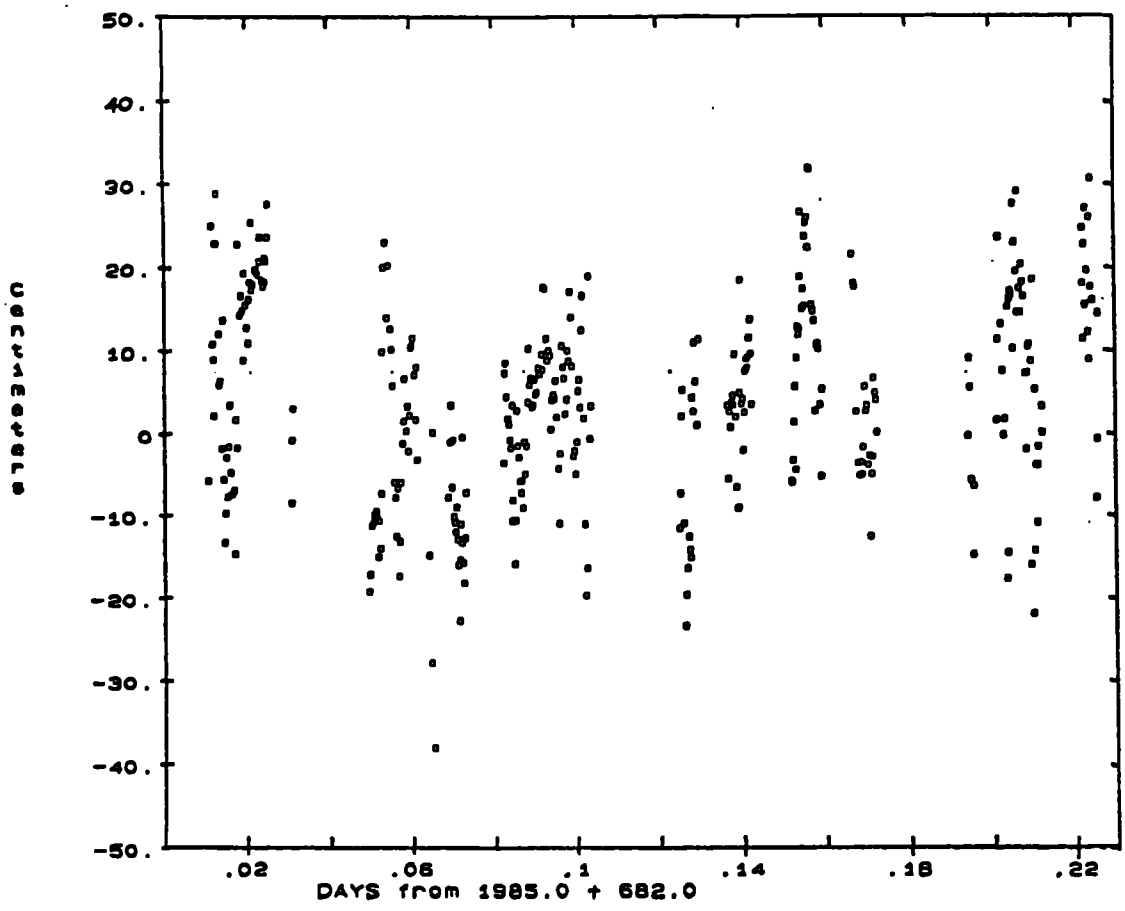

Figure 2d.–Residuals of smooth STH differences after orbit reduction: first overlap, segment G, Geosat ERM, first three revolutions. Notice marked reduction in range of these residuals compared to the source data in fig. 2c. At an expanded time scale the "tidal" correlation of these residuals is evident.

To anticipate this result before I discuss it, fig. 2d shows the residuals after the orbit reduction of this cycle pair of segment G (over the full data set in fig. 2b) for the first three revolutions. The changes here (with power about 12 cm) seem systematic over a correlation length of 20° to 50° degrees and so are a good candidate for real tidal anomalies.

ORBIT ERROR REDUCTION

The statistically independent 2° averages for all the Geosat STH differences were reduced of apparent "orbit error" signals by a least squares solution for two near 1 cpr frequencies as well as a constant and a secular term. The need for two frequencies arises because these are differences with respect to two independently determined orbits (in two different ERM cycles for every case) where each has its its own error characteristics (primarily the error generated by an imperfect adjustment of initial conditions).

First, consider all the geopotential-caused orbit errors with integer periods within the ERM cycle. These are the dominant ones on a near circular orbit such as Geosat. The only one which will generate a significant 1 cpr adjustment signal is that usually associated with the odd zonal harmonics with a periodicity of the satellite between nodal crossings, close to the exactly 1 cpr anomalistic mean motion. The orbit adjustment to such close-to-1 cpr errors produces the characteristic "bow tie" pattern discussed at length in Colombo (1984). [See also Wagner (1990).] Errors at other frequencies farther away from 1 cpr are increasingly orthogonal to 1 cpr, thereby producing much less adjustment error. However, if these errors are nonconservative they may not be repetitive in successive ERM cycles and so have direct effects on differencing. Haines *et al.* (1990) have established that the radial orbit error for Geosat using Gem T1 is dominated by such a bow tie pattern by examining the crossover differences in 3-day windows between two successive orbit determinations over two successive ERM cycles in 1987. They found that the crossover differences in the windows at the ends of the cycle were significantly greater than the differences in the middle windows. What is not clear is the cause of this characteristic. Without a more detailed

error analysis I can only say that any errors in the frequency band close to 1 cpr (say from drag, radiation pressure, or station misposition) can cause such a significant 1 cpr (mis)adjustment which Haines *et al.* (1990) found to be of the order of 1 m (rms).

A bow tie orbit error (here) is a 1 cpr signal modulated at a much longer period. It can be empirically modeled as either a sinusoid with secular coefficients or two frequencies close to 1 cpr. I chose the latter representation. The two frequencies with the anomalistic and nodal periods are both known to be associated with major orbit perturbations from a variety of sources and are well known for the Geosat ERM. The latter frequency is the precisely maintained 244 revolutions in 17.0505 days that ensures a repeating ground track for Geosat's 108° inclined (near circular) orbit. The former is the frequency which carries (nearly) all initial orbit adjustment information. The respective periods of these orbit frequencies (from first order J_2 theory) for the Geosat ERM are 6,035 and 6,037 seconds. It is true that some advantage (in absorbing residuals) might be gained by using the alternative bow tie formulation as a single frequency with secular coefficients since the solution for the secular parameters does not uniquely determine the small frequency shift. Thus if the fixed frequencies were in error for a particular orbit pair the secular coefficients could accommodate this error to some extent, at least for a short time. However, to guard against over-accommodation of frequencies outside a narrow 1 cpr band defined by the two conventional "mean motions" of the satellite, which might prejudice the following tidal solution, I prefer here to limit the orbit error solution to these frequencies alone.

To illustrate the great simplification and reduction of orbit error that using overlaps entails I give an example from two nearly independent orbit determinations in the Geosat ERM. (See figs. 3a-d.) The geographically overlapping arcs considered are 2-day "windows" (starting at day 4) in ERM cycles 6 and 7 on February 3 and 20, 1987. The original Naval Astronautics Group (NAG) orbits for Geosat (Cheney *et al.* 1987) covered 2-day spans of Doppler data (from a limited number of stations in the United States). The geopotential field used was Gem 10 (Lerch *et al.* 1979) based on both (early) satellite tracking and surface gravity data. The orbit software was developed at the Johns Hopkins University (JHU/APL 1981). I compare these orbits for the two window openings with those computed by Haines *et al.* (1990) using the Gem T1 geopotential (Marsh *et al.* 1988) with the same Doppler data but spanning more than two weeks of data. The orbit program used for this purpose is called Geodyne (Putney 1976). Both programs use numerical integration for solving the orbit and variational equations but the non-gravitational models (for atmospheric drag and radiation pressure, in particular) differ. In Geodyne, for example, the scale of the drag is found empirically from the tracking through separate drag coefficients for each day of the trajectory since the predicted density of the atmosphere at satellite altitude depends strongly on poorly modeled sporadic solar storms. The Doppler station positions used by each program differ also, presumably at the meter level.

In any case, fig. 3a shows the difference in the radial ephemerides for Geosat between these two systems for the 2 days starting 3.0 February 1987. Since the orbital period for Geosat is about 100 minutes, these differences are clearly dominated by near 1 cpr effects but they also show considerable power at other frequencies. Notice especially how the differences appear to be smaller in the middle of this span, which covers a complete tracking period for the NAG orbit but only a short portion near the beginning of the 17-day Gem T1 trajectory arc No. 7 (Haines *et al.* 1990). The NAG ephemeris should be "best" near its (tracking) midpoint while the Gem T1 orbit in this relatively short span (for it) should be more nearly uniform in quality. Considering the higher quality of the Gem T1 gravity field, this comparison suggests that at best the NAG orbits are in error (at orbital periods) by a few meters.

Examining these differences in more detail, I removed the two strong frequencies near 1 cpr from these data and, as seen in fig. 3a also, the residuals are still at a level of a few meters with a fairly rich (but mostly low frequency) spectrum. Figure 3b shows this (residual) spectrum. Vertical lines represent the measured spectrum; dashed lines connect points on a theoretical spectrum for radial differences on Geosat due to just the geopotential's Gem T1-Gem 10. While a good portion of the actual spectrum seems to be accountable from this source, there are clearly significant departures (mostly near 1 cpr) which are probably nongravitational in origin.

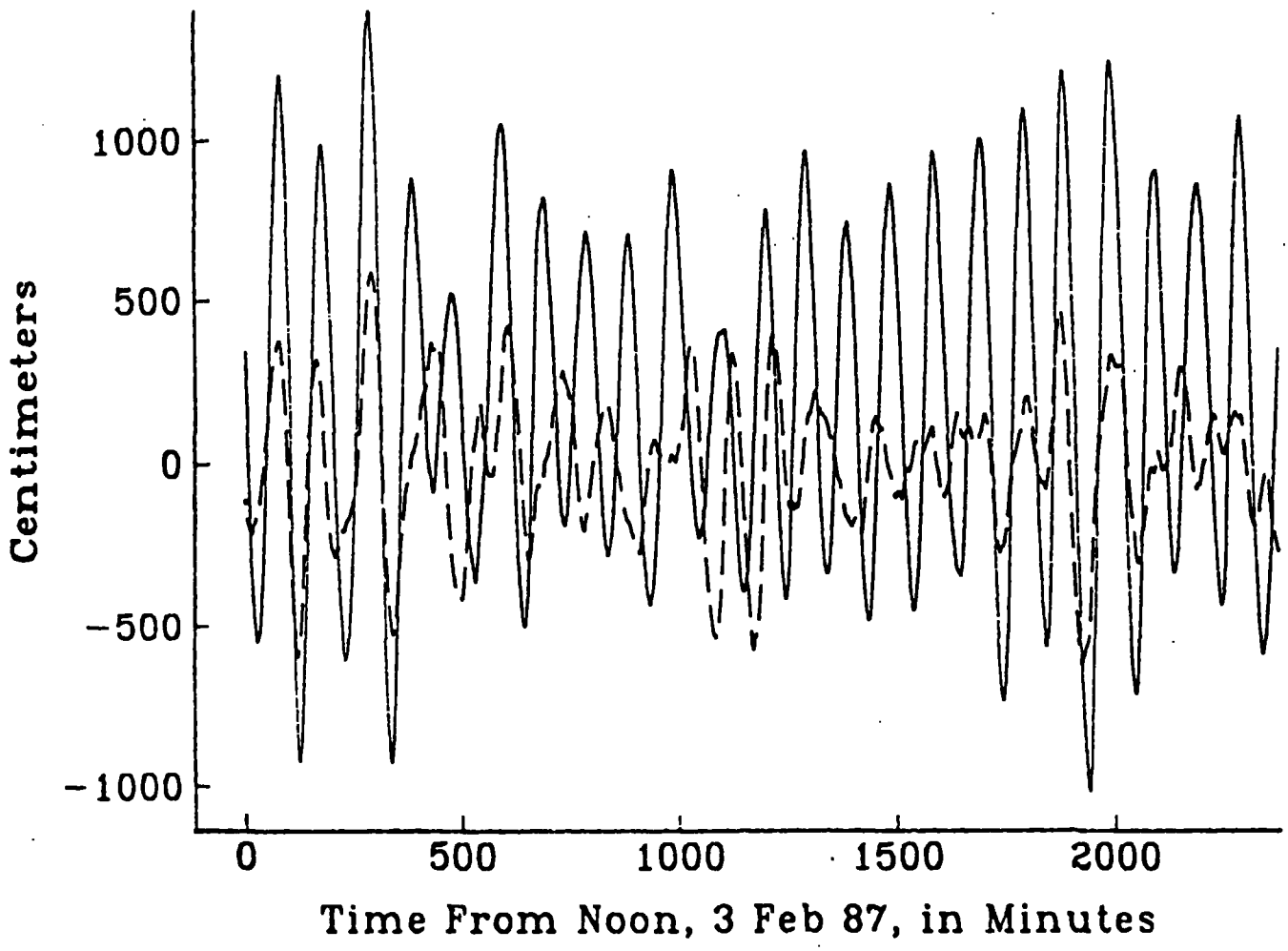

Figure 3a.–Geosat radial orbit differences: Gem T1-NAG ephemerides: 3-5 February 1987 (cycle 7). The solid curve gives these differences before an empirical reduction of them is made using a constant, 1 cpr and near 1 cpr terms. The rms values of the raw differences are 566 cm. The dashed curve gives the residuals after the empirical terms have been determined by a least squares fit of the data (every minute) in the solid curve. The rms values of the reduced discrepancies are 223 cm, presumably arising mainly from errors in the older Gem 10 geopotential used in the NAG ephemeris.

I then compared the two ephemerides in the same window (days 1 and 2) of cycle 7 (beginning on 20.0 February 1987) for nearly 2 days (again using a complete NAG tracking span) by repeating the same geographic track. The 17-day Gem T1 orbit covering this window was almost identical in geographic aspect as the one covering cycle 6. The gross features of the differences in these following arcs are almost identical to those seen in fig. 3a, showing that the bulk of the gross orbit differences between the two systems is repetitive in an ERM and removable by simple differencing. Of course it is already known that the geopotential-caused errors have this feature in an ERM. Figure 3c depicts the overlapping differences between the two orbit differences.

Note in fig. 3c that the level of orbit differences has come down an order of magnitude from 1,000 to 100 cm and the spectrum appears to be almost entirely at 1 cpr with a slight modulation (at a much longer period). This behavior is just that expected for orbit errors dominated by geopotential effects and tracking deficiencies (such as station position errors and poor data distribution) which manifest themselves also at (and near) 1 cpr. What is gratifying is that the level of the nonconservative force errors, that part which is not geographically correlated, is so low here. Some of these errors are expected to show up at and near 1 cpr, and they can also be removed empirically (as we did routinely with the actual Geosat STH differences). The remaining tracking errors are shown

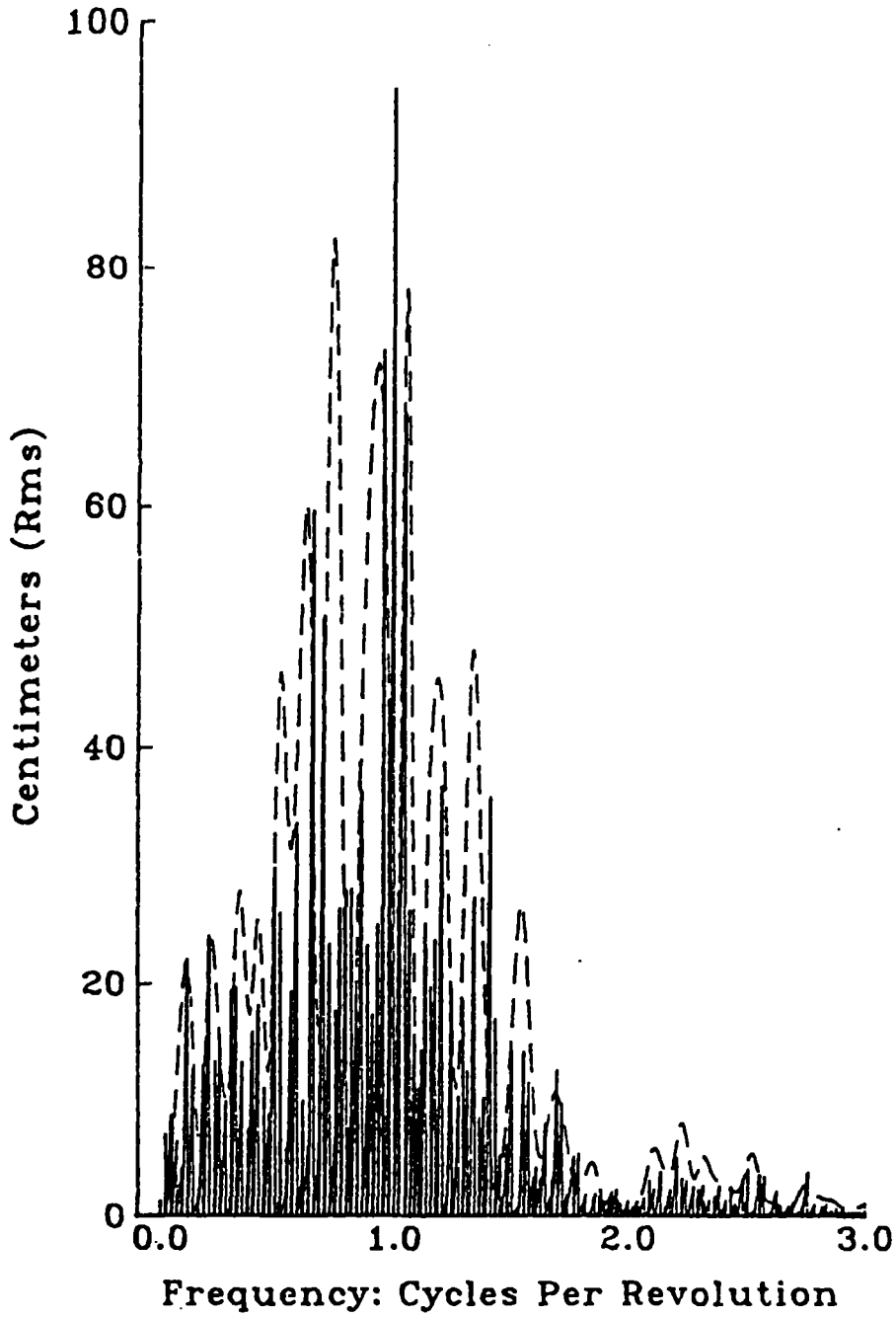

Figure 3b.–Geosat radial difference spectrum: 3-5 February 1987: Gem T1-NAG ephemerides. Shown (in solid) is spectrum of actual differences less two lines at and close to 1 cpr (which have power greater than 1 m) associated with errors in initial orbit adjustment or datum discrepancies between the two orbit determination systems. Dashed spectrum gives theoretical result just for gravitational frequencies from differences between Gem T1 and Gem 10 [e.g., using linear analysis in Wagner (1989)]. While comparison between measurement and theory (assuming only geopotential differences) is fairly good (some extra power in measurement arises from nonperiodicity of time series in fig. 3a), it is also apparent that not all differences between Gem T1 ephemeris and NAG are due to the geopotential.

by the residual dashed data in fig. 3c. Unexpectedly there is a significant slope (10 cm in 2 days) to these residuals after the 1 cpr reductions. Calculation shows the likely cause is a constant drag difference between the NAG and Geodyne orbits. Calculation also shows the difference would only have to be at a level of 0.1 percent of the full drag effect to cause this secular drift between the two trajectories. Presumably the Gem T1 drag computations are more accurate because they encompass data over 17 days compared to 2 days for the NAG orbits. Nevertheless, since only a very small drag error can give rise to so large an effect, the actual orbit reduction (of the overlap differences) included a secular rate term, both for the 1-day arcs (segments L, A, and E) deriving from the NAG computations, and also for the Gem T1 arcs to be on the safe side.

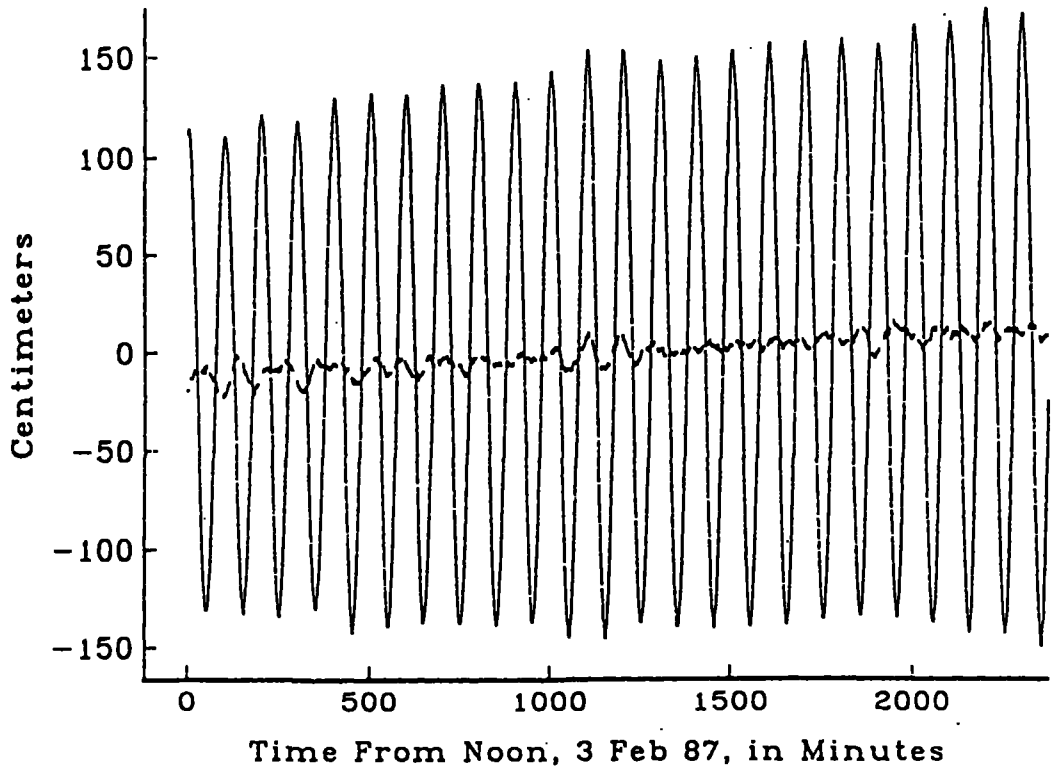

Figure 3c.--Differences of Geosat radial ephemerides differences: (Gem T1-NAG) for cycle 7 minus 6 referenced to cycle 7. A conservative assessment (with regard to Gem T1 ephemeris which is considered superior) of the likely orbit error in a 2-day window of Geosat ERM altimetric sea height differences at overlapping points. Compared to 3a, scale is greatly reduced and the character of the variation (solid line) is almost entirely at 1 cpr. There is also a slight long period modulation of this primary oscillation. After removing these two effects (and a constant) from these observed differences of differences (i.e., changes of orbit errors over an ERM cycle) the dashed curve results. These residuals are dominated by a secular trend that is attributed to differences in drag modeling between the two ephemerides.

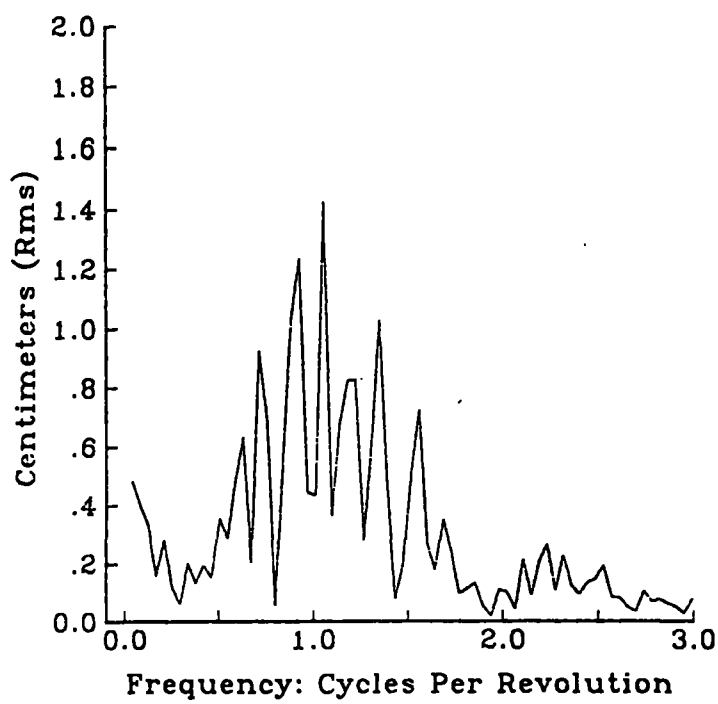

Figure 3d.--Spectrum of differences of Geosat radial ephemerides: (Gem T1-NAG) after empirical correction for a constant, a secular trend, a 1-cpr, and a near 1-cpr frequency. Note the very low power of this "orbit reduced" data (rms=3 cm) and its concentration around 1 cpr. These residuals show the effects of nongeopotential differences (e.g., atmospheric drag and radiation pressure mainly) between the two ephemerides for these time periods. The result may not be a completely independent assessment of these uncertainties, however, because of common modeling in the two systems especially regarding radiation pressure. (Both systems use a simple spherical shape for the spacecraft.)

Finally, fig. 3d shows the spectrum of residuals of these overlapping "orbit discrepancy" differences (with the secular term removed by matching the ends of the data span). The level and character of this spectrum, with a broad peak around 1 cpr at 1 cm, if representative of likely remaining time variations associated with the orbit (from drag effects, say), promises to pose few problems to the tide reduction that follows.

Returning to the processing of the 2° by 2° smoothed STH differences (in fig. 2b), I made a series of (least squares) reductions of these data to remove their "orbit" effects using combinations of two near 1 cpr frequencies, a single 1 cpr frequency with secular coefficients, a pure secular term, and a constant to fit these data. The constant term was meant to absorb any change in the overall altimeter calibration from the reference cycle. But, in addition, I wanted it to serve as an indicator of global sea level change if such calibration changes can be assumed to be sufficiently small and random. Of course by calibration I also include all media effects (such as the ionospheric correction) whose mismodeling might be biased over the 1- to 2-day window here. However, just as important to modeling what should be removed from the data, I also recognize these "orbit" parameters may remove some tidal signal, which I discuss in a later section.

Table 1a gives the results, in terms of the rms residuals, for the various combinations of empirical terms in removing "orbit signal" from the data in fig. 2b. From these runs I concluded that though a single (near 1 cpr) frequency makes by far the greatest reduction of this signal, additional parameters, beginning with a second (near 1 cpr) frequency, or secular sinusoids also are effective. This particular arc does not show a significant constant or secular bias but I retained their use for other arcs which did (also see tidal simulations below).

An interesting aspect of the runs shown in table 1a arises from the optimization for a single frequency, which turns out to have a period 9 seconds longer than the true mean motion of the satellite. Clearly the true period of the satellite is known (from the tracking) to a fraction of a second so this "empirical period" for the two-cycle data differences is an artifact of the slightly different (by perhaps a few seconds) fundamental orbit periods in the two cycles. In fact, even if there were no orbit disturbance near 1 cpr (such as from nonconservative force mismodeling) but just two pure 1 cpr signals from imperfect orbit adjustments in the two cycles, the existence of the two different fundamentals in the signals demands that two frequencies be included in the reduction of these overlap data.

Unfortunately the solution for the optimum two (close) frequencies (or one frequency with secular variations) is highly nonlinear. In table 1a I show that after iterating to a minimum for a single frequency, the introduction of secular rates on the sinusoidal coefficients (equivalent to absorbing a close neighbor frequency) yields residuals which are significantly smaller than the fixed two-frequency result. This should not be surprising because the fixed

Table 1a.--Orbit reduction results for arc segment G: Cycle 2 minus Cycle 1

The data (for reduction) consists of 3,263 2° by 2° averages of differences of sea topographic heights (STH) from 1-second Geosat altimetry fully corrected for: significant wave height (induced bias), wet and dry troposphere delay, 11 ocean tides and the solid Earth tide, ionosphere delay, the inverse barometer surface response, and a detailed geoid. The power of these observed STH differences is 52.36 cm, rms. Forty-five of the original 3308 (2°) observations in this arc were edited at a 3-sigma level from results of a preliminary orbit reduction. All orbit runs determined at least a constant and two 1 cpr harmonics.

Run No.	Rms Residual (cm)	Constant (cm)	Sat. Alt. (km)	ERM orbit	Other parameters determined	Period(s) (sec)
1	11.370	0.66	792.0	yes	secular, near 1 cpr	6035.519, 6037.551
2	11.381	0.70	792.0	yes	near 1 cpr	same
3	12.212	0.57	792.0	yes	none	6035.519
4	11.828	0.86	798.0	no	none	6042.640
5	11.802	1.00	800.0	no	none	6044.663
6	11.844	1.13	802.0	no	none	6046.689
7	11.366	0.67	792.0	yes	sec, sec 1 cpr	6035.519
8	11.381	0.64	800.0	no	same	6044.663

result was only meant to encompass the average condition for Geosat ERM orbits. Aside from the difficulty of implementing this optimum solution, I consider the gain in removing real orbit effects not to be worth the risk of absorbing tidal information in the additional parameters over a sensibly wider band around 1 cpr.

EFFECTIVENESS OF MEDIA AND SURFACE CORRECTIONS

The low level of signal in the difference data reduced of orbit effects indicated by fig. 2d (12 cm, rms) affords an opportunity to test the effectiveness of the media and surface corrections applied to the original sea heights on the GDRs. In order of importance these are the 11 lunisolar tides (order of 40 cm, rms, for one-way correction), the inverse barometer correction (order of 15 cm), the wet troposphere correction (order of 2 cm), and the electromagnetic bias correction (a function of the significant wave height, order of 1 cm).

The reality of these corrections can be judged most directly by viewing the correlation of them with the actual height differences computed without them. To find the latter I reprocessed the original STH data in both the reference and following cycles without the correction in question and arrived at residuals of 2° smoothed (orbit removed) differences in the same way as previously for this (first) arc G segment. Table 1b gives the results of this processing.

Figures 4a-d show the four correlations of the differenced (2° smoothed) corrections with their respective (corrections removed) residuals. In an ideal case where only the particular medium affects the data (without model error) and that medium correction has no power in the "orbit parameters" (e.g., near one cycle per revolution) the correlation should fall on a straight line with a slope of 1.0. In reality, of course, both conditions do not hold strictly, but this result is well approximated for the all-tides model [dominated by the Schwiderski (1983) solution for the M_2 ocean tide]. The strong inverse barometer correction is similarly well seen in the altimeteric residuals. (See fig. 4b.)

Table 1b.--Orbit reduction results with removal of media and surface corrections.

The source of these data is the same as in table 1a with a constant, secular term, 1-cpr, and near 1-cpr terms determined in each run. The residual with all corrections is 11.370 cm, rms.

Run No.	Rms Residual (cm)	Power of cancelled correction (cm)	Cancelled correction
1	16.793	10.86	All tides
2	13.585	9.86	Inverse barometer
3	11.190	2.86	Wet troposphere
4	11.745	1.24	Sig. wave height (induced bias)

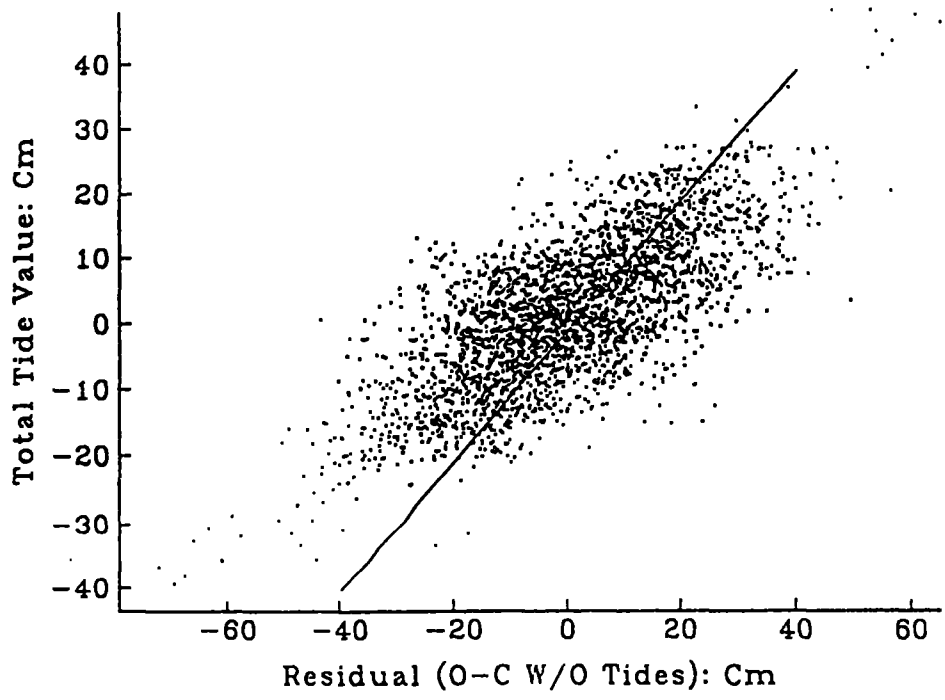

Figure 4a.--Correlation of Geosat STH residuals (after orbit reduction) and tides (ocean plus solid): arc segment G (cycle 2-minus-1 data). As indicated, residual data arise from orbit correction of overlap differences without using tide information on Geosat geophysical data records (GDRs). Text shows only a small portion of error that this incurs is removed by empirical orbit correction. Residuals are evidently strongly correlated with corresponding lunisolar tide values though they are also disturbed strongly by other effects (e.g., media errors, not completely smoothed mesoscale dynamics, ocean weather, and lunisolar tide error).

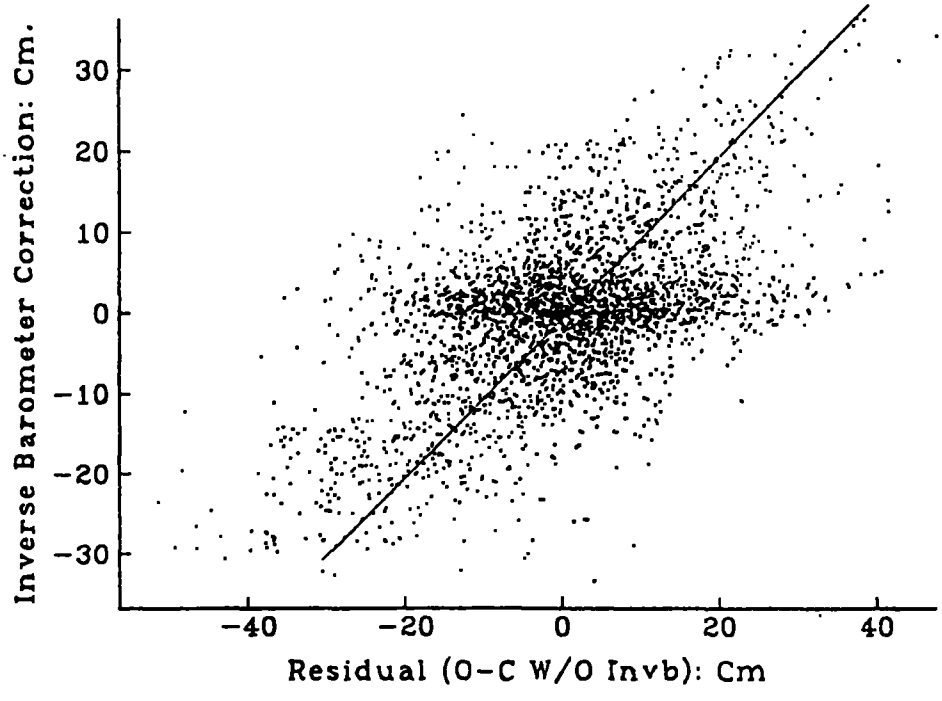

Figure 4b.--Correlation of residual STH differences and inverse barometer correction. Circumstances of data here are same as in fig. 4a except STH differences were computed without using inverse barometer correction. There is fair correlation of residuals (after orbit reduction) with full correction (computed from air pressure data on GDRs) in spite of narrower range of effect compared to luni-solar tides. Horizontal band with small inverse barometer effects arises from those parts of track in the tropics where atmospheric pressure is nearly constant. Notice there is still a strong correlation here in spite of significant 1 cpr signal in inverse barometer (resulting from day-night variation of track) removed by the "orbit correction."

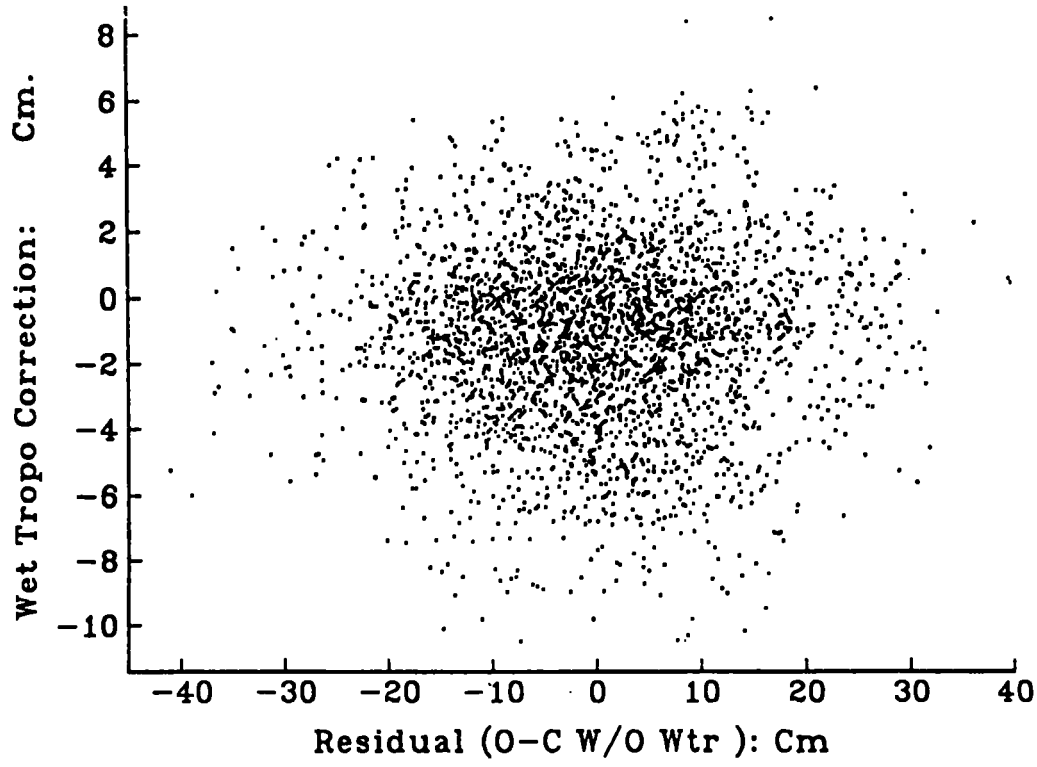

Figure 4c.–Correlation of STH difference residuals (after orbit reduction) and wet troposphere correction. Circumstances of data are same as described in figs. 4a,b but with regard to wet troposphere correction on Geosat GDRs. This correction also has a fairly large 1 cpr (day-night) component, but its overall power (about 3 cm rms) is considerably reduced from previous corrections. There is no noticeable correlation with residual data here. Note from table lb that inclusion of this correction actually degrades residuals slightly.

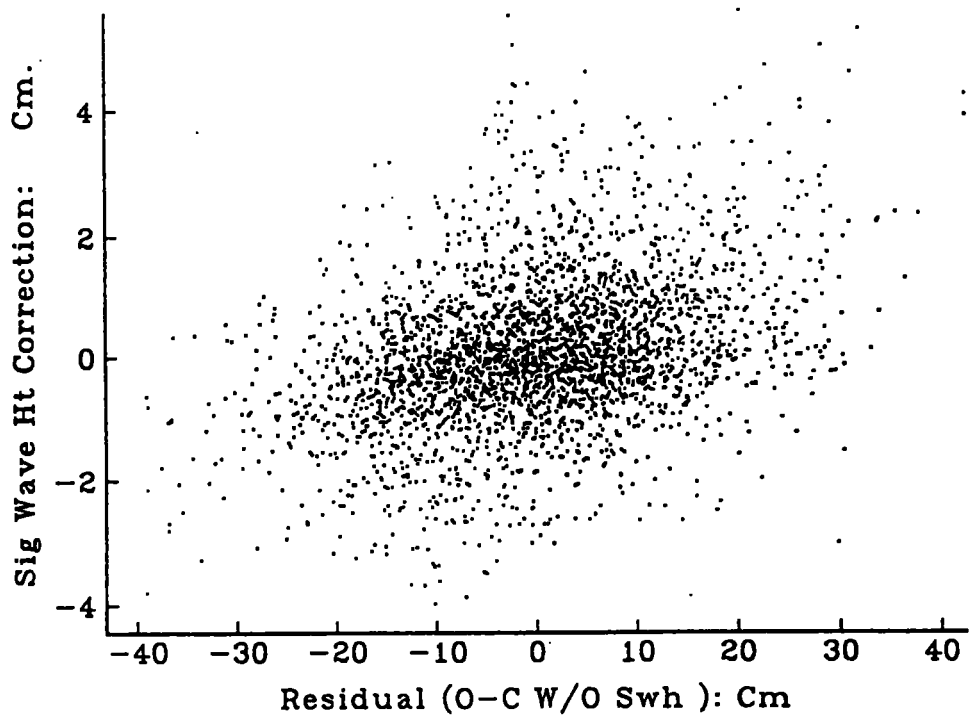

Figure 4d.–Correlation of residuals and electromagnetic bias correction (from significant wave height): arc segment G, ERM 2 minus 1. There is a noticeably positive correlation here in spite of the fact that power of this correction is significantly less than that of the wet troposhere. Concentration of points near zero correction arises from tropical location of these data. Here absolute wave activity is diminished and differences are likewise small.

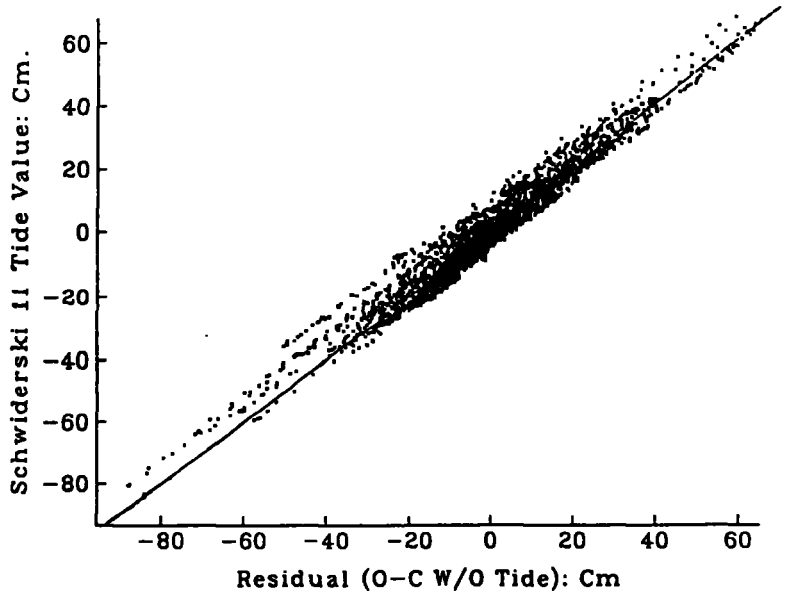

Figure 4e.–Correlation of residuals and total tides: arc segment H, ERM 2 minus 1. This arc passes over a large number of high tide areas in the ocean emphasizing the utility of the model correction.

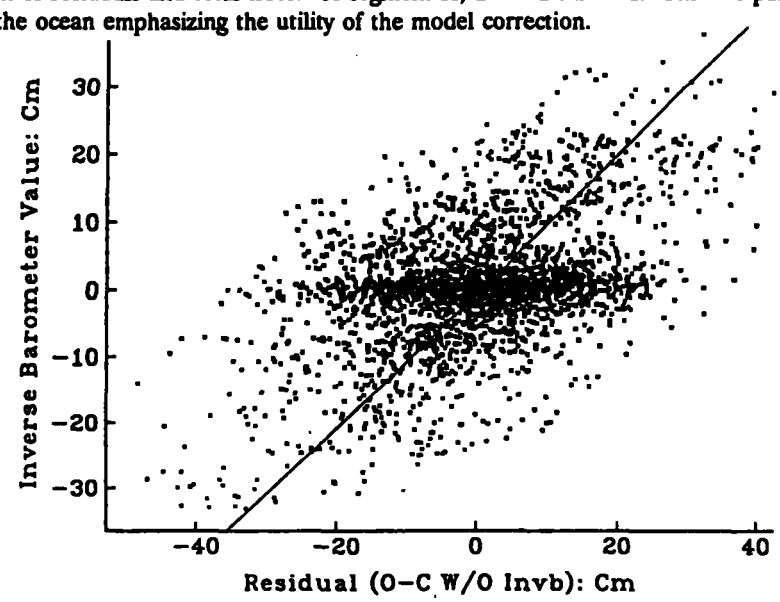

Figure 4f.–Correlation of residuals and inverse barometer correction: arc segment H, Geosat ERM 2 minus 1. Data here are less disturbed by other error sources (than inverse barometer) compared to fig. 4b, so correlation is better. Again, notice band of values near zero correction that occurs in the tropic zone.

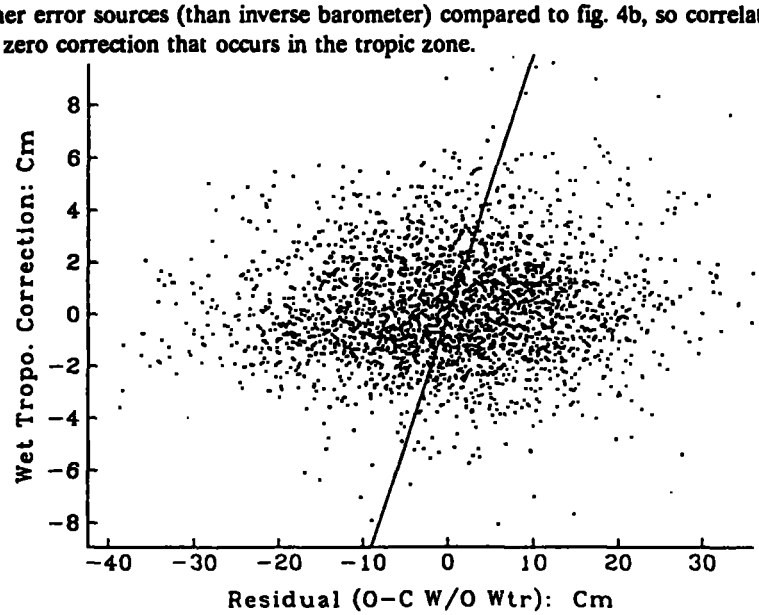

Figure 4g.–Correlation of residuals and wet troposphere correction, arc segment H, Geosat ERM 2 minus 1. Again, as in fig. 4c for arc G, correction is negligible and deletion of this modeled correction actually reduces residuals slightly.

On the other hand, the much smaller wet troposphere correction is not well correlated to the media removed residuals. In fact, as table 1b shows, smaller residuals would have been achieved for this arc without the wet troposphere correction. Yet the still smaller electromagnetic bias correction resulting from the enhanced return from wave troughs does show a positive correlation with these residuals (fig. 4d and table 1b). These results while fairly typical for the 126 arcs processed are by no means the "best" in bringing out the efficacy of the media and surface corrections. For example, figs. 4e-g show the results of similar processing of arc segment H for cycle 2 minus cycle 1 in the tides, inverse barometer, and wet troposphere correction. The effects of the tides and inverse barometer are better seen in these residuals than for arc G, but again the correlation of the wet troposphere correction is poor (fig. 4g) though barely positive here compared to fig. 4c.

THE EFFECT OF ORBIT REDUCTION ON THE TIDAL SOLUTION

The basic premise of this work is an iterative solution for the tides. It is well known that the tidal surface over the deep oceans at any time has most of its power at long wavelength, roughly between 2 and 8 cpr along a satellite's track. For example, spherical harmonic decompositions of the Schwiderski (1980, 1983) M_2 model (including zero land values) have peak power at degree 6 (Christodoulidis *et al.* 1985). Nevertheless some tides, especially those of the longest periods are computed by Christodoulidis *et al.* (1985) to have considerable correlation even at fully global scales. Fortunately this does not appear to be the case for the semidiurnal tides such as M_2, but before proceeding I made tests to confirm this with typical along-track spectra for such tides.

To test the effect of an uncoupled "orbit reduction" of the sea height difference signal on the subsequent tidal recovery, I simulated perfect M_2 tide values from the Schwiderski (1983) model every 400 seconds for a day along a 244-revolution/17-Day orbit of 108° inclination (Geosat ERM equivalent) starting at Greenwich on the Equator (proceeding north). I repeated these 1-day track samplings for every other ERM cycle for a total of 10 samples (to cycle 20) exactly overlapping the reference track. (The reason I extended the difference sampling to cycle 20 was to simulate a full aliased M_2 period for Geosat and to cover roughly the same time span as with the "real" Geosat data. These aliased tide periods will be discussed in a later section. Taking the difference (with cycle 1) of the 10 following cycles of the M_2 tide heights at corresponding along-track points resulted in 411 deep ocean time series each with 10 tide difference observations. I show the full 1-day arc of such difference data for cycles 2 minus 1 in fig. 5a.

Since Geosat has a mean motion of about 14 cycles per day it is clear from fig. 5a that most of this tidal variation will pass through undisturbed by a "high pass" filter of it at this frequency (also including a constant and a secular term). I proceeded to solve for such "lower frequency" orbit signals from these pure tide data just as from the actual data. The residuals from this artificial orbit "fit" (for this first global overlap pass) are also shown in fig. 5a and are close to the actual data except near the ends of the data span (as expected). Over the whole arc the distortion from the "orbit removal" process does not appear to be severe, since only a small amount of power in these data has been removed.

Table 2 shows the power reductions from filtering all 10 arc differences. The average reduction is about 2 percent but rises for the more powerful arcs in the midcycles (corresponding to difference samples of the tide at any one station over a phase of about 180°). This may not seem like a significant reduction, but statistically the effect on a given tide harmonic may be considerably more severe. For example, if all the tides at midcycle (10) were being sampled across their full range, then the result from table 2 indicates that the distortions in this range could be as high as 15 cm $[60^2 - (0.97x60)^2]^{1/2}$. This range distortion represents an error of 25 percent from the true range of 60 cm. Indeed this magnitude of distortion by the filter is indicated in fig. 5b where I compare the true tide difference at the beginning of the arc with the one computed from the residuals of the 10 along-track "orbit fits."

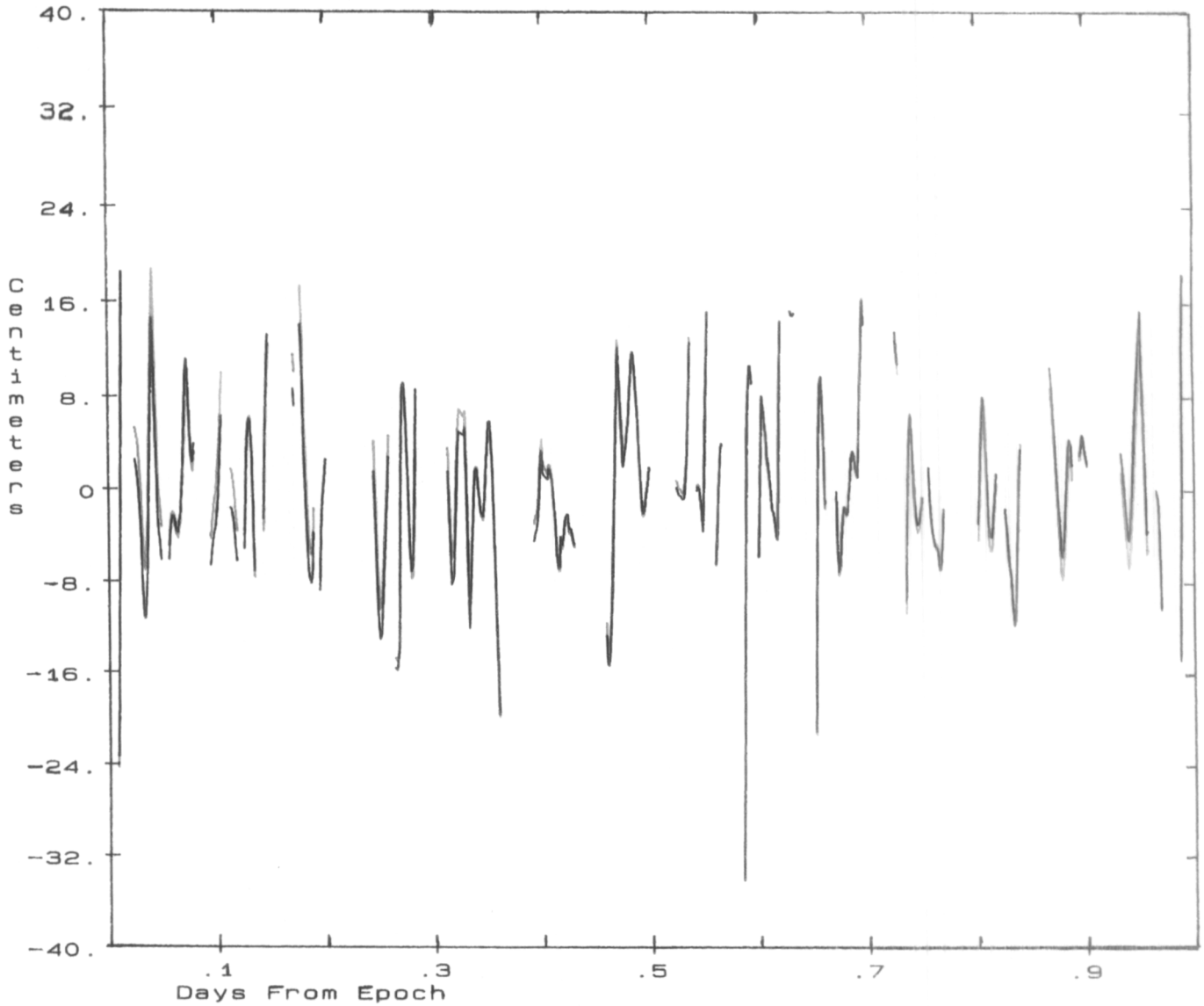

Figure 5a.--Simulated M_2 ocean tide differences: Geosat ERM 2 minus 1. Black lines show simulated M_2 ocean tide height differences using the Schwiderski (1983) model (as on the Geosat GDRs) under ground tracks arising from an orbit of 244 revolutions/17 days inclined at 108°, like Geosat but starting at latitude 0°, longitude 0°. Data were generated every 100 seconds on this track at deep ocean points for 1 day. Ten such global sets were generated overlapping the first set here but lagged at every other 17-day cycle. Shown are the overlapped height differences from cycles 2 minus 1. The red lines are the residuals of these height differences after an orbit adjustment of the simulated data removed a constant, a secular rate, a 1-cpr, and near 1-cpr frequency from the simulated data at the 411 discrete points along the track. While overall the tide signal does not seem to be strongly disturbed by this (uncoupled) empirical adjustment, distortions can be seen most prominently at the ends of the data span here.

A more comprehensive picture of the pattern of these distortions is seen in figs. 5c-d where errors in the power of the tides and the power of the errors themselves (not the same quantity for a vector function like the tide) are displayed along the reference 1-day track.

Table 2.--Residuals of orbit reductions of perfect along track M2 tide difference data (simulated)[1]

Reference 1-day Geosat orbit arc generated from Lat; Long. = 0,0 starting at 1987.0 using the Schwiderski (1983) M_2 ocean tide. Generation for 411 deep ocean points on the Geosat track separated by (normally) 100 seconds (about 664 km). Following arcs of the M_2 tide heights were taken to overlap this base at multiples of 17.0505 days with lags of 1,3,...19 exact repeat mission cycles. The overlap differences with the reference were taken and each cycle pair independently reduced of a constant, two frequencies (1 cpr and near 1 cpr), and a secular term (linear in time). The power of the difference data in these pairs at the 411 along track points before and after the artifical orbit reduction follow:

Following cycle No.	Cycle lags	Uncorrected differences (cm,rms)	Residuals after orbit correction (cm, rms)	Determined constant (cm)	% reduction of power
2	1	7.03	6.88	-0.32	2.13
4	3	20.38	19.92	0.89	2.26
6	5	32.05	31.27	4.02	2.43
8	7	40.73	39.64	7.67	2.68
10	9	44.86	43.59	10.25	2.83
12	11	43.35	42.11	10.63	2.86
14	13	36.29	35.29	8.83	2.76
16	15	24.97	24.33	5.14	2.56
18	17	11.33	11.07	1.69	2.29
20	19	2.887	2.824	-0.21	2.18

[1] Note the rise and fall of the difference data power in the aliased M_2 period of 18.6 ERM cycles lags. For further information on the "errors" revealed by this simulation, see figs. 5a-e.

Fluctuations of these error distortions have a periodicity of roughly 2 cpr, reflecting the interaction of the various 1 cpr orbit adjustments with the systematic phase changes of the tide over its aliased period. It is interesting that while the average power change is negative (-3 percent), there are some stations which actually show increased power after the orbit reductions. The total tide errors (rms), as indicated in table 2 (and seen, for example, in fig. 5d) average 14 percent and reach a maximum of 31 percent compared to a true global M_2 tide of 30 cm (rms). While certainly significant, and a cause for concern in this kind of analysis, the actual Geosat data analysed represent an errored tidal signal that is perhaps one-fourth of the full one since the Schwiderski (1983) model has been removed in forming the STHs. Thus I expect an average M_2 (residual) signal of only 6 to 7 cm, implying only a few centimeters of distortion (on average) from this source in my analysis.

Even the severity indicated here may be tempered further by the actual circumstances of the reduction with real data which use mainly arcs longer than 1 day and from a variety of ERM window segments with both ascending and descending passes at most stations. In any case, these simulations show that a careful calibration of the tidal results is necessary when the orbit reduction is uncoupled from the (later) time-series tidal solution.

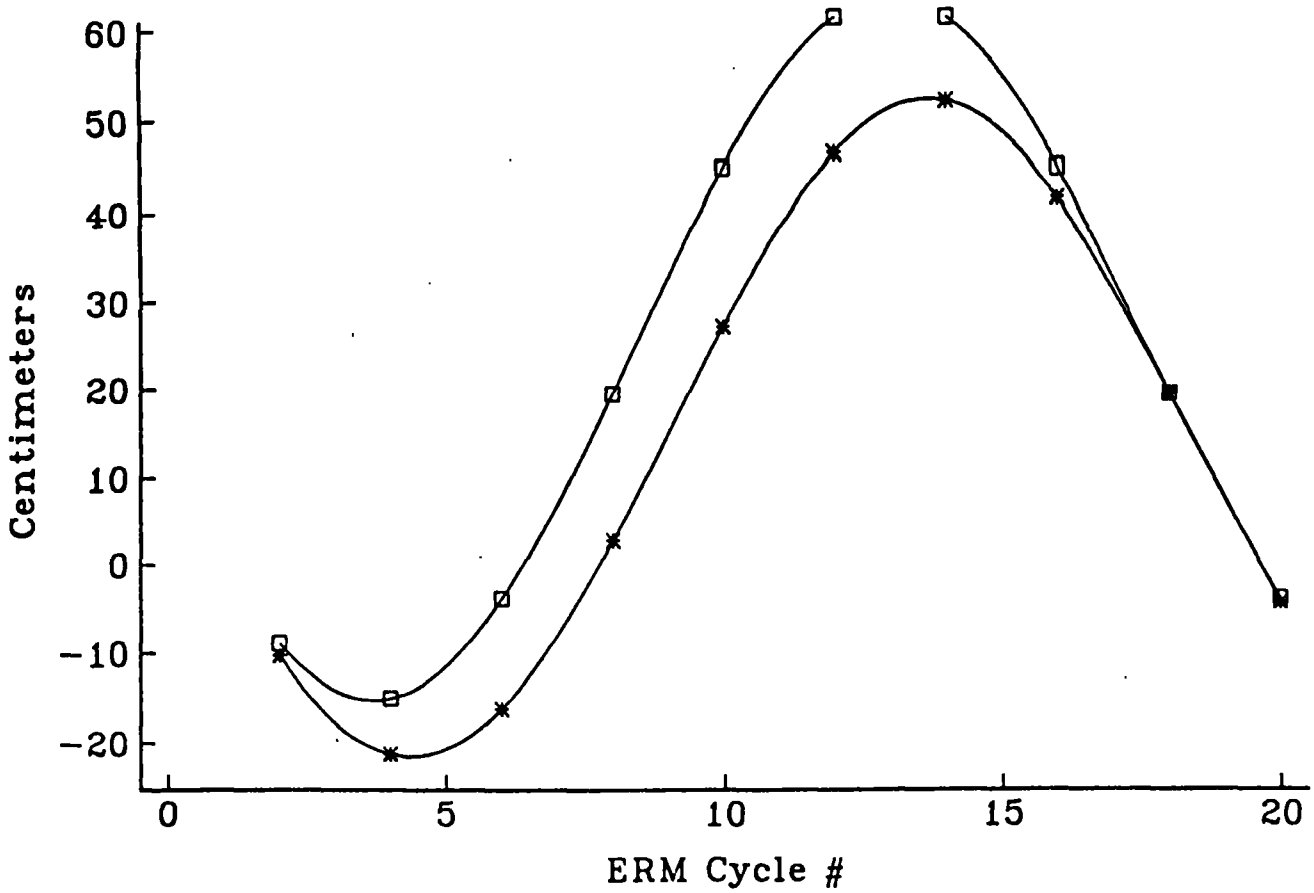

Figure 5b.–Simulated M_2 tide differences (with respect to heights in cycle 1) at latitude 0°, longitude 0°0 for a Geosat ERM. Shown are the simulated differences before (squares) and after (asterisks) orbit reduction for the 10-cycle pairs of 1-day arcs. The first point here is the same as the first point in fig. 5a (before and after results). Note the orbit corrections have systematically distorted original data with a periodicity of the aliased M_2 effect for the Geosat ERM (18.6 cycles). Thus the M_2 tide solution for this station will have little apparent error from examination of residuals alone. Systematic error from the false orbit reduction is about 20 percent of the true variation here over the full M_2 period but distortion in the power of the data is much less (only about 2 percent).

RESULTS OF ORBIT REDUCTION OF OVERLAP DIFFERENCES

I have reduced 126 1- to 2-day arc segments of Geosat ERM overlap differences of sea heights averaged into 2° by 2° deep ocean areas in the same manner as described above for segment G. Figures 6a-c give an overview of this reduction from (media corrected) STH values to 2° averaged residuals of difference values after "orbit removal." In fig. 6a note the significantly greater power of the Gem 10 topographic height data over using the Gem T1 radial ephemeris, a result of the poorer orbits using Gem 10 as implied earlier. Indeed, as seen in figs. 1a-b many of the Gem T1 STH arcs are as much disturbed by the poor detailed geoid of Rapp (1978) as by "orbit error." However, there is much less discrepancy in the STH differences when using these two ephemerides (fig. 6b). The Gem 10 orbits are undoubtedly strongly deficient at 1 cpr. Much of these errors are geographically correlated and removed on differencing as well as all of the geoid error and periodic orbit error due to the geopotential. Finally, after orbit filtering there is little to distinguish one ephemeris use from the other (fig. 6c). Indeed the distinguishing character of the fully reduced 2° data is a clear rise and fall of power in the "aliased" period of the M_2 tide (near 1 year) which demands a more complete explanation. (See next section.) Before proceeding with this, however, note that the data are still too sparse to verify this effect in the second year of the ERM for which (as yet) only the operational Gem 10 orbits are available.

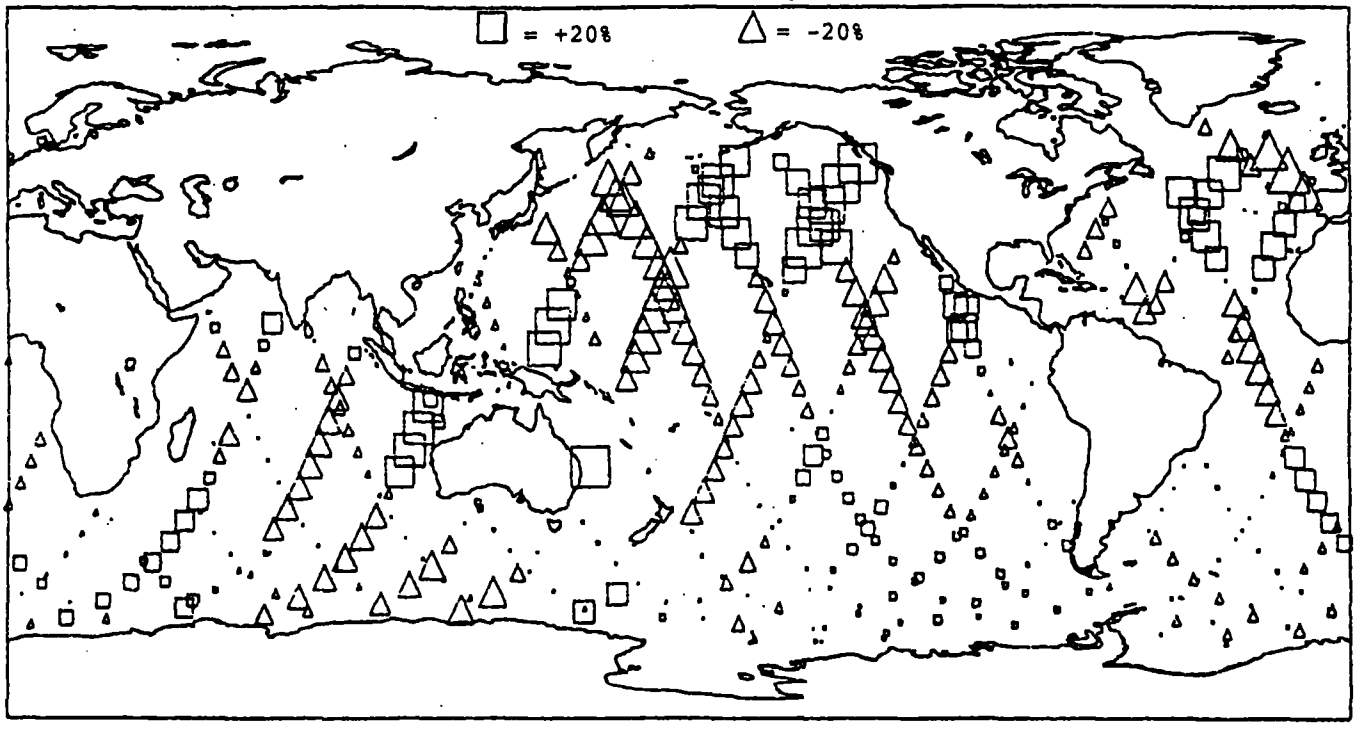

Figure 5c.–Error of orbit-reduced simulated M_2 tide for a Geosat ERM (20 cycles). Shown are the percentages of errors in the power of the solution (with respect to 30 cm) from the simulated M_2 tide at 411 stations along track for 1 day (repeated every other ERM cycle, with orbit reduction performed on each arc pair of differences with respect to cycle 1). The (scaled) squares show where the power of the solution from the orbit reduced data is larger than the original (simulated) tide. The (scaled) triangles show where the power has been reduced. The maximum discrepancy is -31 percent; the average is -3 percent.

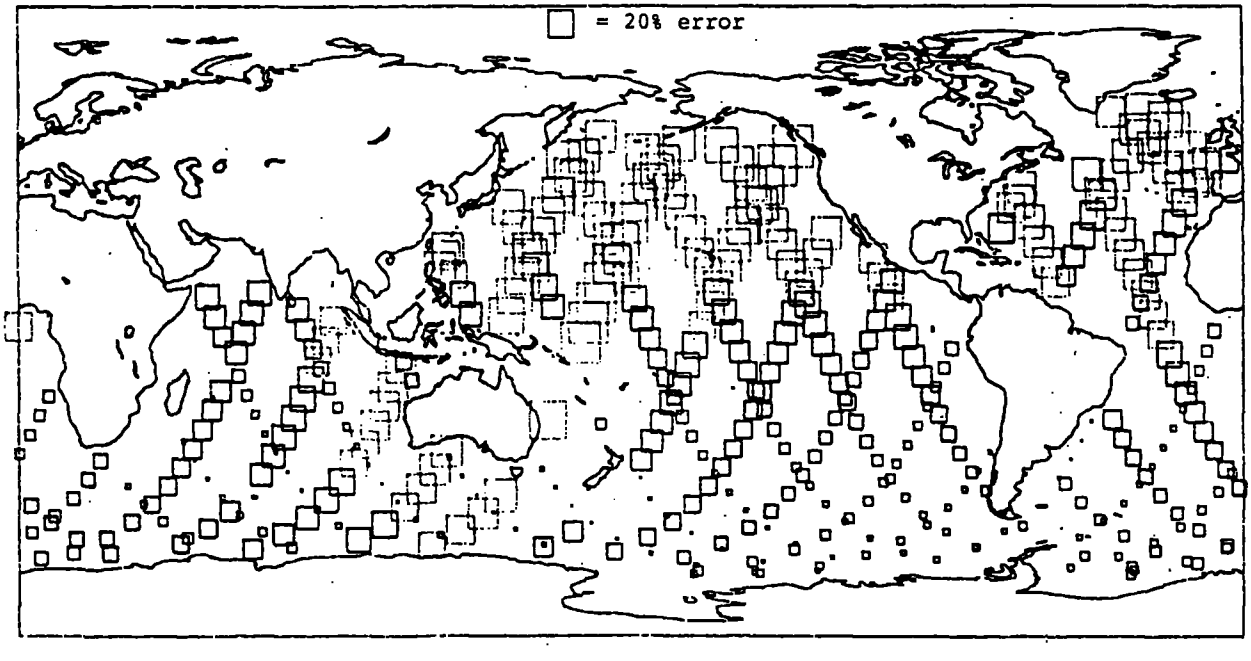

Figure 5d.–Errors of M_2 tide derived from orbit-reduced simulated data. Shown are rms errors of solutions described in figs. 5a-c. The average error is 14 percent (of a global M_2 tide of 30 cm,rms). The maximum error is 31 percent; as seen, the station errors along track vary predominantly at 1 cpr. Here the (411) station solutions (of 10 overlaps each) contain only a single pass of data in each cycle of the same kind (with no averaging). In the actual solution most of the stations contain more than one kind of passes (ascending and descending) and arc segments through the area bins which should reduce the distortions seen in figs. 5a-d.

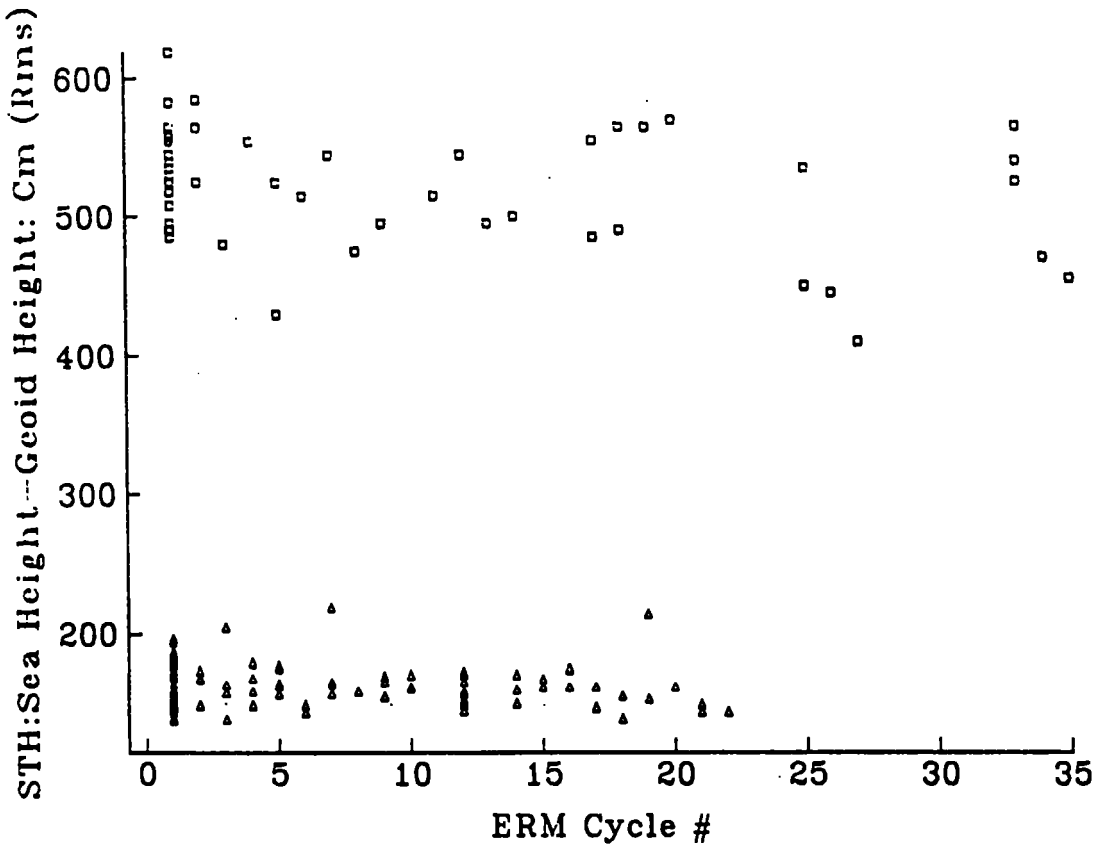

Figure 6a.–Global sea level residuals from Geosat altimetry. Squares represent rms of sea topographic heights (STH) (sea height corrected for media and surface effects minus a detailed geoid) using the NAG radial ephemerides of Geosat that employed the Gem 10 geopotential. Triangles are the same data (from different windows or arc segments) using ephemerides that employed the Gem T1 geopotential. As seen in fig. 1b, the Gem T1 STHs show both orbit and geoid height error signals (dominating) as well as tide and other mismodeled and unmodeled effects (such as from ocean dynamics).

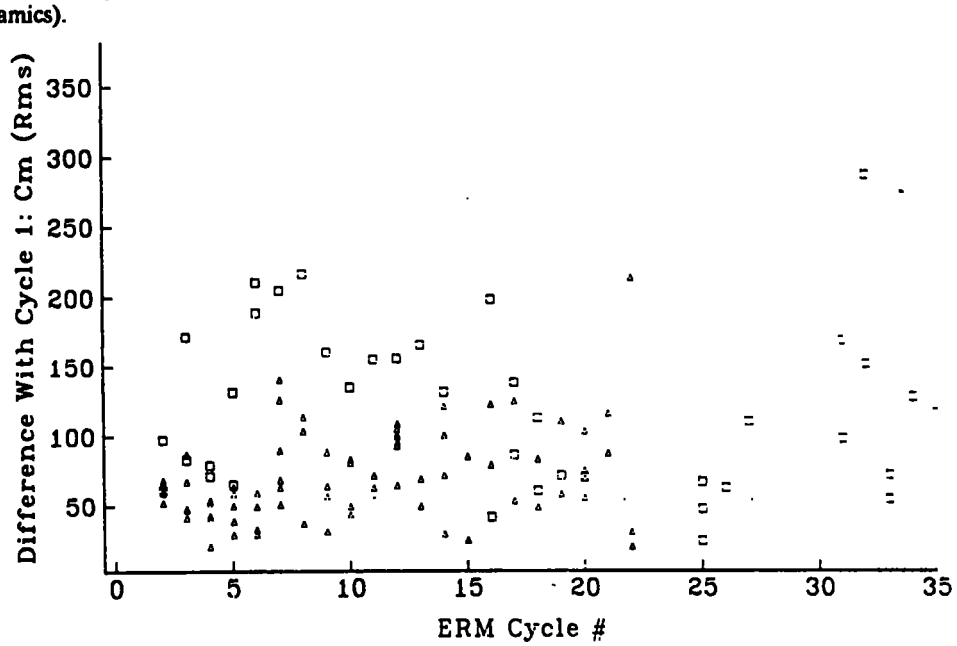

Figure 6b.–Global sea level differences from Geosat altimetry. These are STH differences from overlapping arcs in ERM cycle 1 (averaged in 2° by 2° bins). Boxes are for 1-day arcs using Gem 10 ephemerides. Triangles are for 2-day arcs using Gem T1 ephemerides. Notice substantial reduction in power of these difference data compared to one-way STHs (fig. 6a). The detailed geoid errors were eliminated and the orbit errors reduced in both power and complexity. Though the power of Gem T1-derived differences is generally smaller, there are many Gem 10 arcs that have less power (in these differences) than Gem T1 arcs, even in the same cycle.

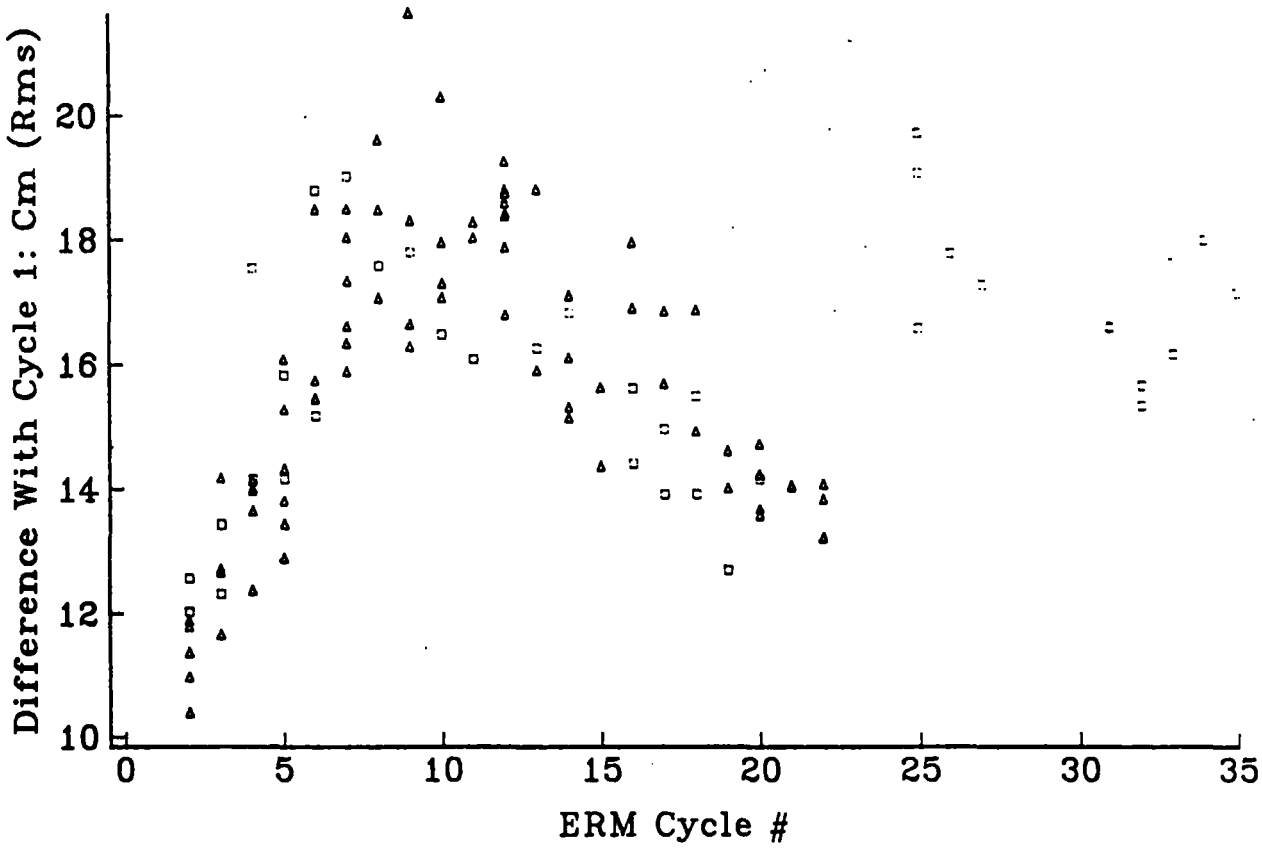

Figure 6c.–Global sea level differences from Geosat altimetry after empirical orbit reduction. The 2° by 2° averaged differences (fig. 6b) have been reduced of a constant, a secular term, a 1-cpr, and a near 1 cpr frequency. Again the boxes represent data derived from Gem 10 ephemerides. The power of the Gem T1-derived data is now almost indistinguishable from the power of the Gem 10-derived data. The primary feature of the power data here is its clear variation with a period near 20 ERM cycles related to both the aliased M_2 period (317 days) and a possible yearly ocean weather tide (say from temperature changes) that is not modeled by the inverse barometer effect which has been removed. Notice how the weakest data in cycles 10 to 20 tend to be from the 1- day arcs. These generally have a significantly smaller data content than the 2-day arcs or even the 1-day arcs in the first 9 cycles.

The Gem 10 orbits are computed in overlapping 2-day arcs so that every day represents a new set of initial conditions and a break in the STH differences here, necessitating a new "orbit" solution. These breaks do not coincide with the "days" of the ERM segments used, but are slowly changing with respect to them. Therefore, the standard 1-day arcs are nearly that long only at the beginning of the ERM. By the end of 20 cycles (the aliased M_2 period as we shall see) the new orbit break occurs in the middle of these segments (L, A, and E), yielding only seven or so revolutions of data, sometimes much less.

I have studied the behavior of the determined constant in the orbit reduction with the number of observations used in this reduction. (See fig. 7.) When the number gets below about 800 (roughly 60 percent of a day's 2° smoothed data) this average can be quite large, which is obviously unrealistic. With so few observations, I feared I might also be absorbing too much tidal energy in the removed orbit parameters, and limited my analysis to arcs with more than 800 observations. Because of the shifting breaks in the Gem 10 ephemerides, I found only a scattered number of these in the second year, too few to verify what was found in the first.

Figure 7 also shows that (disregarding the excessive values) the average of these global shifts of sea level of the arcs in following cycles with respect to cycle 1 is positive by a few centimeters. This bias, indeed the variability of the constant determined here, may be due to global coherence of the residual tide (errors in the low-degree spherical harmonics of the tide), changes in the altimeter calibration, or systematic errors in the other medial and surface corrections to the altimeter data. Another fundamental source of the variability of

the constant is undoubtedly the varying tracking conditions and data underlying the orbits computed for Geosat. Thus an error of only 1 millisecond in the period of this satellite is equivalent to an uncertainty of 80 cm in its altitude, since no direct range data were used in determining the orbit.

ALIASED TIDAL PERIODS IN THE GEOSAT ERM

Whenever a periodic function is regularly sampled (as in an ERM) it is possible to fit the sampled data to an unlimited number of other (aliased) frequencies. The danger, of course, is that other phenomena with natural periodicities near these "other" frequencies can easily become confused with the fundamental periodic function we wish to investigate. The simplest and best known example is aliasing to higher frequencies. If spacing of the samples is S in time, then every wave with period 2S/n (for integer n) is compatible with the original data (n=1 is called the Nyquist limit after the scientist who first studied regular sampling). In our case though (at least for the most prominent tidal species) we sample (in the ERM) at regular intervals (of 17.0505 days) much longer than the fundamental tides of near 12 (semidiurnal) and 24 hours (diurnal). In such cases, as we might guess, the aliased periods are longer than the sampling interval. The aliased period(s) in this case is more complicated to describe algebraically (e.g., Mazzega 1985) but just as easy to visualize if one asks for the period fraction (of the fundamental) remaining after an integer number of such periods closest to the sampling period. This "closest" period fraction (or remainder) increases steadily until, after a (usually nonintegral) number of "long" sampling periods a total fundamental period fraction of 1.0 is covered. That number (1/closest period fraction in ERM units) is the longest aliased tidal period. (There is always another one of less than twice the ERM cycle from 1.0 minus the "closest" period fraction, but the description of the data is the same in any case and much easier to "see" with respect to the longest period.) With this prescription, and using the fundamental lunisolar tidal periods from Melchior (1978), table 3 lists the longest aliased periods for the Geosat ERM for the 11 principal (strongest) tides.

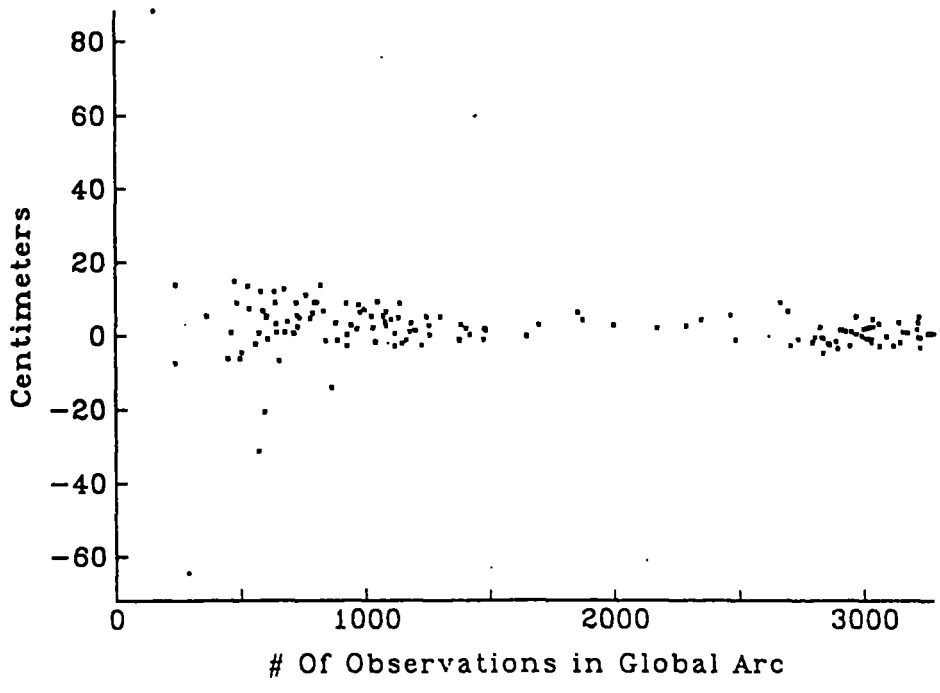

Figure 7.–The constant from the orbit reduction of global overlap sea height data. The data here are results from the orbit reduction of 2° by 2° STH differences described previously. For data arcs less than about 1,000, there is a tendency for the constant to be excessive, suggesting a poor separation from the 1 cpr orbit signals.

Table 3.–Aliased periods of principal tides for the Geosat ERM
ERM cycle = 17.0505 days

Tide name	Equilibrium[1] Amplitude (cm)	Period (hrs)	Aliased period Days	ERM Cycles	Cycle No. at repeat tracks
M2	24.2	12.42060	317.1	18.60	19.6, 38.2,...
K1	14.2	23.93447	175.5	10.29	11.3, 21.6,...
S2	11.3	12.00000	168.8	9.90	10.9, 20.8,...
01	10.1	25.81934	112.9	6.62	7.6, 14.2, 20.9,...
P1	4.7	24.06589	4466.5	261.96	263.0, ...
N2	4.6	12.65835	52.1	3.05	4.1, 7.1, 10.2,...
Mf	4.2	327.84046	68.7	4.03	5.0, 9.1, 13.1,...
K2	3.1	11.96724	87.7	5.15	6.2, 11.3, 16.4,...
Mm	2.2	661.301	27.6	1.6	2.6, 4.2, 5.8,...
Ssa	1.9	4383.	182.6	10.7	11.7, 22.4,...
Q1	1.9	26.86816	74.0	4.3	5.3, 9.6, 13.9,...
Annual	5.0?	8766.	365.3	21.4	22.4, 43.8,...
Semiannual	2.5?	4383.	182.6	10.7	11.7, 22.4,...
Biannual	2.0?	17532.	730.5	42.8	43.8, ...

[1] Estimates: lunisolar-tides [Christodoulidis *et al.* (1985)]; remaining (ocean weather) tides [Wyrtki and Leslie (1980)].

A few points from table 3 should be especially noted. First, the aliased M_2 period (317 days) is close to both annual and twice semiannual periods, which are natural "weather" periods for ocean surface changes due to seasonal temperature and water fluxes. Second, many of the other tidal constituents have similar aliased periods which may also be difficult to separate from the Geosat data. Here though I want to describe specifically how the power of differenced heights is evinced over these long (aliased) periods.

Let the tide height at a given ocean point, j, be given for tide constituent i as:

$$H_j = \sum_i C_{ij} \cos w_i t + S_{ij} \sin w_i t \tag{1}$$

where C,S are harmonic coefficients at a reference time for point j, and w_i are the frequencies of the respective constituents. If the reference time is taken as the time in the reference cycle for passage over that point (different for ascending and descending passes), then the difference tide height is expressible from eq. (1) in terms of the aliased period T' and the ERM sampled time difference t' from the reference cycle as:

$$\Delta h_j = \sum_i C_{ij}[\cos 2\pi t'/T_i' - 1] + S_{ij}[\sin 2\pi t'/T_i'] + e_j(t') \tag{2}$$

where e_j is the difference in signal errors between the two cycles at this time at location j.

An interesting aspect of eq. (2) is that e_j as written cannot be completely random over the sampling pairs since it always depends on the same error in the reference cycle. It is therefore permitted, in theory, to include a resolvable constant for each time series of similar passages at an ocean point. (This is equivalent to the practice of other authors who have worked with overlapping altimetry of referencing the data to an average profile of a long arc or time series in a small ocean bin (e.g., Mazzega 1985; Cheney et al. 1989). In

practice (at least for this solution) there may not be sufficient data to resolve these individual reference pass constants as well as the other tide parameters at a station. However, this possibility for future solutions promises a significant gain in the signal/noise ratio because without it the noise must be gaged as a two-way process.

The power of these difference data over all the passes in a cycle (with respect to the base cycle) is easy to calculate when we realize that the quantities in brackets in eq. (2) are (as t' is) constant over all the points in the ERM cycle. Let these bracket-factors be C^* and S^* respectively for the cosine and sine of the tide harmonics. Then the power of the difference data at a point j is:

$$(\Delta h)_j^2 = \{ \sum_i [C_{ij} C_i^*(t')] + e_j(t')\}^2 = \{\sum_i C_{ij}^2 C_i^*(t')^2 + S_{ij}^2 S_i^*(t')^2 + 2[\sum_{k \neq l} C_{kj} C_{lj} C_k^* C_l^* \tag{3}$$

$$+\text{all other cross-terms in } C_{kj}S_{lj}, S_{kj}S_{lj} \text{ and } C_{kj}S_{kj}] + e_j(t')^2 + 2e_j(t')[\sum C_{ij} C_i^*(t') + S_{ij} S_i^*(t') + \ldots]\}$$

Taking the average of eq. (3) over all the points j in the given cycle at t' and assuming that:

$$<C_{kj}C_{lj}, C_{kj}S_{lj}, C_{kj}S_{kj}> \approx 0, \text{ and } <e_j(t')[C_{ij}, S_{ij}]> \approx 0 \tag{4}$$

in relation to the other terms in eq. (3) I can write over the j points:

$$<(\Delta h)^2>_j \approx \sum_i C_i^*(t')^2 <C_{ij}>_j + S_i^*(t')^2 <S_{ij}>_j + <e_j(t')^2>_j \tag{5}$$

for the power of a difference arc at lag time t' with respect to the aliased period T_i' for a tide constituent. Using the further expectation that over a large number of globally dispersed points:

$$<C_{ij}^2> \approx <S_{ij}^2> \tag{6}$$

I can reduce the power expectation to the even simpler form:

$$<(\Delta h)^2> = \left\{ \sum_i 2<C_i^2> [1 - \cos(2\pi t'/T_i')] \right\} + <e^2(t')> \tag{7}$$

However, because the global tide power is dominated by only a relatively few high amplitude regions in the oceans (between amphidromes), the expectation in eq. (6) is not exactly realized. Nevertheless in resolving the evolution of the signal in fig. 6c, I am naturally limited to only a few parameters for the 22 samples of cycle-pair data (with full global estimates). For this purpose I find that I can still use eq. (7) to obtain a rough estimate of the tide correction power using a single value for each constituent without incurring significant distortion of the result.

THE 4° BY 4° DATA SET OF TIME SERIES

As discussed above, of the 126 arc segment pairs I reduced to 2° (orbit removed) data, I used only those with more than 800 observations in each arc pair (of differences with cycle 1). Another limitation was that I did not go beyond cycle 37 in further processing, because at this cycle the detailed geoid height data on the original GDRs I used were corrected. This possibly introduced height anomalies of up to 1 m in differences with uncorrected cycle 1 data. It is not likely that the anomalies arising from an interpolation change for the 1° detailed geoid height grid can be near this large for the smoothed data over wide zones however, even in areas of rough topography. Still I wanted to be conservative and, as the few arcs involved were all small (less than 1,100 observations), I also eliminated them from further consideration. Finally, I averaged the remaining arcs into 4° by 4° deep ocean bins, yielding the distribution given in figs. 8a-c.

Figure 8a shows that, while the data are stronger in the earlier ERM cycles, the maximum density is actually found near the midpoint of the M_2 aliased period which repeats near cycle 20. For future reference I estimate that the 1-second GDR data content (more than 4,000,000 records) of the 4° set through cycle 22 represents more than one-third of the full set for deep ocean points.

Figure 8b shows how the power of the time series has grown from the 5° data sets (Wagner 1990) to the present 4° sets. The current set contains more than twice as many GDR records as the previous set, averaged into different and slightly more refined ocean areas. The distribution of this new observation set in the deep oceans is shown in fig. 8c. Notice that the highest observation density is in the far southern oceans while the northernmost Atlantic is poorly covered. The latter is an artifact of the rather poor coverage of the North Atlantic in cycle 1 of the ERM. The groundtrack patterns of density in fig. 8c reflect that the observation set is still dominated by only a few of the 2-day arc segments (F, G, and I) which together have this rather coarse spacing. Recall that during the Seasat summer of 1978 the coverage of the southernmost oceans was poor because of heavy ice conditions. Here, since most of the data used are in the first 7 months of the ERM (to cycle 12) from November 1986, the ice-free conditions at that time have provided excellent coverage there. This region will provide a critical test of the Schwiderski (1983) M_2 model far from the boundary data used therein.

The southern oceans also are well represented in this data set because all the tracks are strongly east-west at high latitudes. The poor coverage of the far North Atlantic is due not only to boreal winter conditions there (storms and ice, conditions which cause data rejections), but also to the particular attitude instability of Geosat for cycle 1, which caused a large amount of data to be lost in this region [e.g., Cheney *et al.* (1987)]. The indication of data over land areas in fig. 8c is spurious. These represent single GDR record passes that belong elsewhere due to a glitch in the grid point assignment for data near longitude 0° in the 4° set. This program anomaly is also responsible for the excess number of low-pass time series seen in fig. 8b. In the final solutions all passes represented by a single GDR point pair were rejected for this reason and because, even in a legitimate pass, a fair estimate of the pass variance could not be verified in this case.

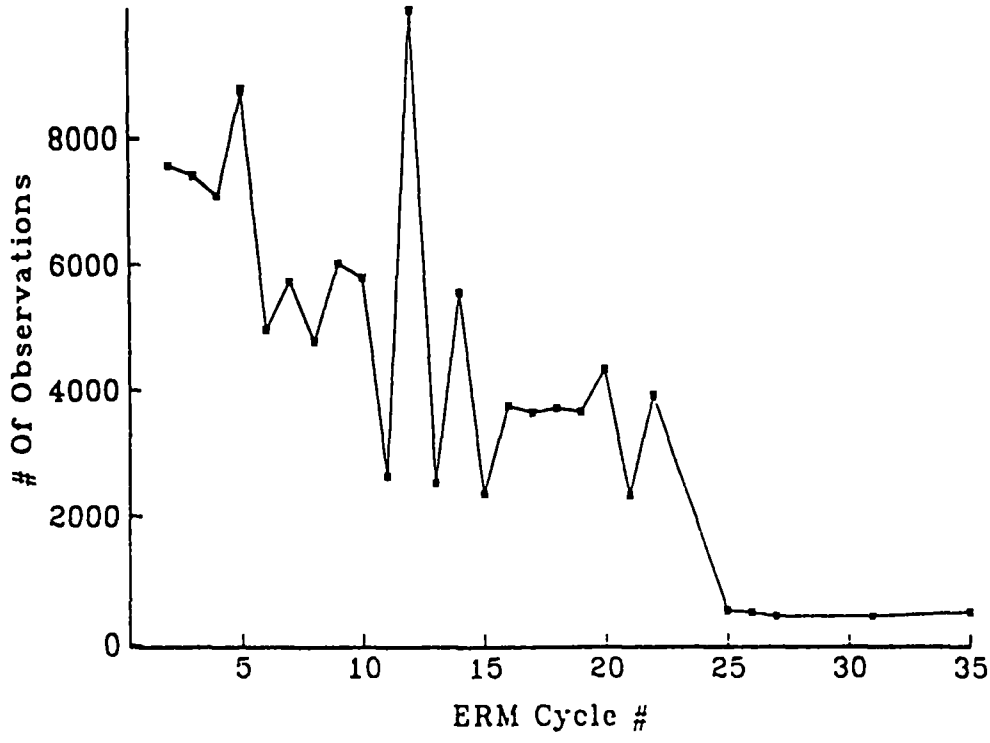

Figure 8a.–Distribution of Geosat difference data: 4° averages. Only arcs with more than 800 2° by 2° average passes were used in forming the 4° pass averages. The early cycles predominate with a particular concentration near cycle 12, where the aliased M_2 tide (or the yearly weather tide) should have maximum power in these differences.

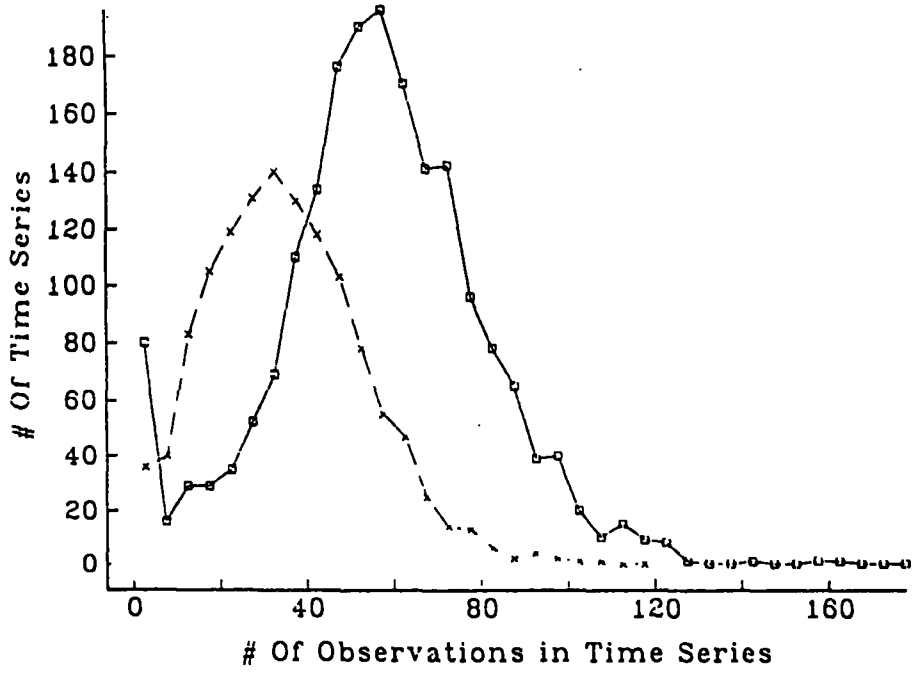

Figure 8b.–Histograms of time series for 5° and 4° data sets. The crosses give the midpoints (for bins of five observation width) for the (preliminary) 5° set. The boxes give the pass or time series distribution for the current 4° set. The total number of passes in the 5° set is 43,654 (for 1,253 grid points). The totals for the 4° sets are 108,993 passes (for 1,953 grid points). As shown, the density of the pass observations for a typical ocean area analyzed has nearly doubled with the current set. However, there are still some grid points with less than six observations which were rejected in the final results.

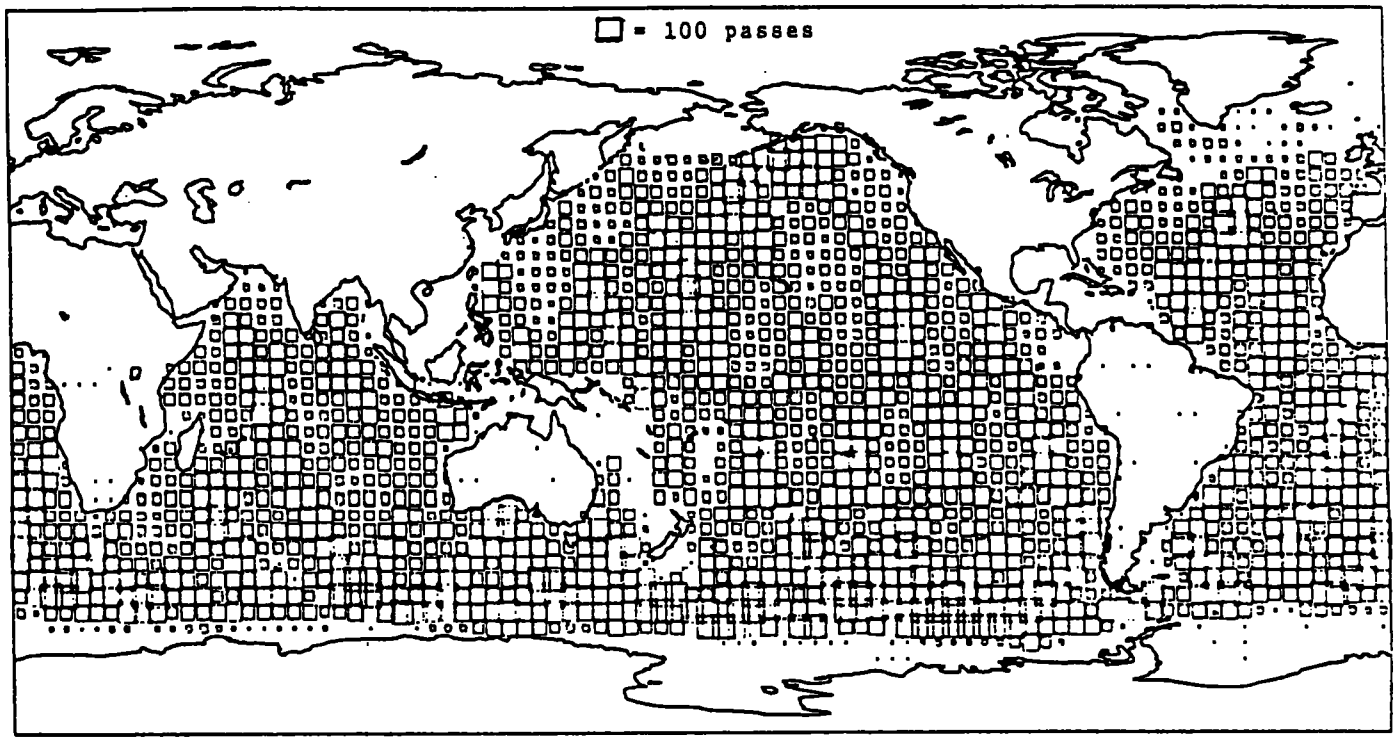

Figure 8c.--Geographic distribution of altimetric time series in 4° by 4° data set. The boxes scale the number of pass observations (actually pass-pairs with cycle 1) in the set at the given grid points.

GLOBAL TIDE POWER FROM THE FIRST YEAR OF THE ERM

In fig. 6c we saw clear evidence of a long-term tide correction signal in the 2° averaged (orbit reduced) STH differences. Ignoring the limited data beyond the first ERM year (past cycle 22) the period of these residuals appears to be at cycles 19 to 22. Referring to table 3, the cause of this periodicity seems to be either the aliased M_2 tide (as a correction to the model on the Geosat GDRs) or a (direct) annual ocean weather tide (above that provided by the inverse barometer). Wyrtki and Leslie (1980) have made an extensive evaluation of the full annual tide from Pacific Ocean island gage data and find the power of the annual tide there is about 5 cm. However, as shown in figs. 4b,e, the inverse barometer is probably effective in removing at least most of the air pressure-caused variation. (The so-called radiational or ocean temperature-induced changes are thought to be a minor part of this tide, as are the seasonal water fluxes compared to the air-pressure component.) The other aspect of fig. 6c, suggesting more than one tide is involved, is a clear indication that the level of the initial minimum is less than the subsequent minimum (at ERM cycles 19 to 22).

If only a single tide is responsible for the results in fig. 6c, it should produce the same minimum effect at the reference and repeat times. Accordingly, I tried to solve for a number of average tides (their average global power) to resolve these data according to eq. (7). Using the 4° data set that included only those arcs satisfying the minimum observation criterion, fig. 9a shows the residual power data used for fitting three such tide functions and an added (constant) noise power. This fit was done using weighted least squares with the data actually being the square of the data in fig. 9a and the weights being proportional to the number of observations in each global estimate of the power from the various arc pairs. These observations range from

800 to 1,400 in the 1-day arc segments L, A, B, D, and E, and from 1,500 to 3,300 in the 2-day arc segments F, G, H, I, J, K, BD, and AE.

The solutions for the 4° individual arcs seem most compatible with inclusion of a BiANnual (BAN) weather tide because the BAN acts to increase the cycle power continuously from cycle 1 to 22. This permits the clear separation of power minima seen in the data, but of course the final three-tide solution is not meant to be definitive, only suggestive. For example, a two-tide solution with M_2 and K_2 does nearly as well as this three-tide solution in separating the minima and fitting the data. Another encouraging aspect of the three-tide solution is the fact that it preserves the one- and two-tide values of its common parameters (within their error estimates which come from the solution inverse scaled by the level of the reduced

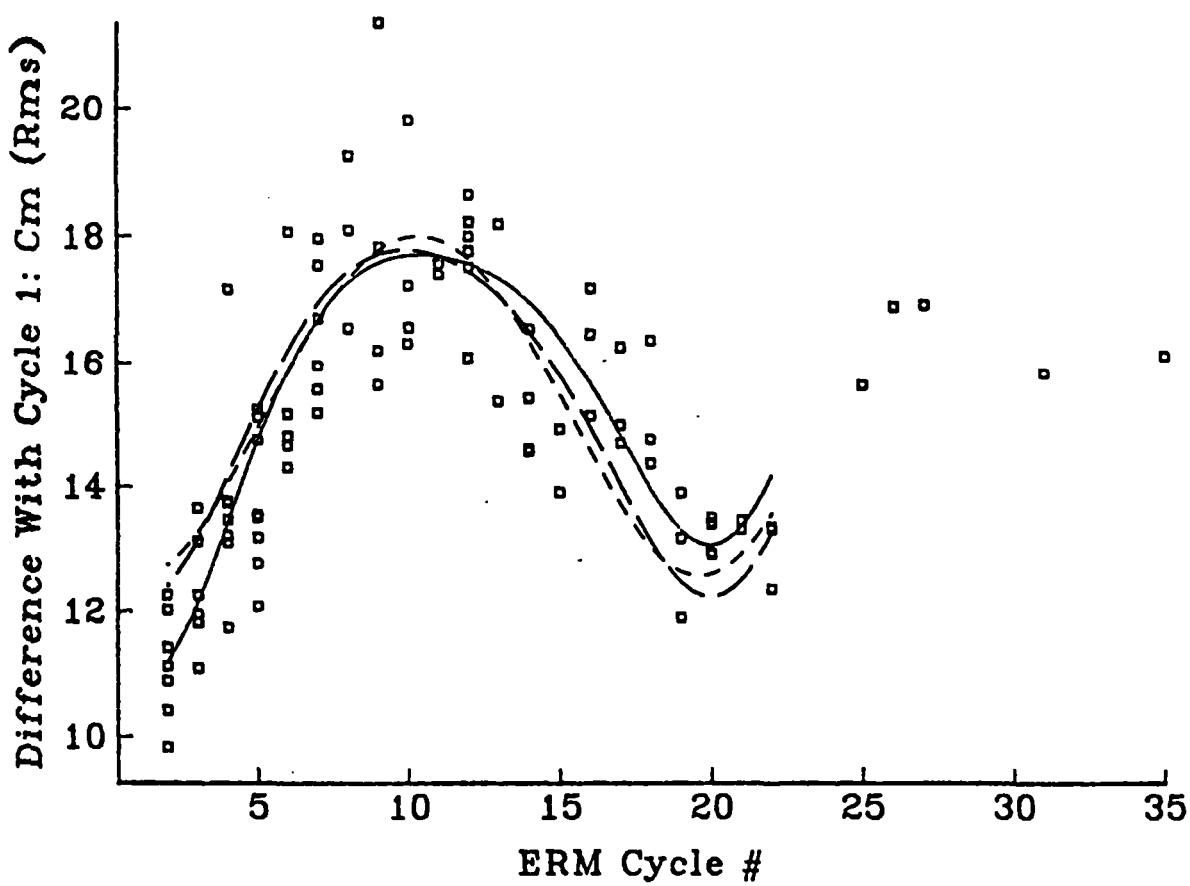

Figure 9a.–Observed and computed power of 4° Geosat overlap differences in 1- and 2-day window segments. Only segments with more than 800 4° observations (passes) were used in this assessment. From these data a few residual tides were estimated by a least squares fit using eq. (7) weighted according to the number of passes in the arc. Because the cycles past 22 were so poorly represented I only used them to check the predictions made from the data in cycles 2 to 22. The short dash curve gives the expected power from a solution for M_2-only plus a noise estimate. Notice that the power level in this solution at the beginning of the second aliased M_2 period (cycle 19) is the same as at the start of the ERM. The long-dashed curve arises from an estimate of both the M_2 and S_2 tides fit to these power data. While there is some separation of the power between cycles 2 and 19, the initial rise is poorly predicted. But for the solid curve, when an additional biannual variation was also estimated, the fit is satisfactory at both ends of the data span. The residual M_2 power in all three solutions is 6.5 ± 2 cm. The solution for S_2 (2.4 cm ± 2 cm), while barely significant, clearly represents a lumped effect of neighboring tide periods. (See text.) The biannual (ocean weather) tide power of 3.6 ± 1.8 cm may also be a lumped effect of interannual variations.

residuals of the fit). A third favorable aspect is a noise level (of 11 cm) closer to the average deviation (of differences) in a 4° pass (9 cm). It should be said though that the "noise" level sensed in this fit is a lumped value from many sources of variation both for the individual pass averages on a short time scale and among the aggregates of these pass-averages on a long time scale where gross tide and media-surface correction errors are involved. If only random noise sources concerned us, the pass averages (averaging 40 GDR observations) should be good to only about $9/\sqrt{40} \approx 1.5$ cm.

To analyze a more representative sample of the global cycle-averaged power, the data in fig. 9a were accumulated into single cycle power estimates and weighted according to the total number of observations in each cycle. (See fig. 8a.) The power averages themselves are shown in fig. 9b along with a "best" soluton for the data through cycle 22. Here I wanted to see how well a solution might predict the sparse data in the second ERM year. As seen, the "best" solution is at least compatible with the sparse data in the second ERM year.

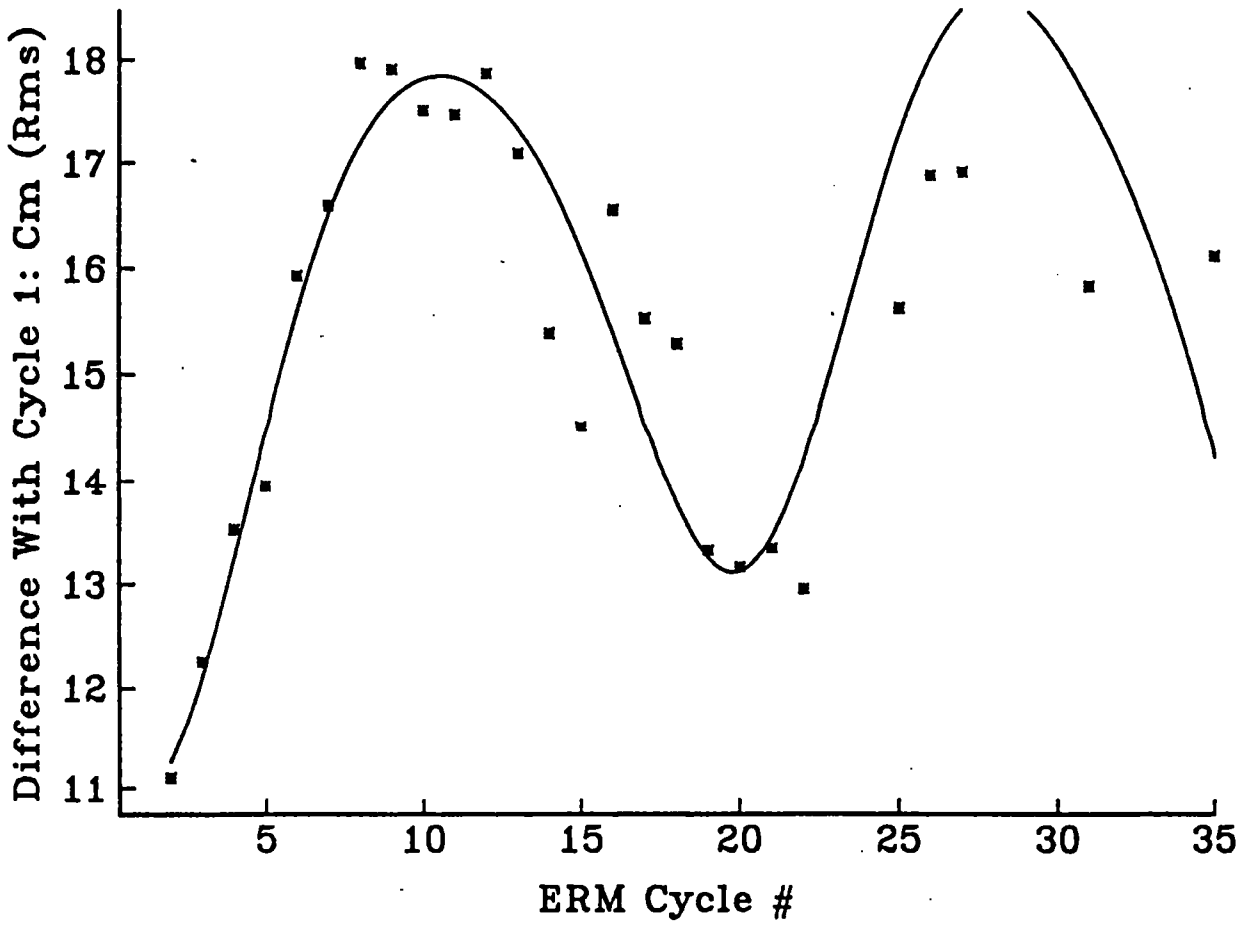

Figure 9b.–Observed and computed power of Geosat overlap differences with corrections for the M_2, S_2, N_2, Q_1 semiannual and biannual tides. The observations here are complete cycle power estimates of the 4° window-arc power data (orbit-reduced differences) in fig. 9a. In the least squares solution of eq. (7) the data have been weighted according to the total number of 4° passes for each cycle. Thus the data past cycle 22 have little weight in the solution and essentially constitute a prediction of the correction power variation for the second ERM year. Considering the poor cycle sampling here in this second year these predictions are adequate (e.g., note the wide variation of power in any cycle over the sub-cycle window segments in fig. 9a).

Table 4 lists 14 such tide solutions using eq. (7), made with the aim of finding reasonably low residuals in groups of one, two, three, four, and five tides. Obviously the tides chosen are not exhaustive. Note that M_2 alone (plus the noise solution) reduces the weighted residuals by an order of magnitude and all other tides added to the solution affect the result by only an additional factor of about 2. A few solutions (8 and 13) were unacceptable because the squared power for certain tides were negative, probably an indication of a poor estimate for the cycle power near the maximum sensivity for those tides [considering the coefficient factors in eq. (7)]. Notice when the ANnual (weather) tide is added to a solution with M_2 (Nos.7 and 9), it is obviously correlated with M_2 since the M_2 solutions decrease significantly. With pure global power data the two periods for these tides are too close for good separation using only 1 year of data.

When I analyzed the individual 4° time series for the M_2 and AN tides I found that, providing there was a reasonable mix of data windows and passes (ascending and descending) in the series, the separation was much better than with the cycle power data. The reason is an aliased tide can be sampled at many different phases in a given cycle and over a time series while a direct tide, such as the weather ones and the long period lunisolar tides M_m and S_{sa}, is always sampled roughly at the same phase for all passes in one cycle. [My colleague Laury Miller first pointed this out to me. See also Cartwright and Ray (1990: 3071-72).] Later we will see that, thanks to this diversity of phase sampling, combined solutions for M_2 and AN disturb the solution for M_2 only slightly for the bulk of the individual time series solutions.

Table 4.–Global tide power from cycle averaged 4° differenced altimetry
Weighted rms of data (cycles 2 to 22 only) = 1203.0

Run No.	tides in solution	Wt rms residuals	Solutions (cm, rms) Noise	M_2	Q_1	S_2	SAN	BAN	Others
1	M_2	121.6	12.0±2.9	6.7±1.6	---	---	---	---	---
2	M_2+BAN	95.8	11.4±2.7	6.6±1.6	---	---	---	3.5±1.7	---
3	M_2+Q_1	115.2	11.6±3.2	6.7±1.8	2.3±1.7	---	---	---	---
4	M_2+S_2	120.9	11.9±3.3	6.7±1.8	---	1.4±1.9	---	---	---
5	M_2+K_1	118.7	11.7±3.3	6.8±1.8	---	---	---	---	(K1)2.0±1.9
6	M_2+SAN	115.8	11.5±3.3	6.8±1.8	---	---	2.3±1.8	---	---
7	M_2+AN	104.4	11.9±2.7	4.7±2.8	---	---	---	---	(AN)4.9±2.8
8	M_2+M_m	119.0	12.4±3.4	6.7±1.8	---	---	---	---	(Mm)<0?
9	M_2+AN+BAN	94.4	11.5±2.7	6.0±3.1	---	---	---	3.1±2.0	(AN)2.9±3.1
10	M_2+Q_1+BAN	88.3	11.0±2.9	6.6±1.6	2.2±1.5	---	---	---	---
11	M_2+SAN+BAN	84.1	10.7±2.9	6.7±1.5	---	---	2.6±1.6	3.6±1.6	---
12	M_2+Q_1+SAN+BAN	64.6	9.7±1.4	6.7±1.4	2.7±1.3	---	3.0±1.4	3.6±1.4	---
13	$M_2+Q_1+K_1$+ SAN+BAN	60.7	9.8±2.8	6.7±1.3	2.7±1.3	---	4.9±2.8	3.5±1.4	(K1)<0?
14	$M_2+N_2+Q_1$+ SAN+BAN	62.9	9.3±3.1	6.7±1.3	2.7±1.3	---	3.1±1.4	3.6±1.4	(N2)1.5±1.4

Examining the "best" power solution (No. 14) in more detail we recognize that only the M_2 and noise solutions are well determined (formally) with M_2 (in particular), being remarkably consistent over all solutions excluding combinations with AN. Again as in the solution with individual arc segments (fig. 9a) the best constant noise solution is closer to 10 than 12 cm (here 9.3 cm, rms). The N_2 and Q_1 results as they stand are undoubtedly lumped values (with respect to the many tides with nearby aliased periods such as

M_f, O_1, and K_2) but their (scaled) formal errors may be fairly realistic (compare with the full equilibrium amplitudes for these tides in table 3). In this comparison, however, note the solutions represent corrections to model values which are undoubtedly not 100 percent in error. I am also assuming that the tidal corrections here and in what follows are strictly to the relatively uncertain ocean component of the geocentric tide model. The Cartwright and Edden 1973 model of the solid Earth part of this tide is not only about 1/3 of the ocean component but is considered much better known with errors of perhaps 1 cm according to Baker (1984; see also Tapley *et al.* 1982).

SINGLE TIDE SOLUTIONS FROM 4° X 4° TIME SERIES

Another indication that the 4° residual data are dominated by the M_2 correction is a series of single tide (least squares) solutions to eq. (2), using all the 108,993 pass-differences over 1,953 stations. The overall rms residual in these station solutions is then reduced (most) from 15.32 cm to 13.15 cm in the M_2 solutions (fig. 9c). The next most influential single tides involving these data appear to be the AN and BAN weather tides with a third set of tides (S_2, P_1, K_2, SAN, and S_{sa}) also showing strong influence. Obviously many of these are lumping the effects of others with neighboring aliased periods (especially weak long-period tides like S_{sa}). These tests confirm the strong influence on these data of M_2, AN, and BAN but leave to the future the specific combination of these and other lunisolar tide corrections (with M_2) which will produce the best result.

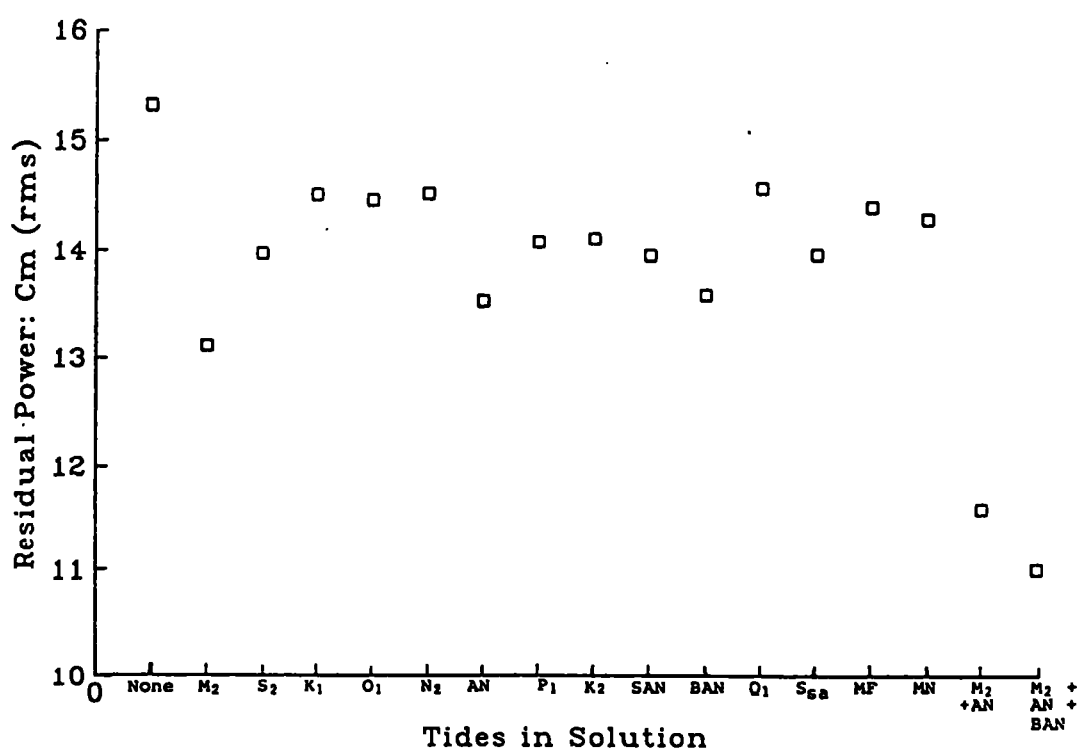

Figure 9c.–Results of single and multiple tide solutions with the full Geosat time series. Shown are the residual power after a least squares solution of the tide difference eq. (2) using data at 1,953 deep ocean stations. The first point on the left gives the data power before any solution. For single tides the M_2 correction has the greatest effect. But the reduction with any single tide is small because the data are small because the data are generally dominated by necessary corrections for many other tides as well as media and surface effects such as mesoscale ocean dynamics. An empirical solution for all 11 principal lunisolar tides as well as the three ocean weather tides listed and a few secular terms (constant, linear, and quadratic) reduces the power in these difference data to 9 cm, rms.

While I believe strongly that the power variation over the ERM cycles shown in fig. 9a,b is an indication of significant M_2 deficiency in the Geosat model I also want to be sure that the specific ocean-area values obtained from its correction using the detailed time series are estimated with realistic errors. Thus, as just seen with the cycle-power solutions, they were dominated by a "noise" component that is probably far from random while being influenced at the sub-decimeter level by systematic errors in the many media and surface corrections that were applied to the GDRs. (See Tapley *et al.* 1982, Cheney *et al.* 1987). As discussed above, I am also particularly concerned about what deleterious effect the uncoupled "orbit reduction" has on the subsequent tide solutions. For both of these reasons I performed an extensive calibration test of subsets of the full 4° data using essentially independent windows on the solution.

SUBSET CALIBRATION TESTS OF M_2 SOLUTIONS FROM 4° TIME SERIES

Table 5 gives some statistics of the subsets of arc-segment windows processed independently for calibration purposes. The windows themselves were described in a previous section above. Recall, for example, that arcs L, A, and E represent (roughly) a window of 1 day of data referred originally to the Gem 10 radial ephemeris and arcs F,G,H,I,J,K represent (roughly) a window of 2 days of data referred originally to the Gem T1 ephemeris. The amount of data (no. of passes) and cycle distribution for each of the 1/4 subsets used is shown in fig. 10. The important point to notice is that passes (actually pass pairs with cycle 1) in each cycle are usually dominated by a different subset (of windows) but in any case the characteristics of each subset is quite distinct. For example set C1 is particularly strong in cycles 5 and 17 while C2 is strong in cycle 12 but D2 has a fairly uniform distribution. This disparate distribution of data by cycles is important

Table 5.--Subsets of 4° Geosat difference altimetry for calibration

Name	Kind	Passes No.	GDR Records No.	Time Series (No. Grid Pts)	(No. Passes) Max	Median	Arc segments (windows)	Data power cm, rms
C1	1/4	27,913	1,154,494	1,750	46	16	B,D,BD,H	14.28
C2	1/4	27,011	1,102,893	1,671	49	14	G,K	16.31
D1	1/4	27,390	1,124,223	1,819	44	12	A,E,AE,I,J	15.90
D2	1/4	26,679	1,086,844	1,503	57	14	L,F	14.72
C1C2 (A)	1/2	54,924	2,257,387	1,904	95	26	(see above) C1+C2	15.31
D1D2 (B)	1/2	54,069	2,211,067	1,890	81	25	D1+D2	15.33
C1D1 (C)	1/2	55,303	2,278,717	1,891	80	26	C1+D1	15.10
C2D2 (D)	1/2	53,690	2,189,737	1,859	91	28	C2+D2	15.54
C1D2 (E)	1/2	54,592	2,241,338	1,858	102	27	C1+D2	14.50
C2D1 (F)	1/2	54,401	2,227,116	1,905	83	26	C2+D1	16.10
CD	1	108,993	4,468,454	1,953	160	53	C1+C2+D1+D2	15.32

because even though different windows of the cycles are processed (reduced of orbit errors) independently the data attributed to the same cycle arises from the same Gem T1 orbits (again always paired with cycle 1) for most of the arc segments here. To eliminate this common underlying orbit dependence we could cull special subsets that would have only distinct cycle information in each. However, for the purposes of this study I feel that the variety and quality of the independent tests is sufficient. It is certainly considerably more sophisticated than was attempted in Wagner (1990), where only two 1/2 subsets were tested with such independent M_2 solutions.

Thus in the station calibrations I resolve the M_2 tide (correction) from as many pairs of fairly equal independent data sets as possible and then see how well the differences between these solution pairs are comparable with the formal (white noise) error statistics (scaled, of course, by the respective solution residuals). For this purpose I performed six tests with 1/4 subsets (C_1 vs. C_2, D_1 and D_2; C_2 vs. D_1 and D_2; and D_1 vs. D_2) and three with the 1/2 subsets (A vs. B, C vs. D, and E vs. F). Originally I had hoped to establish that the 1/2 subset calibrations would be closer to a white noise result than the 1/4 set ones.

More precisely if H_1 and H_2 are two harmonic coefficients arising from independent tidal solutions (at a given ocean grid station) and σ_1 and σ_2 are their formal (scaled) error estimates (e.g., from the least squares inverse of the difference data normals), then I have used here the following theoretical "z" statistic to gage a calibration factor for the two solutions:

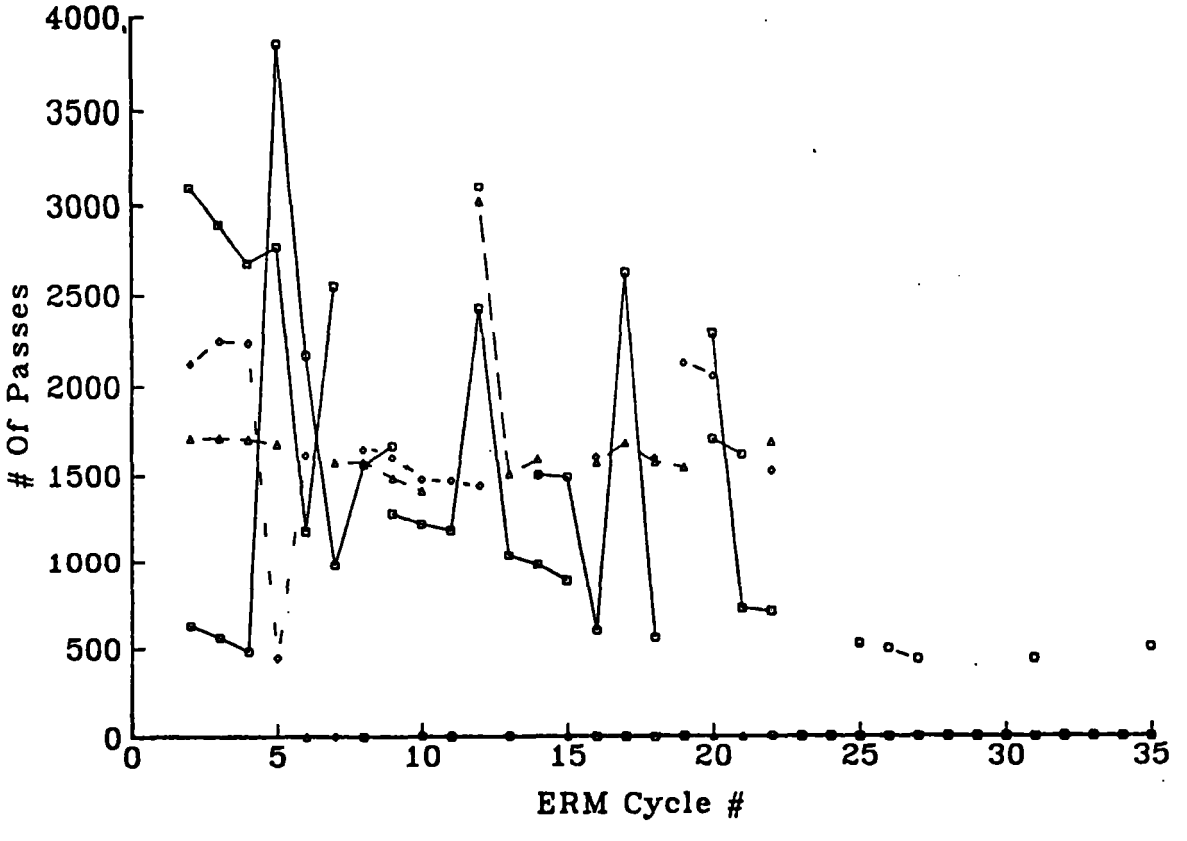

Figure 10.–Distribution of Geosat difference altimetry in 1/4 subsets of the full 4° time series. Squares are for subset C_1, triangles for subset C_2, octagons for subset D_1, and diamonds for subset D_2. For a description of the ERM day windows of these subsets, see table 5. Each 1/4 subset has a fair amount of data over the 19 cycles of the aliased M_2 tide. Each also emphasizes data at different cycles. Thus not only are the ERM windows distinct in these sets but the cycles (mainly) are also, as well as the ephemerides that govern the orbit corrections.

$$z = (H_1 - H_2) / [\sigma_1^2 + \sigma_2^2]^{1/2} \tag{8}$$

If the signal analyzed is only disturbed by random (white) noise, I would expect z in eq. (8) to have a unit normal distribution. Over many such independent samples a good judgment can be made of the likely calibration factor "f" that should scale the formal error estimates by computing for a large solution set:

$$f = \text{rms } z. \tag{9}$$

For (random) normally distributed errors, the expected value of f^2 should be 1.

To be specific, for each time series (of differences) at a station I solved (by least squares) the harmonic equation:

$$\begin{aligned} \Delta h &= [\sum_i \sum_{j=1}^{2} Y_{ij}] \pm e \\ Y_{ij} &= C_i [\cos(w_i t) - \cos(w_i t_o)] , \qquad j=1 \\ Y_{ij} &= S_i [\sin(w_i t) - \sin(w_i t_o)] , \qquad j=2 \qquad , \end{aligned} \tag{10}$$

for best values of C_i, S_i with respect to the difference height data Δh, where i is a tidal constituent with frequency w_i, t_o is the time in the reference cycle (here, cycle 1) from a certain base time, and t is the time in the following cycle from the same base time. I have based the harmonics C_i , S_i on the time at the start of the Geosat ERM, 8.0 November 1986, but these can be easily converted to harmonics with respect to a conventional tide system referenced to the time of the Moon's passage over the Greenwich meridian [more precisely, the time when the particular tidal argument is zero (Schwiderski 1983)].

Table 6 provides statistics of the nine subset calibrations for the M_2 tide solutions. They show that there is no substantial difference between the two divisions of the full data set; that is, in either case a calibration factor near 2.0 is appropriate. Evidently the degree of non-randomness in the errors (e) of eq. (10) has not decreased from the 1/4 to the 1/2 set even though the data have about doubled. I consider the major systematic error sources in this equation to be other tidal constituents as well as the distortions due to the uncoupled orbit error reduction. The latter has been shown (above) to generate tidal errors with the M_2 aliased period of about 20 ERM cycles. (See fig. 5b.) Clearly the data distribution is highly weighted towards the early cycles (fig. 8a), so that this and other likely systematic error sources of period greater than about 1/2 year will not be well randomized over any arbitrarily chosen subset as here. This is probably the reason why an improvement in the calibration with data size is not seen. But since the full set is also poorly distributed in time (relatively more early cycles than late) we must settle (conservatively) for the (near) 2.0 factor even if the cause is known.

Figures 11a,b show the distributions of the raw differences seen in some of these subset calibrations. They are roughly the order of magnitude of the coefficient solutions themselves, which is sobering but still understandable (within a factor of about 2) from "normal" statistics. If this seems excessive, contrast it to the error calibration factors of from 3 to 10 found for Goddard Earth Models currently and from the earliest days of satellite geodesy (e.g., Lerch *et al.* 1988).

Figure 12 summarizes the overall M_2 calibration for tests involving a single aggregation of the 1/4 to 1/2 subsets, namely C_1/C_2, D_1/D_2 and A/B. The aggregate test here (A/B) appears to have a genuinely better calibration than any one of its 1/4 constituents (but see table 6 for other subset results).

Table 6.--Subset M_2 correction calibrations. Minimum number of passes in either set = 10.

Sets	No. of common stations for calibration	Coeff. sol. (cm, rms)	Coeff. diff. (cm, rms)	Calibration Factors Avg local[1]	global[2]	rms z[3]
C1/C2	938	8.22	10.80	1.99	2.05	2.42
D1/D2	958	7.30	8.55	1.67	1.80	1.99
C1/D1	1129	7.43	8.54	1.64	1.73	1.93
D2/C1	981	7.85	9.52	1.65	1.71	1.94
C2/D1	964	7.77	8.56	1.75	1.95	2.09
C2/D2	826	7.79	9.18	1.74	1.89	2.08
(Wt Avg)	(966)			(1.74)	(1.85)	(2.07)
A/B	1616	6.79	7.29	1.69	1.89	1.98
C/D	1595	7.13	8.25	1.86	2.05	2.20
E/F	1576	6.90	8.15	1.89	2.07	2.21
(Wt Avg)	(1596)			(1.81)	(2.00)	(2.13)

1. $\bar{f} = (1/N)\sum_{n=1}^{N} f_n$: $f_n = \{[(c_{n1} - c_{n2})^2 + (s_{n1} - s_{n2})^2]/[\sigma^2 c_{n1} + \sigma^2 c_{n2} + \sigma^2 s_{n1} + \sigma^2 s_{n2}]\}^{1/2}$

for *solutions* 1 *and* 2 *at station n*

2. $\bar{f} = \{\sum_{n=1}^{N} [(c_{n1} - c_{n2})^2 + (s_{n1} - s_{n2})^2 / \sum_{n=1}^{N} [\sigma^2 c_{n1} + \sigma^2 c_{n2} + \sigma^2 s_{n1} + \sigma^2 s_{n2}]\}^{1/2}$

3. $\bar{f} = \{(1/N)\sum_{n=1}^{N} [(c_{n1} - c_{n2})^2 + (s_{n1} - s_{n2})^2]/[\sigma^2 c_{n1} + \sigma^2 c_{n2} + \sigma^2 s_{n1} + \sigma^2 s_{n2}]\}^{1/2}$

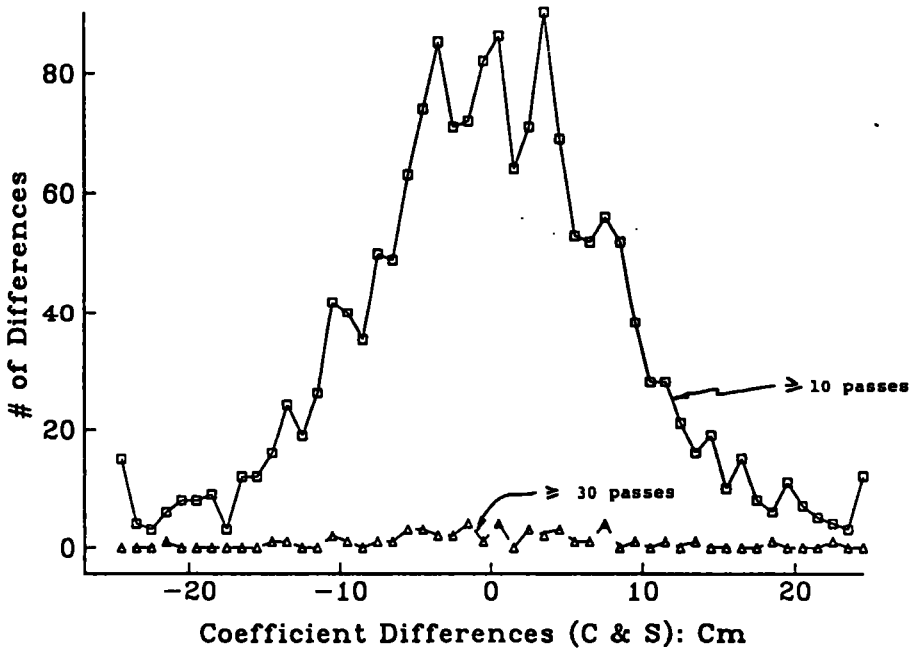

Figure 11a.--Histograms of the M_2 solution differences: 1/4 subsets C_2 vs. D_2. Upper histogram gives distribution of differences considering all common stations with 10 or more passes in each independent subset. There are 826 such stations. The power of the differences in the solutions (rms) is 9.2 cm. The power of the correction coefficients themselves in all the solutions is only 7.8 cm (rms). A somewhat sharper result is achieved when at least 30 passes define the two subset solutions for a common station (lower histogram). However, only 23 such common stations are available for these subsets. The power of the differences here is reduced to 8.3 cm (rms) while the power of the correction coefficients determined is 7.5 cm (rms).

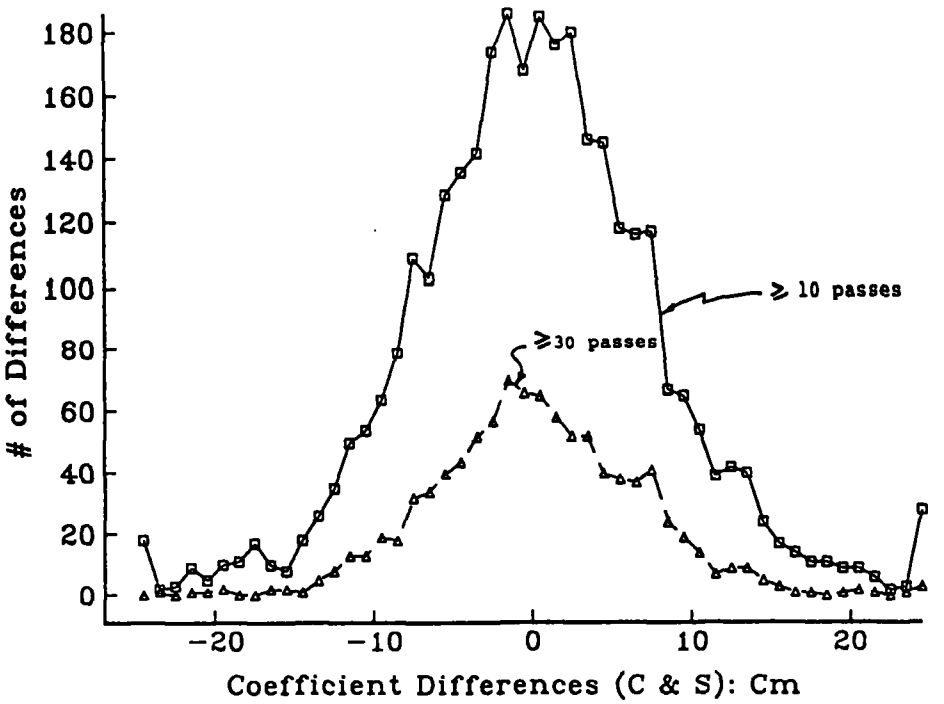

Figure 11b.–Histograms of M_2 solution differences: 1/2 subsets C_1D_1 vs. C_2D_2. Upper histogram is for 10 or more passes in each solution (of which there are 1,595) while the lower is for 30 or more passes (of which there are 482). With a more robust data distribution these subset solutions are more compatible. When 10 or more passes are present the differences are only 8.2 cm (rms), while the differences are only 6.5 cm (rms) when 30 or more passes are present.

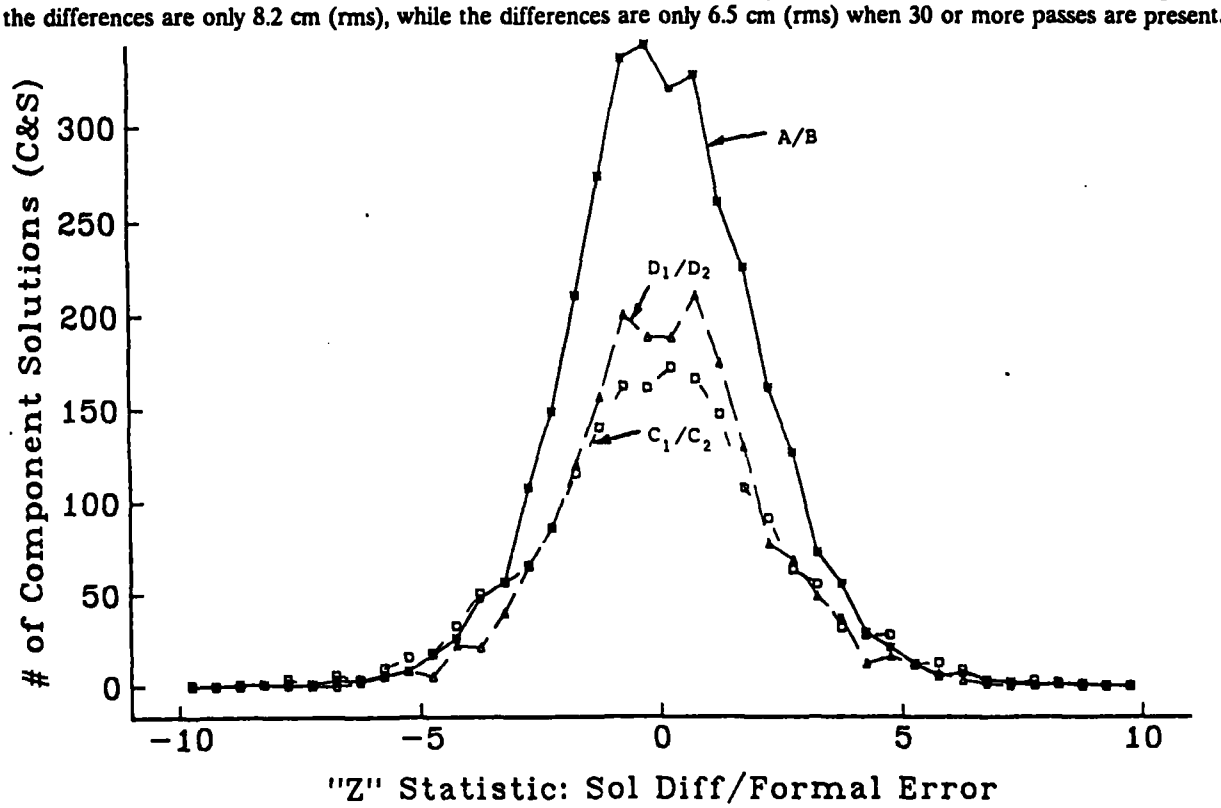

Figure 12.–Calibration of 4° M_2 solutions: 1/4 sets C_1 vs. C_2, D_1 vs. D_2 and the 1/2 subset A vs. B. These new comparisons again emphasize the somewhat sharper results when better conditioned 1/2 subsets are used. Here only common station solutions with more than 10 passes are considered. The overall global calibration factor derived from C_1/C_2 comparisons was found to be 2.05. (See table 6.) For D_1/D_2 comparisons the factor was 1.80 while for A/B comparisons the factor was 1.89, showing that though the 1/2 subset solutions agree better the agreement is matched by a reduction of formal errors yielding roughly the same calibration result.

Finally, in table 7 I show the detailed calibration results from two stations that experienced enough passes to be represented in all nine subsets, at latitude -64°, longitude 254°; and at latitude -56°, longitude 222°. Notice that in the former the 1/4 subset calibration factors are (with one exception) less than 1.0. While it is gratifying in one sense to obtain such results I attribute them to a lack of sufficient sampling. While each test individually involves independent data, as a whole these tests are not independent since each 1/4 subset is used in three of these confrontations. The same is true of the 1/2 subset tests, which again for the first station, appear much more believable than the 1/4 subset ones. On the other hand, the data mix for the second station seems to be fair for both the 1/4 and 1/2 subsets; each result is consistent for a calibration factor of about 1.5 at this station with no advantage gained by the larger 1/2 subset sampling.

Table 7.--Consistence of calibration factors from independent 4° time series-M_2 solutions

Station lat: (degrees)	lon:	Subsets	Min No. Passes	Pass No. discrepancy[1]	Max. correlation	Calibration factor[2]
-64°	254°	C1/C2	34	0.278	0.471	1.250
		C1/D1	24	0.609	0.604	0.767
		C1/D2	45	0.235	0.471	0.591
		C2/D1	24	0.345	0.604	0.343
		C2/D2	34	0.505	0.455	0.629
		D1/D2	24	0.815	0.600	0.479
(average)						(0.68 ± 0.32)
-64°	25°	A/B	79	0.025	0.409	1.079
		C/D	69	0.275	0.518	0.427
		E/F	58	0.550	0.447	1.338
(average)						(0.95 ± 0.47)
-56°	222°	C1/C2	27	0.169	0.194	1.999
		C1/D1	27	0.286	0.194	1.568
		C1/D2	25	0.077	0.194	2.080
		C2/D1	32	0.118	0.090	1.532
		C2/D2	25	0.246	0.048	0.508
		D1/D2	25	0.361	0.090	1.310
(average)						(1.50 ± 0.57)
-56°	222°	A/B	59	0.033	0.079	1.193
		C/D	57	0.100	0.038	2.275
		E/F	52	0.267	0.124	1.267
(average)						(1.58 ± 0.60)

[1] [no. passes (set 1) - no. passes (set 2)]/ average no. passes (both sets).

[2] Average local calibration factor (see definition, table 6).

The three auxiliary data in table 7 show an early attempt to explain these calibration factors. I originally hypothesized that a large number of passes in both of the two test solutions would be associated with the best calibrations. Table 7 shows this is not true in general (an exception is the 1/2 test for the second station). Then I thought perhaps the best calibrations would be associated with tests which had nearly the same number of passes (a minimum of 10 was always necessary for a valid test). Again, this is realized only for the 1/2 subset tests at the second station. Finally, I thought that those tests which yielded the best data distribution with respect to their M_2 solutions (as measured by the correlation coefficient between sine and cosine terms) would have the best calibrations. Aside from the question whether this correlation is a proper measure of the distribution in a difference determination (see appendix A), again only in one of these four groups of tests (the 1/4 tests at the second station) is this hypothesis confirmed.

To gain more understanding of the calibration process I display representative calibration results from solutions experiencing the largest reductions in residuals using the full data set. (See figs. 13a-f.) In these figures both the data and the solutions are displayed as if they referred to a direct times series.

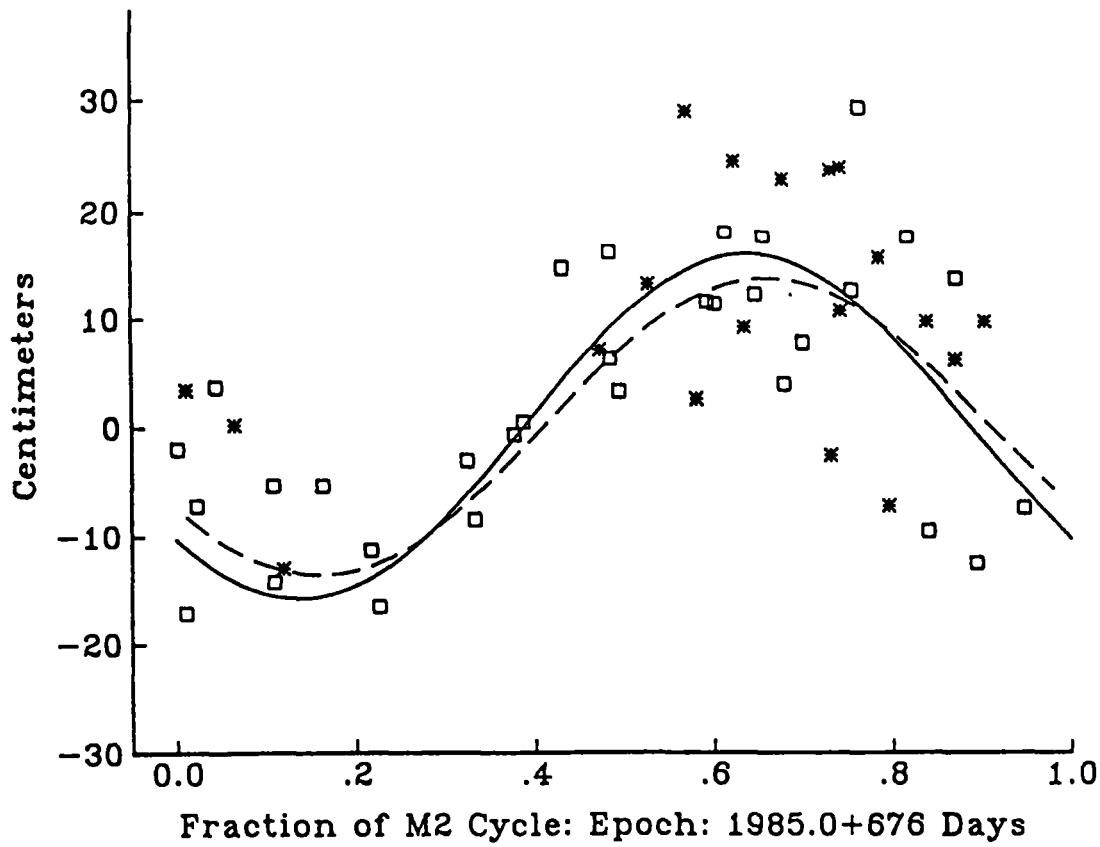

Figure 13a.–Residual M_2 tide in North Atlantic (lat. 16°, long. 318°). Solid line gives correction tide determined from 1/2 subset C_1D_2. Dashed line gives same (M_2) correction tide determined from independent 1/2 subset C_2D_1. Asterisks display actual difference data of solid line solution as though all of the error belonged to the following or lagged ERM cycle observation and none to cycle 1 observation of sea topographic height. Distribution of the following ERM cycle data is shown (but not labeled by cycle). The fraction of the M_2 cycle (from epoch) for the ERM cycle 1 that passes here is also not shown so the full impact of the data distribution in these solutions cannot be appreciated from this and the following figs. 13. However, in general, cycle 1 data act to fill in the gaps of this distribution with respect to the M_2 cycle (or phase). Boxes give the same following ERM cycle errors with respect to the dashed solution arising from subset C_2D_1. The C_1D_2 solution has reduced data power from 20.4 cm (rms) to residuals of 10.0 cm (rms). The C_2D_1 solution has reduced data power from 16.7 cm (rms) to residuals of 7.8 cm (rms). Local calibration factor for this comparison is 0.74. (See table 6 for factor definition.)

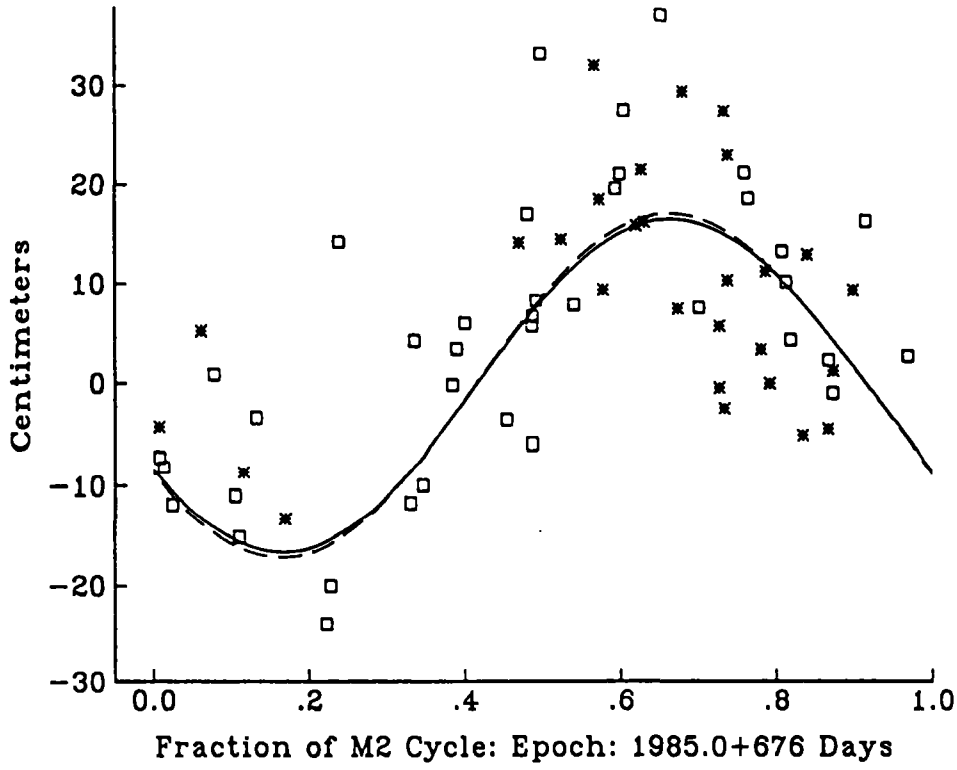

Figure 13b.–Residual M_2 tide in the North Atlantic (lat. 8°, long. 322°). Solid line and asterisks refer to solution with 1/2 subset C_1C_2 while dashed line and boxes refer to solution with independent 1/2 subset D_1D_2. (See fig. 13a for general interpretation of this data display.) The C_1C_2 solution has reduced data power from 19.4 cm (rms) to yield residuals of 9.7 cm (rms). The D_1D_2 solution has reduced its data power from 21.4 cm (rms) to yield residuals of 10.0 cm (rms). Local calibration factor for this comparison is 0.18.

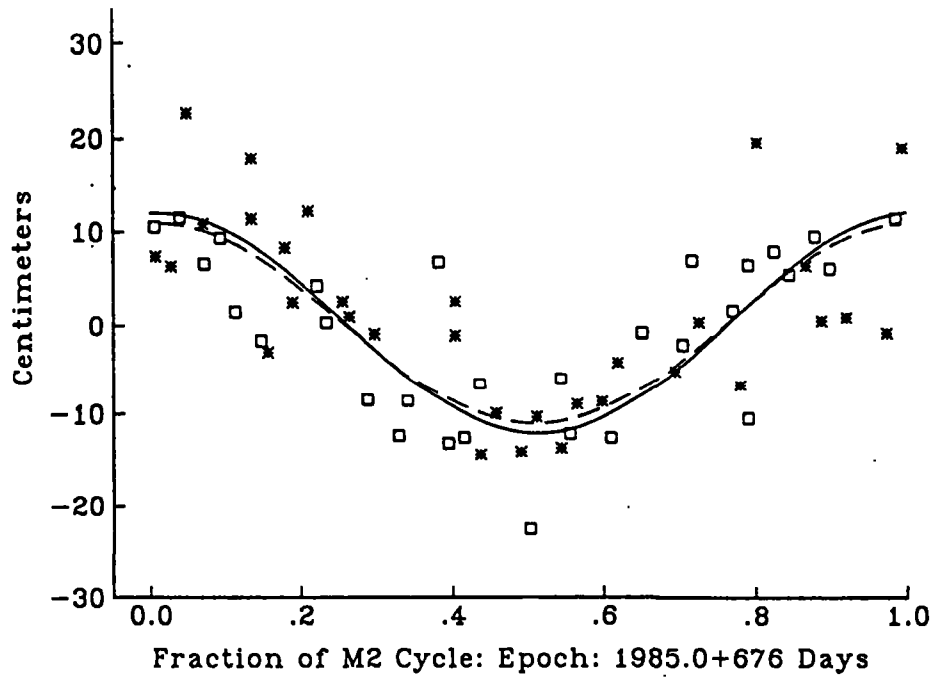

Figure 13c.–Residual M_2 tide in the South Pacific (lat. -16°, long. 250°). Solid line and asterisks refer to solution from 1/2 subset C_1D_1 while dashed line and boxes refer to solution from independent 1/2 subset C_2D_2. The C_1D_1 solution has reduced its data power from 15.1 cm (rms) to yield residuals of 6.7 cm (rms) while the C_2D_2 solution has reduced its data power from 10.6 cm (rms) to yield residuals of 5.8 cm (rms). (See fig. 13a for more details on the form of this display.) Local calibration factor for this comparison is 0.46.

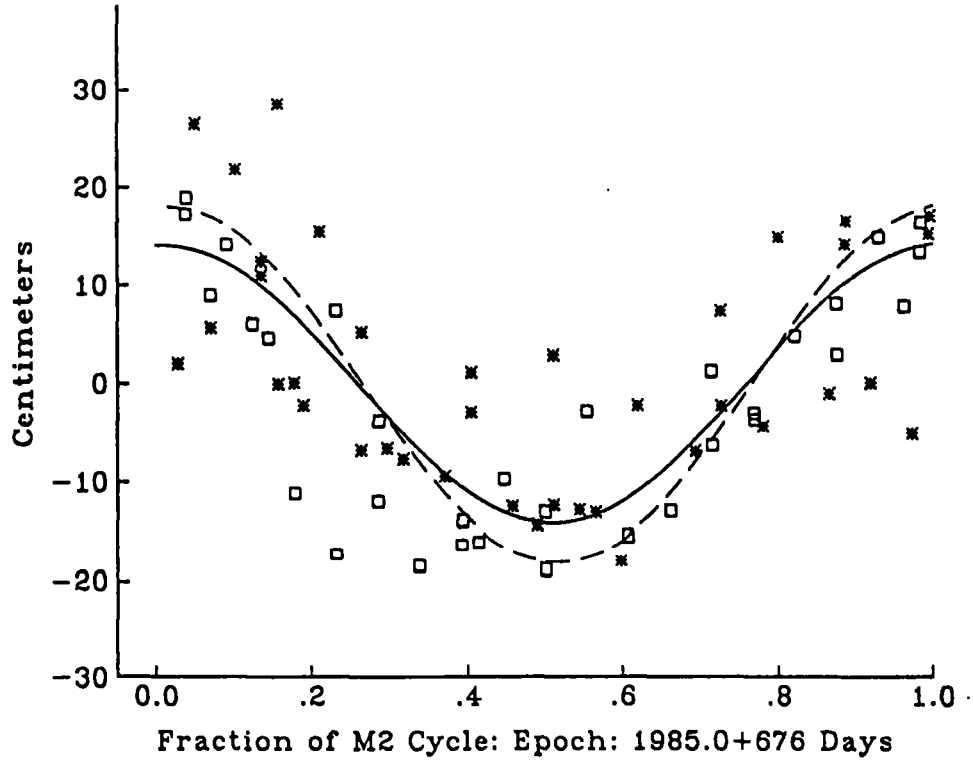

Figure 13d.–Residual M_2 tide in the South Pacific (lat. -20°, long. 250°). Solid line gives solution from 1/2 subset C_1D_1 with respect to the asterisk data while dashed line gives solution with respect to the independent 1/2 subset C_2D_2 (and data in boxes). The C_1D_1 solution has reduced its data power from 18.6 (rms) to residuals of 8.6 cm (rms) while the C_2D_2 solution has reduced its data power from 18.8 cm (rms) to 7.7 cm (rms). Local calibration factor for this comparison is 1.40.

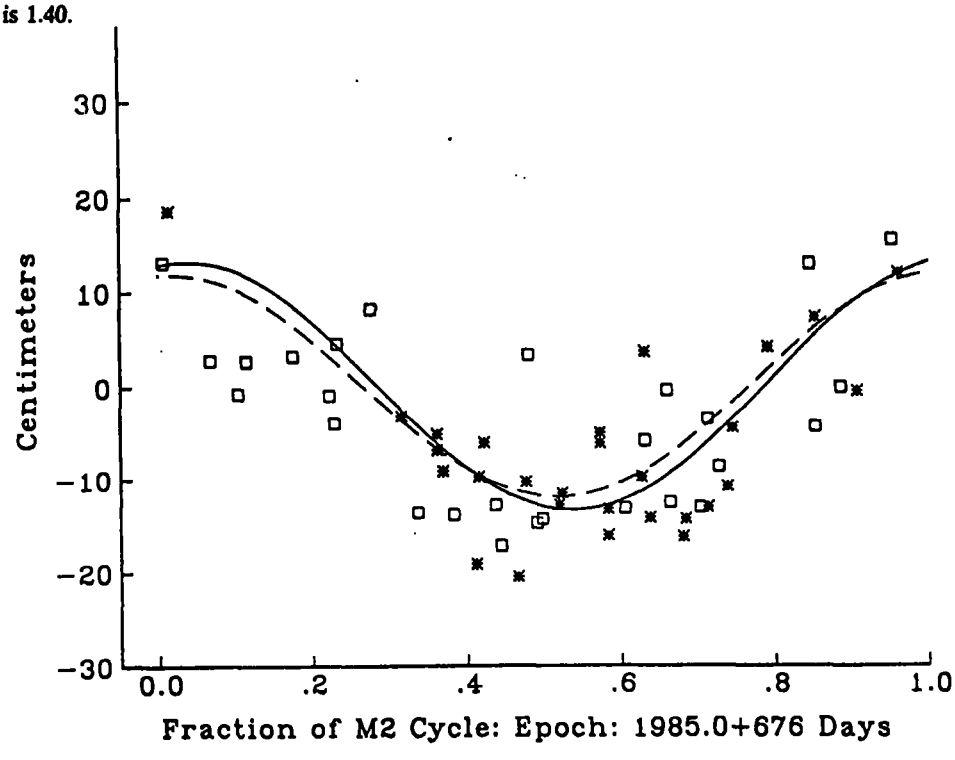

Figure 13e.–Residual M_2 tide in the South Atlantic (lat. -44°, long. 10°). Solid line refers to solution from 1/2 subset C_1C_2 (with asterisk data), dashed line to the solution from independent 1/2 subset D_1D_2 (with boxed data). The solution from set C_1C_2 has reduced its data power from 15.4 cm (rms) to 5.6 cm (rms); the solution from set D_1D_2 has reduced its data power from 14.5 cm (rms) to 6.8 cm (rms). Local calibration factor from this comparison is 0.91.

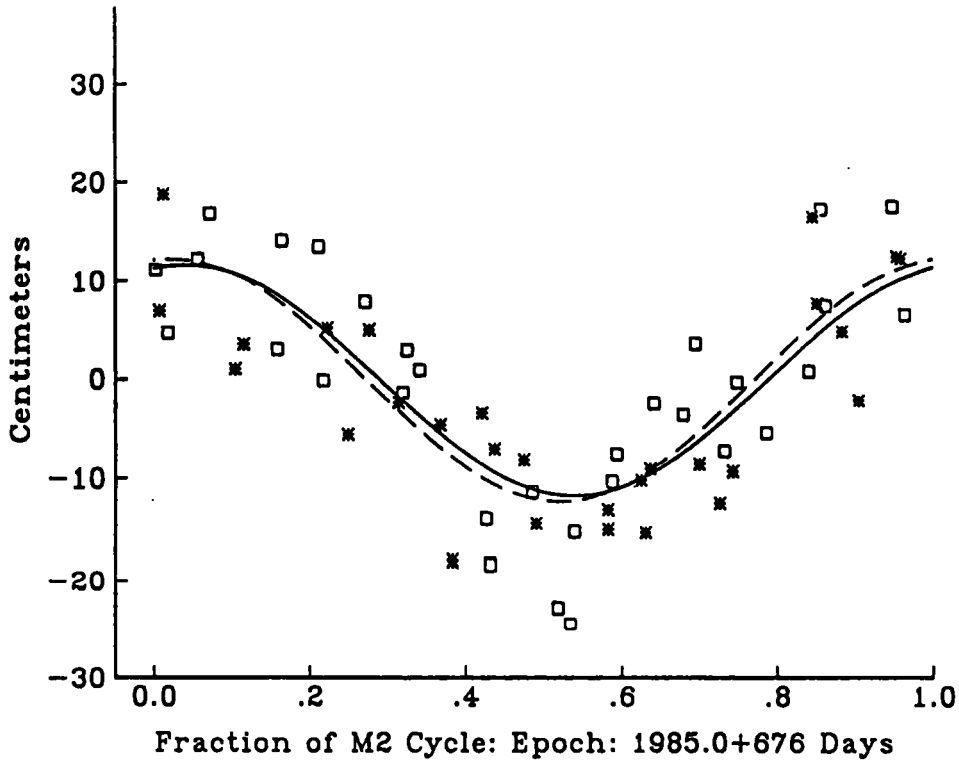

Figure 13f.–Residual M_2 tide in the South Atlantic (lat. -44°, long. 10°). Solid line refers to solution from 1/2 subset C_1D_1 (with asterisk data), dashed line to solution from independent 1/2 subset C_2D_2 (with boxed data). Solution from C_1D_1 has reduced its data power from 14.2 cm (rms) to 5.7 cm (rms). Solution from C_2D_2 has reduced its data power from 14.1 to 6.1 cm (rms). M_2 appears to be only residual tide affecting this station significantly. Local calibration factor for this comparison is 0.68.

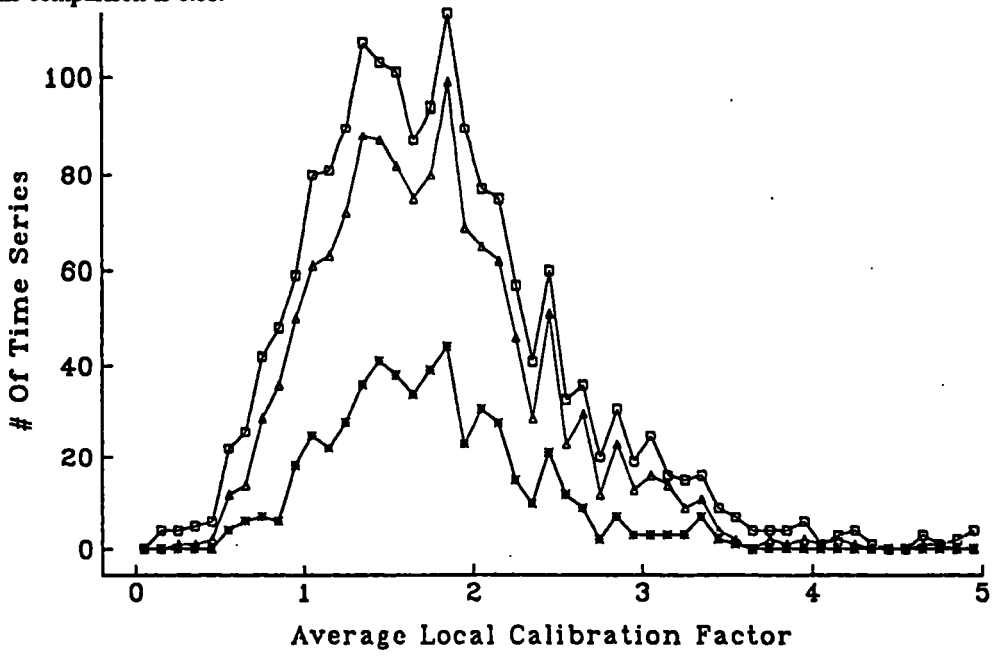

Figure 13g.–Histogram of significant calibration factors from subset analyses showing distribution of average local calibration factors with respect to number of subset analyses that apply to a particular station's time series. (For a definition of local factor, see table 6.) Boxes give the distribution when at least one of the nine possible independent subset comparisons could be applied to a common station. There are 1,736 such stations and the grand average of all the local calibration factors determined was 1.79 with a standard deviation of 0.76. Triangles give the (sharper) distribution when four or more subset comparisons could be made (1,342 stations) yielding a grand average of 1.76 with a (reduced) standard deviation of 0.66. Asterisks give the distribution when all nine subset comparisons applied (528 stations) yielding the sharpest overall average calibration of 1.74 with a standard deviation of 0.58.

The actual data refer to time-difference pairs. Thus I do not know how much of the residual belongs to the reference cycle-1 arc and how much to the following cycles. For convenience, in these displays I assume that there is no error in the cycle-1 heights. The difference between the data heights and the solution curve is the full difference residual at its correct M_2-cycle fraction for the following ERM cycle. Thus many months in time may separate adjacent data points in these figures. The independent variable here is not time but fractions of an M_2 period (of 12.4206 hours). The display shows that for most of the independent data sets in these particular (1/2 set) calibrations the M_2 cycle is well covered and the tide (correction) stands clear above the "noise" of the observations. It should also be said, however, that these solutions have effected the maximum residual reduction (over 50 percent), but that the average reduction is much less (about 15 percent). Recall that the average power in the orbit-reduced data was 15 cm, rms. Since the average power of the M_2 corrections here is only about 6 cm, we see that the solution (if orthogonal to the data) should effect a reduction of the residuals of only about 10 percent. On the other hand we saw from the cycle power analysis that the addition of a few more tides in the solution should drive the residuals down to about 9 to 10 cm, which would leave most solutions of about equal power with their remaining residuals (signal/noise ≈ 1). Unfortunately therefore, there are not sufficient data here for most stations to yield precise corrections for more than a few tides in combination.

While not explaining the calibration results in detail, I adopted from many of these trials the following simple conservative rules for the full set M_2 solutions. The normal calibration factor for a station was 1.8 if no superseding local information was applicable. Considering the experience I had assuring the consistency of the subset results I only used the (average) local calibration factor (from the subset tests) when all nine of the possible tests were performed under the conditions described above (e.g., a minimum of 10 passes in each subset at a station).

Figure 13g shows the overall distribution of these factors under these varying conditions with regard to subset test samples. While the average factor does not change significantly when I relaxed the sample-test requirement, note that the number of factors less than 1 (obviously unrealistic) increased markedly as fewer tests were used to determine an average local factor. Likewise, many of the factors greater than 2 or 3 in the sparse sampling must be considered just as unrealistic, even though using them would give a conservative result. Wagner (1990) used only a single 1/2 subset analysis to define a local factor, but included many additional conservative criteria which effectively vitiated this local information in a complex way. Here I simply applied the global average factor of 1.8 for most of the station solutions and used the nine-sample average for the 528 well tested ones except for the few showing factors less than 1.0 which was held as a minimum.

To recapitulate, 1,736 of the 1953 4° by 4° stations with time series in the current (full) data set had at least one local calibration. Only 528 of these were actually used (as described above) to calibrate (locally) the errors of the full set M_2 solutions, which I now describe.

DEEP OCEAN M_2 TIDE SOLUTIONS

In solving eq. (10), by least squares fitting of the height-difference data (cleared of orbit effects) I adopted (first) the simplest assumption that all the data had the same uncorrelated weight (a unit error of 5 cm was used). As can be appreciated from the variations seen in arc segment G (fig. 2a for example) there may be justification for using the information on these variations as well as the averages themselves to weight the data variably in these tide solutions. However a counter argument must also be entertained; namely, that since this time-local "bin noise" may only be a small part of the true error "e" in the tidal eq. (10) we should not use this more refined information until at least eq. (10) has been expanded to include more than just the M_2 tide.

The (least squares) solution of eq. (10) also used a very mild a priori constraint on its error (or normal) matrix, which embodied the information that the M_2 harmonic coefficients sought should have zero expectation with errors of 30 cm. A covariance analysis of the Schwiderski (1983) M_2 model actually shows that in the deep oceans (sampled here) the power is closer to 24 cm. (See below.) In any case this constraint (competing with data weighted at 5 cm) only affected solutions significantly when fewer than 10 observations were available at a station. (These were also discarded in displaying the "best" results). In fact the power of the data for small solution sets (when poorly distributed) tended to yield not small but unrealistically high M_2 solutions, which was the principal reason why these small set results were discarded.

A concern arises that a considerable number of stations in the full data set still had fewer than 10 observations (fig. 8b). Figure 14 shows that many of these (probably) have unrealistically high power. In fact when the calibration procedure above is applied and all solutions with fewer than 10 observations or calibrated errors greater than 5 cm are rejected, the remaining solutions all have power less than 16 cm. These 1,652 "best" solutions have an average power of 5.71 cm contrasted with 6.33 cm, rms for the set shown in fig. 14, which rejects only solutions with fewer than three passes. However, both of these values agree reasonably well with the global predictions made for the M_2 corrections from the cycle-power data above (figs. 9a,b). Nevertheless even after eliminating the obviously poorer solutions I was still concerned by the possibly excessive power at the sparser grid points. This would indicate overadjustment in the presence of significantly nonrandom errors for a relatively poorly sampled solution. For example, on fig. 14 I have drawn a best fit line through the power points of the 1,652 best solutions (weighted by the estimated errors for them, all less than 5 cm). The slope of this line is indeed slightly negative and it is also negative if just unweighted data are used.

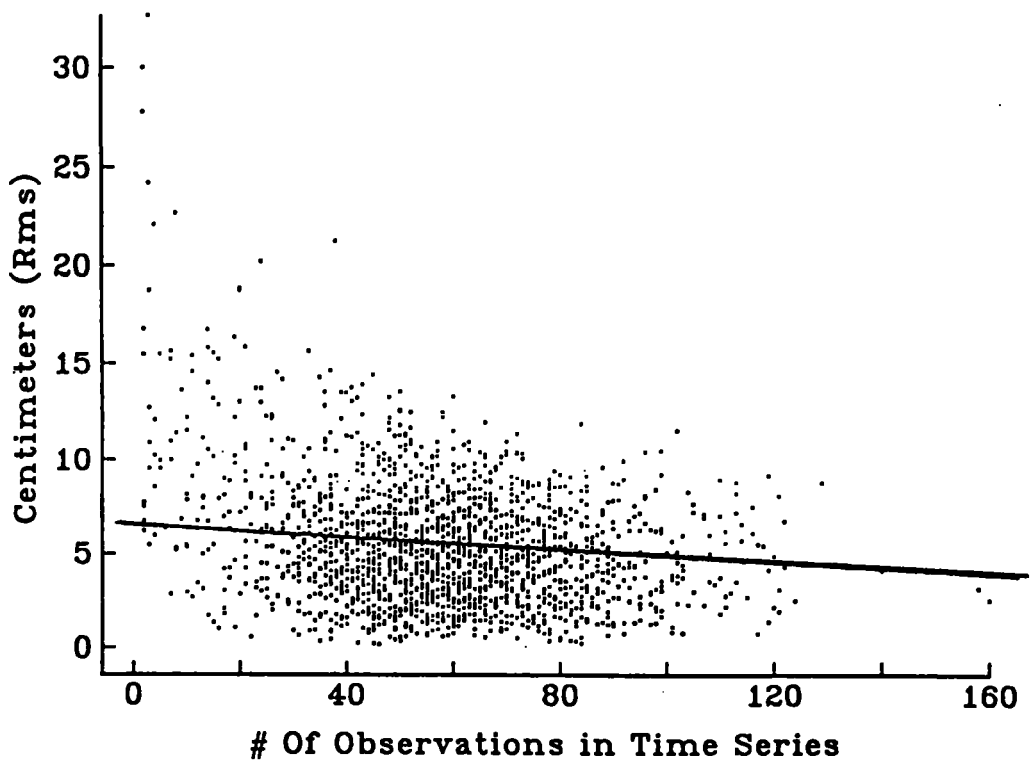

Figure 14.–Power of M_2 correction solutions from 1,895 time series. The only selection criterion here was that at least three passes had to be present for each time series (actually pass pairs with cycle 1). The solutions were carried with the use of mild a priori information (assuming initial harmonic errors of 30 cm). However, difference data were weighted at 5 cm. Clearly solutions with fewer than about 10 passes tend to yield excessive power and the tendency for the stronger solutions to yield lower power persists even beyond 10 passes.

Because of the nonuniform sampling of equiangular ocean areas by the ERM ground track, a wide range of passes always appears in the solutions. Figures 8b and 14 show, though, that in spite of the additional selectivity imposed by the incomplete windows here, there is still a fair degree of concentration of pass density between 30 and 80 observations in this particular analysis. Still the existence of this power bias, even if slight, emphasizes the importance placed on the thorough calibration of the solutions which indicates that the mean (calibrated) error of an harmonic is roughly 50 percent (signal to noise ratio: 2/1) of the mean power globally. (See fig. 15.)

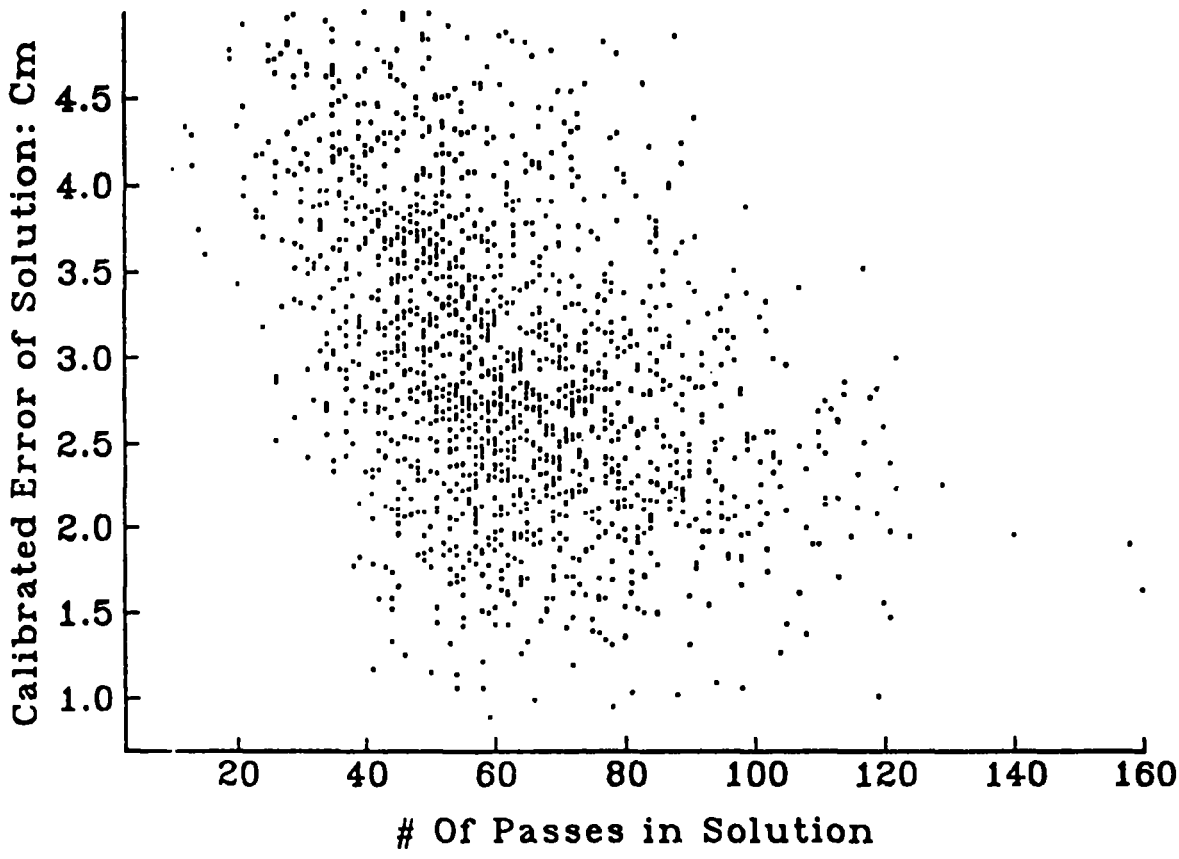

Figure 15.–Strength of M_2 correction solutions from 4° Geosat altimetry. If only errors of unit variance (here 5 cm for the data) were taken into account, the distribution would closely follow a declining curve inversely proportional to the square root of the passdensity (with a fairly wide scatter), an encouraging sign the solution will improve even more when the full ERM data set is employed (roughly 3 times the data used here).

As a final test of the stability of my M_2 solutions I examined the differences in the station solutions for M_2 only and those for M_2 from a combination of what seem to be the most influential tides, M_2+AN+BAN. (See fig. 9c.) Figures 16a,b show the results of this comparison. For stations with more than about 30 passes the order of magnitude of the differences is from 2 to 3 cm. Note however that for solutions with less than about 30 passes the differences can be quite large (up to 60 cm), indicating poor data distribution with respect to these long-periodic tidal variations. Summarizing, the comparison is good and the great majority of the solutions are at the level of the estimated errors from the calibration results.

OCEAN LOADING CORRECTION

Before interpreting the corrected M_2 tide solutions as "errors" in the Schwiderski (1983) M_2 ocean tide model however, I acknowledge [following Rao and Sanchez (1989)] that the GDR values for these tides (solid and ocean) do not account for the so-called ocean loading tide (OLT). The OLT is merely the effect on the ocean bottom of the modeled ocean load. [See fig. 17, adapted from Schwiderski (1980: fig. 4).]

Disregarding the solid Earth tide which displaces the ocean bottom and the sea surface equally, fig. 17 shows that the geocentric tide measured by the altimeter is simply the ocean tide minus the ocean loading tide. Since I have assumed that the solid tide (of order 10 cm amplitude) is not likely to be significantly in error (e.g., Baker 1984) I interpret the measured M_2 corrections here to be the difference of ocean tide corrections and the ocean loading tide which should have been (but wasn't) included in the model tides on the GDRs. [See also Francis and Mazzega, 1990]. What is the order of magnitude of the OLT? According to Schwiderski (1980) the OLT is effectively a simple elastic response of about 10 percent of the full tide (over most of the ocean) so that OLT equals about 3 cm rms globally. But Wagner (1990) ignored this small secondary tide as being within the errors of most of the Geosat tide corrections and interpreted the results directly as ocean tide corrections. Here, following Goad (1980) I removed from the M_2 tide corrections that part belonging to the OLT which should have been included in the model on the Geosat GDRs. Goad (1980) used an integrated Green's function approach to this load calculation (with an indicated accuracy of order 0.3 cm) while Ray and Sanchez (1989) used a spherical harmonic approach (maximum degree: 36). I have verified that both approaches yield virtually the same OLT for the deep oceans. (The comparison is not as good for near shore and land areas.)

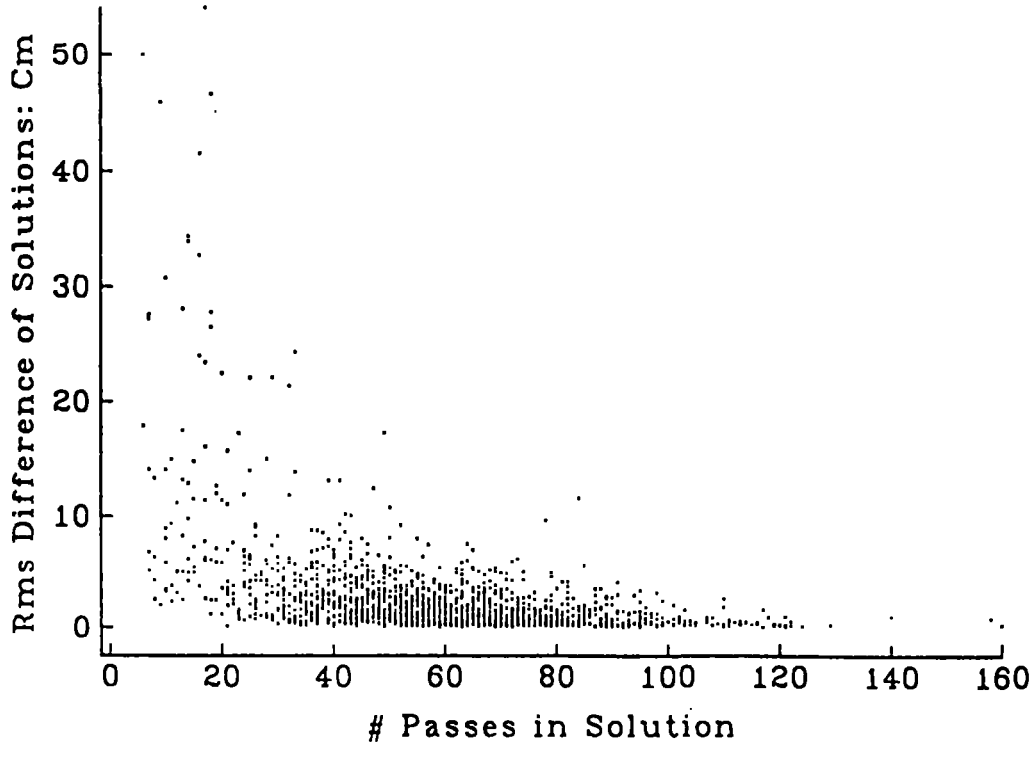

Figure 16a.–Differences of M_2 correction solutions: M_2 only vs. M_2 plus annual plus biannual. In spite of close correspondence between periods of aliased M_2 tide (in the Geosat ERM) and yearly ocean weather tide, the M_2 solution appears to be well separated for most solutions with more than about 10 passes, even with an additional biannual weather tide included. For example, for overall solutions with more than 10 passes (1,857 stations) the average M_2 harmonic coefficient difference is only 4.3 cm (rms), while for solutions with at least 30 passes the difference is only 2.6 cm (rms).

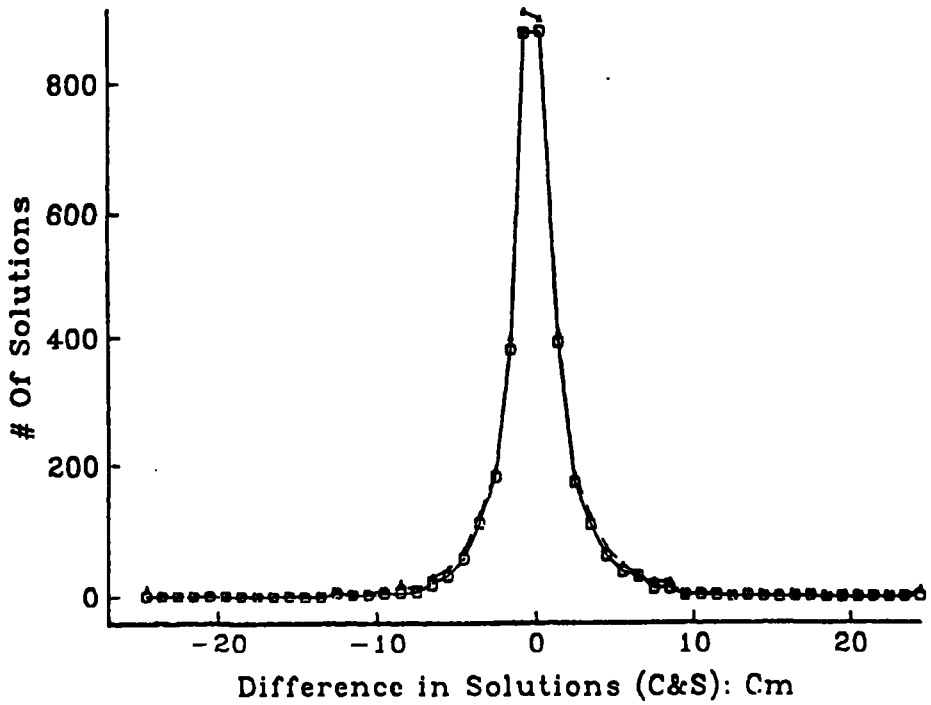

Figure 16b.–Histogram of M_2 correction solution differences: M_2 only vs. M_2 plus annual plus biannual. Solid line between boxes; minimum no. of passes = 10, overall differences (1,857 grid points) = 4.27 cm, rms. Dashed line between triangles; minimum no. of passes = 30, overall differences (1,712 grid points) = 2.60 cm, rms. Notice the comparison is much sharper (more central) than for a normal distribution, which means it has an excessive number of outliers or anomalous points where the data distribution (for the given number of passes) is not sufficiently uniform to effect an adequate separation of these tides. This situation should improve with added data more uniformly distributed among the ERM cycles. In the meantime the use of local calibration factors where appropriate and global ones at all other grid points can help to get a better judgment of the true errors of the M_2-only solutions.

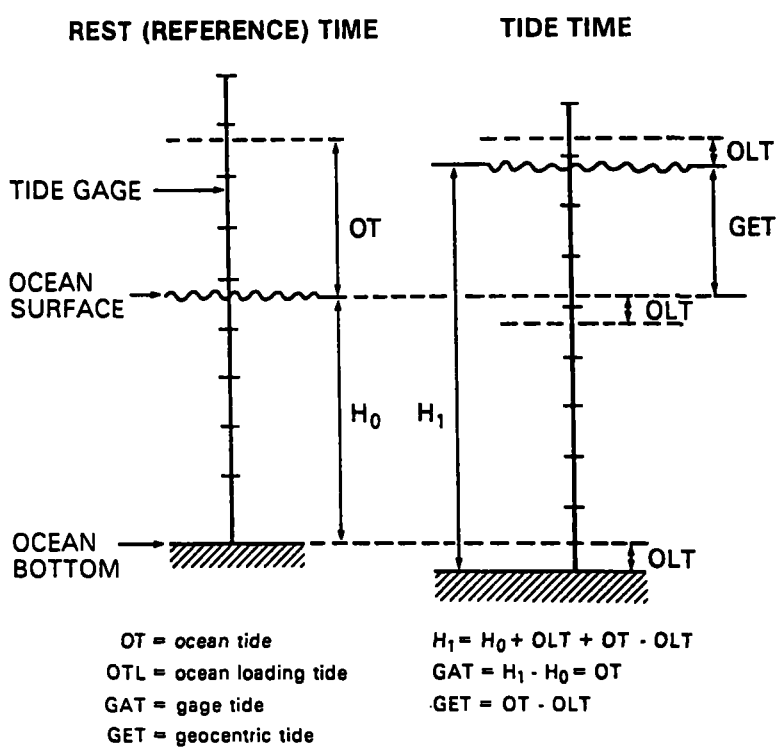

Figure 17.–Ocean, ocean loading, gage, and geocentric tides.

Note that the M_2 tide corrections here (without adjustment for the ocean loading) have a power of about 6 cm, so that a substantial correlation between it and the M_2 ocean load tide might be expected if the Schwiderski M_2 ocean tide model only has errors of order 1 to 2 cm, for example. But how well are the M_2 corrections here correlated with the OLT from Schwiderski's model?

Before giving this result I should discuss what is meant by the coherence or correlation of tide functions. In particular I have defined the tides in this study from a reference at the beginning of the ERM and not, in the standard way, from the time when the tidal argument is zero (conventionally stated as the time when the moon is at the Greenwich meridian). In the conventional notation (e.g., Schwiderski 1983) the tide is given as:

$$h = A\cos(wt - \gamma) \tag{12}$$

where w is the frequency (as seen on the Earth's surface) and γ is the phase (with respect to a tidal argument $wt = 0$). But if this same tide is given by C,S harmonics with respect to another reference time t_0:

$$h = C\cos wt' + S\sin wt' \tag{13}$$

where $t' = t - t_0$, which is equivalent in the standard (tide) notation to:

$$h = A\cos(wt' - \gamma') \tag{14}$$

where $A = [C^2 + S^2]^{1/2}$ and $\gamma' = tan^{-1}[S/C]$. Thus we see that if the tidal argument at the new reference time is $\alpha = wt_0$, the conventional phase of the tide γ (in terms of C,S) is:

$$\gamma = \alpha + \tan^{-1}[S/C] \tag{15}$$

Furthermore, appendix B shows that the coherence or correlation (r) in time between two tides of the same frequency but different phases γ_1 and γ_2 does not depend on their amplitudes but is just:

$$r = \cos[\gamma_1 - \gamma_2] \tag{16}$$

Another useful concept related to coherence is the compliance or best fit between two such tidal functions of amplitudes A_1, A_2 and phases γ_1 and γ_2. (This is also discussed in app. B). In terms of a linear accommodation factor (β) expressing the relation of one tide to the other:

$$h_1 = \beta h_2 , \tag{17}$$

I find that the least squares solution for a constant β (over a tide cycle) is:

$$\hat{\beta} = A_1\cos(\gamma_2 - \gamma_1)/A_2 \tag{18}$$

In fact, the load tide is indeed nearly a linear elastic response to the generating ocean tide in the deep oceans. According to the integrated Green's function approach of Goad (1980), the average coherence is nearly 90 percent for the deep ocean areas here. (See fig. 18a.) Using eq. (18) I find the least squares compliance factor between the ocean and load tides to be -0.052 on average for our best 1,652 stations, much smaller than the -10 percent recommended by Schwiderski (1980). More important though, I find the coherence between the actual tide correction for the best 4° solutions and the ocean loading to be much poorer but discernible. (See fig. 18b.) Using the Goad (1980) loading effect, the power of the 4° corrections is reduced from 5.71 to 5.53 cm, rms, a small but significant adjustment. Now let us examine this ocean load adjusted solution in detail.

THE M_2 OCEAN TIDE CORRECTION FOR 4° BY 4° AREAS

As previously described, an M_2 ocean tide correction to the Schwiderski (1983) model has been determined from Geosat difference altimetry at 1,652 4° by 4° deep ocean grid points to a calibrated accuracy of better than 5 cm. Figure 19a shows the power (rms) of these corrections. The power in a similarly derived solution from less than half of this data set averaged into 5° by 5° areas (Wagner 1989b) appears in fig. 19b.

The two solutions are consistent overall.. Evidently major corrections to the Schwiderski model are necessary in all oceans, particularly in their southernmost portions. Even in the North Atlantic consistently strong corrections are necessary for north of Brazil and in some areas west of Europe. Notice, however, that the new solution does eliminate a number of anomalously large corrections reported previously (in Wagner 1990) at scattered locations such as near Pakistan in the Arabian Sea, in the Central Pacific near Tahiti, and in the Sargasso Sea of the western Atlantic.

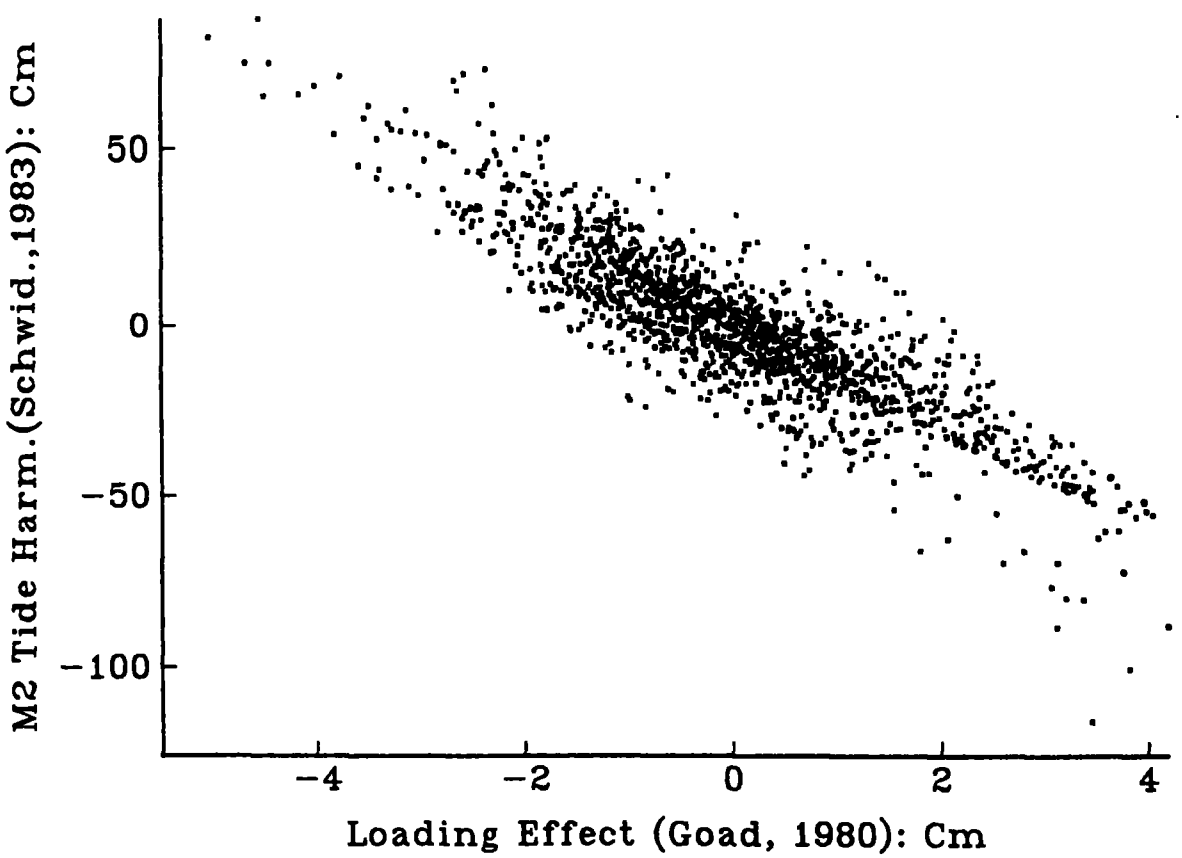

Figure 18a.–Correlation of full M_2 ocean tide and its load effect. Tide harmonics (C and S) are derived from Schwiderski (1983) for the 1,652 deep ocean stations with best solutions here (referenced to 8.0 November 1986). The ocean load tide was derived from the Schwiderski model by an integrated Green's function method (Goad 1980). Correlation here contains both C (tide) vs. C (load tide), and S (tide) vs. S (load tide). Average correlation coefficient for the pair of harmonics at a station is -0.88, the global average (rms): 0.80. Response of the ocean bottom to the tidal loading is evidently not perfectly linear. The best linear accommodation coefficient (β) to these data, however, is -0.052 (response = $\beta \times$ load).

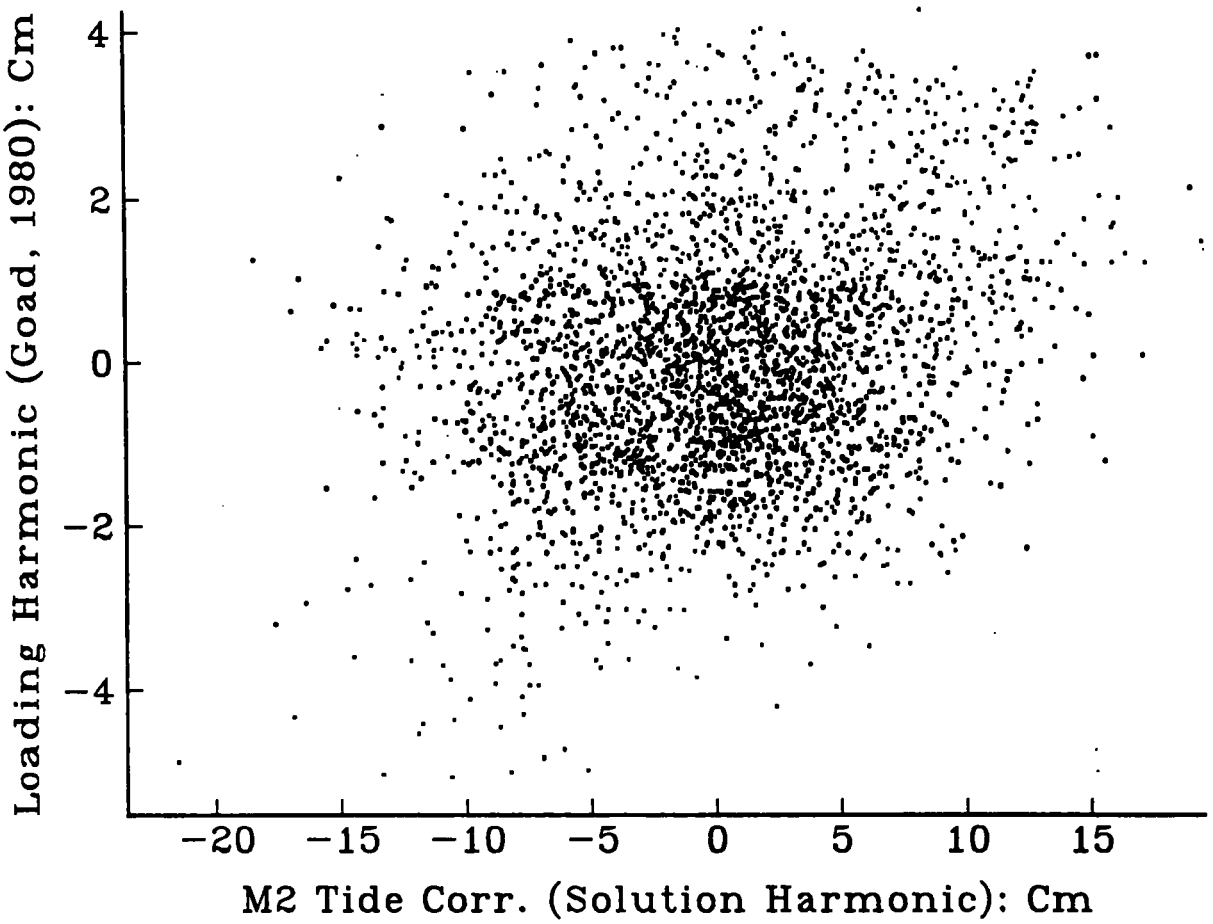

Figure 18b.–Correlation of M_2 tide correction and model ocean load response, showing correlation of *C* and *S* coefficients for M_2 correction tide [to the Schwiderski (1983) model] derived from Geosat overlap differences with the Goad (1980) ocean load response. This response was not included in original Geosat tide model. While the appearance here is of no correlation, the average correlation is actually 0.16, rms: 0.48. Furthermore, when the ocean load response is subtracted from the tide determined from the data, the power of the tide correction is reduced from 5.71 to 5.53 cm (rms).

Figures 19a,b also show the locations of the deep sea tide gages used by Schwiderski (1983) to compute (arrows) and calibrate (crosses) his own hydrodynamic-empirical solution. The tide gage data at these point locations all (are claimed to) agree to within 5 cm of the Schwiderski (1983) model used on the Geosat GDRs. It is evident that most of these gages cannot be used to test the Geosat solution here, but of the ones that can, it appears the new 4° by 4° corrections agree with more than twice as many gages as those with which they disagree. The earlier solution (Wagner 1990) was less compatible with the gages, using even fewer reasonable tests. It should be emphasized that the tide gages give point readings of the tide, but since the tide is generally a long wave phenomenon (see below), the point values should be valid over a wide area (5° to 10°), although perhaps not with 5 cm accuracy.

We can appreciate the most significant Geosat results if we concentrate only on those corrections which are, say, greater than 10 cm and have signal-to-noise ratios better than 2:1. [Recall the average correction is only 5.4 cm while the average noise level is about 3 cm (fig. 15)] Figure 19a depicts these grid points filled with asterisks. Note their concentration north of Brazil, which, because the tide is especially energetic in Schwiderski (1983) does not cause a particularly major change in that model there. It is still disconcerting though to see what we consider to be these most significant corrections seeming to disagree with the tide gage data at two locations in the eastern and western Atlantic. These two grid points have a fair, if not the best, data representation (fig. 8c) in the current solution.

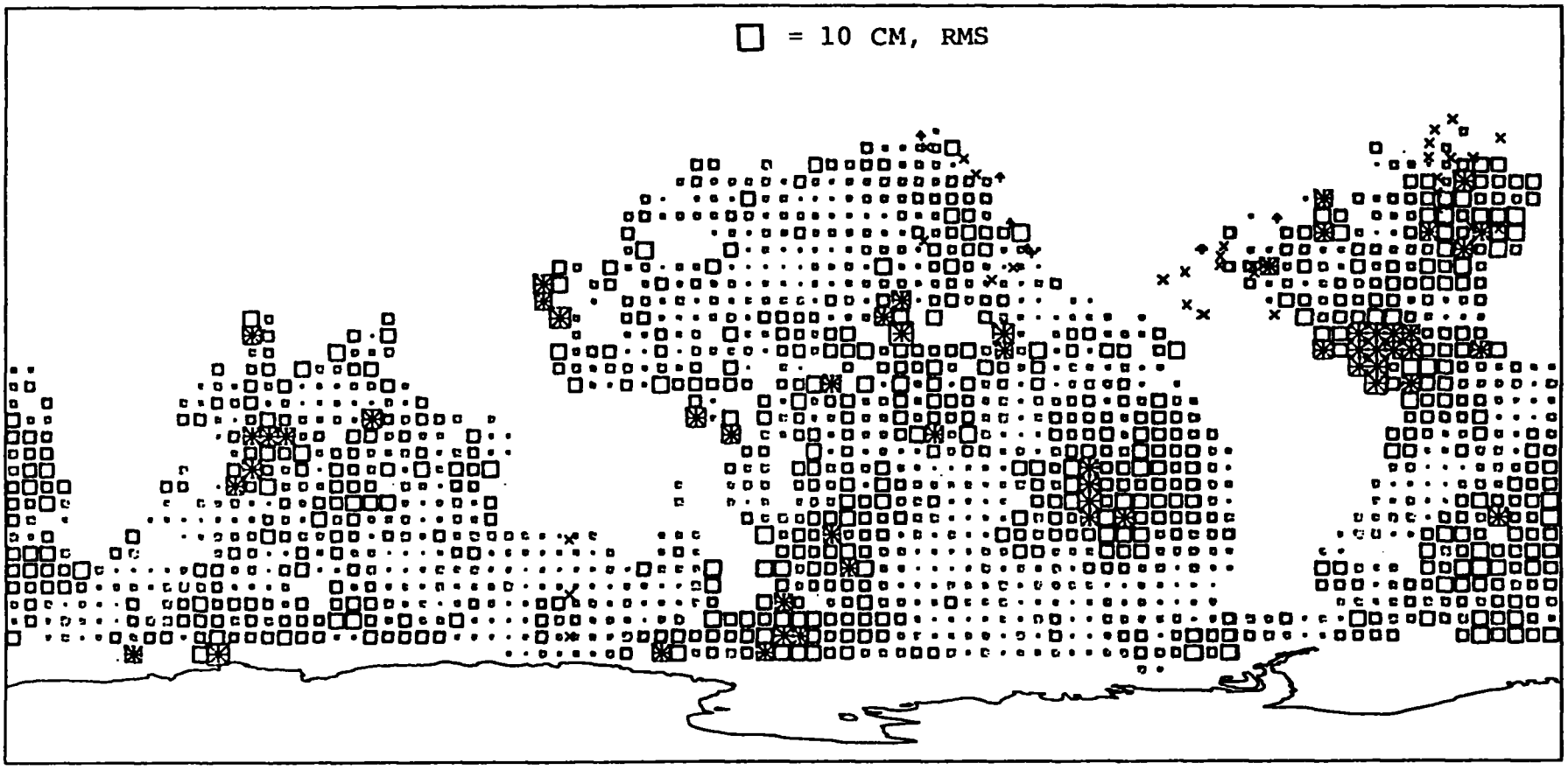

Figure 19a.–Best M_2 solution power (ocean tide only) from 4° Geosat altimetry. The size of boxes centered on deep ocean stations scales power of determined solution. Only solutions with calibrated errors less than 5 cm (rms) and containing 10 or more passes are shown. Ocean load tide [computed from Schwiderski (1983) model] was removed from these data. Maximum power over 1,652-station solutions here is 14.59 cm (rms). Also displayed are locations where point ocean tide gage data have been found to be compatible to Schwiderski model within 5 cm (crosses). Location of additional gage data (arrows) is also shown. These gage results are reported to be similarly agreeable with the Schwiderski model, but at these locations that model used these data. Comparing the Geosat power solutions here with gage locations unused by Schwiderski, I find that of 37 distinct gages (with respect to 4° grid here) only 26 are directly verifiable by the Geosat solution. Of these, 10 agree and 5 disagree (fall too close to grid points showing greater than 10 cm corrections, rms). Without detailed interpolation of my solution, I cannot decide upon compatibility of 11 tide gage locations.

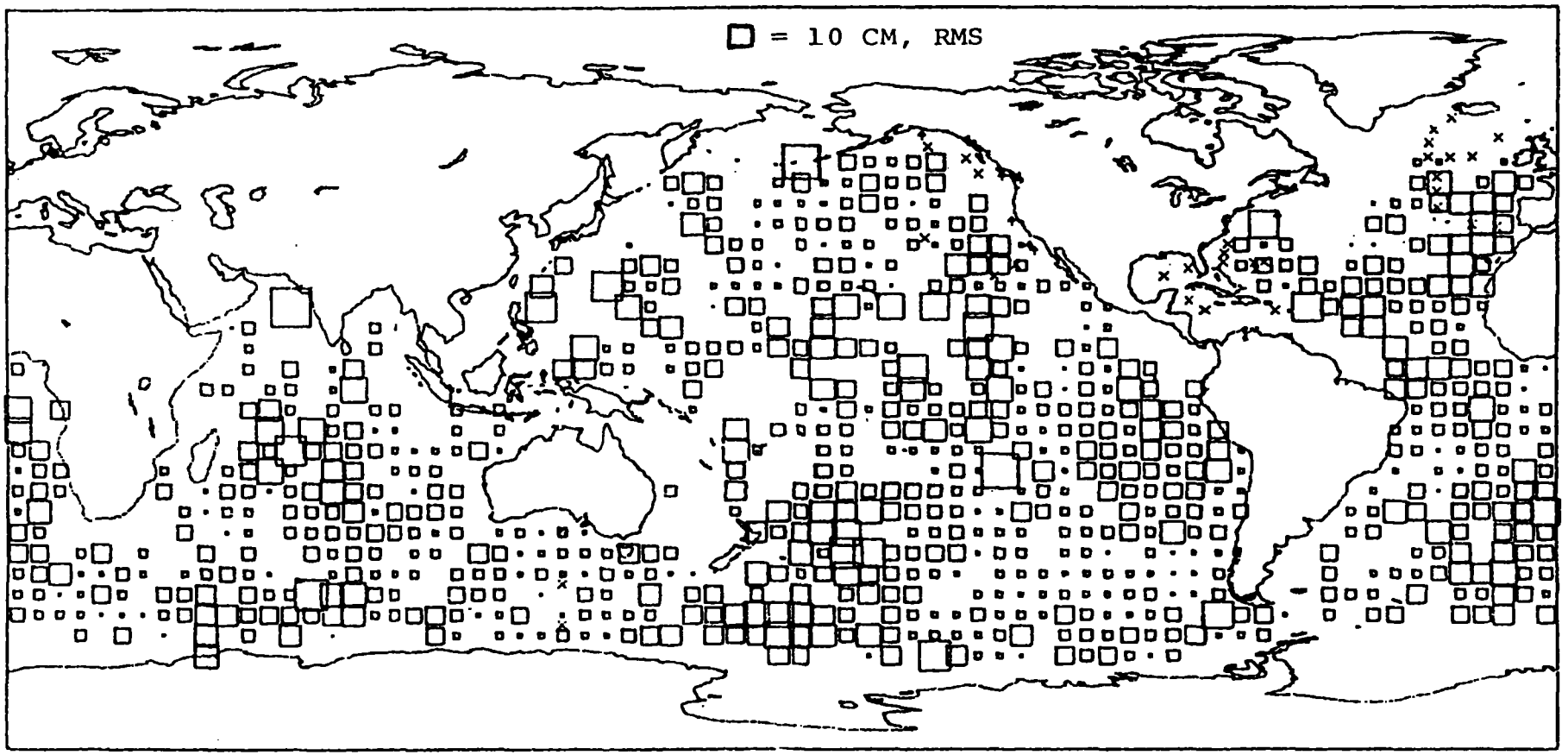

Figure 19b.--Best M_2 solution power (ocean tide only) from preliminary 5° Geosat altimetry. This is the solution reported in Wagner (1990) from about half of the data analyzed here (but here with ocean load removed). The method of solution from the differences of overlapped altimetry is otherwise the same. Maximum correction power (for 5° averages) is 15.30 cm, rms. Of 35 distinct gage locations (with respect to 5° grid) only 18 are directly testable by this (sparser) solution. Of these, four agree with it, six disagree, and eight cannot be decided without detailed interpolation of gridded solution (compare fig. 19a).

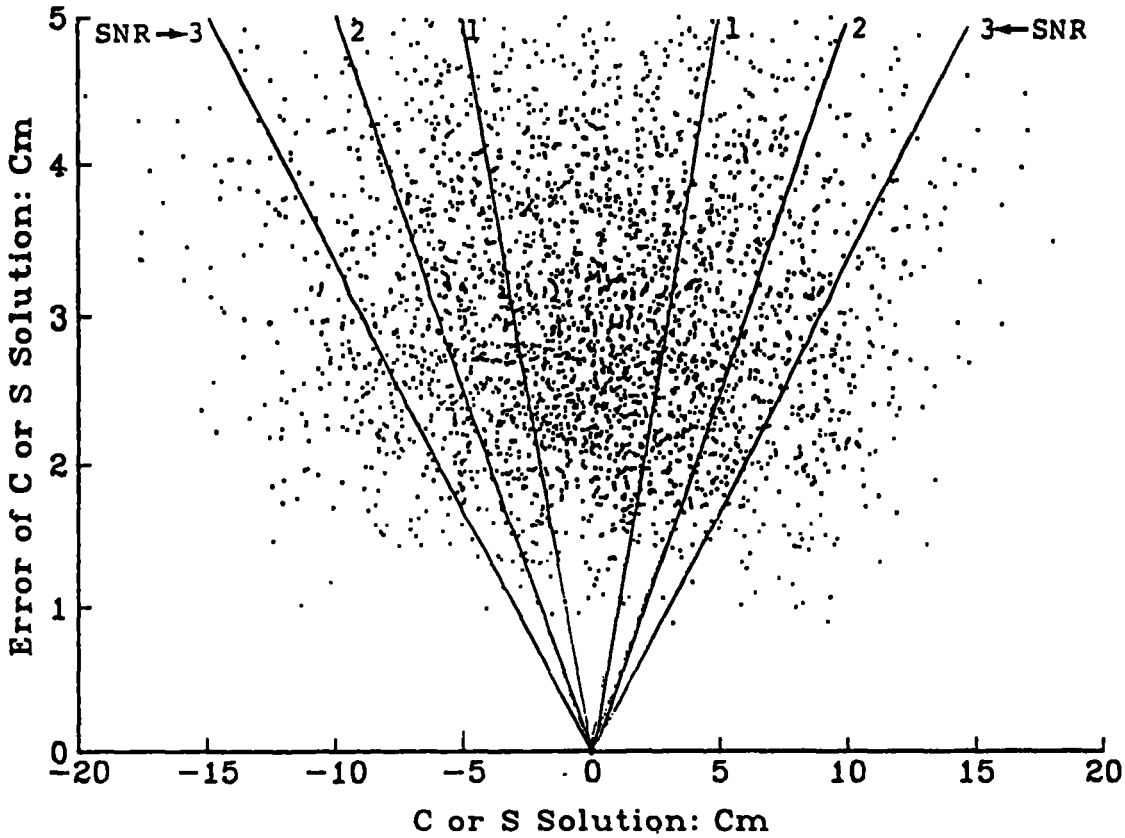

Figure 19c.--Comparison of Schwiderski's model with Geosat solution for M_2 ocean tide. X-axis coordinates are Geosat *C* and *S* corrections to the Schwiderski model. Their corresponding calibrated errors are given as y-axis coordinates. Lines radiating from zero on x-axis divide the space by signal-to-noise ratio. Thus all points falling outside the lines SR = 1 refer to corrections that have significant signal-to-noise ratios (e.g., >1), about half of the 1,652 grid point solutions here (all of which have calibrated errors less than 5 cm).

A further breakdown of the signal-to-(calibrated) noise ratio of these best (less than 5 cm error) solutions suggests that over half have ratios greater than 1 (fig. 19c), but since the average power is still small (5 to 6 cm, rms) the overall effect on the Schwiderski model is minor. Still, since virtually every area of the deep oceans is covered by these calibrated Geosat solutions it is interesting to compare the complete M_2 ocean tide from Geosat with the original model. Note that since nonlinear effects are not expected to play a prominent role in the straightforward metric solutions here (aside from the orbit error distortions, whose remedy is discussed at greater length below) the Geosat solution might as well have been made from a zero tide model on the GDRs.

Before comparing the full Geosat model I computed a covariance function for the corrections and compared it to a similar one for the Schwiderski model over the 1,652 best grid points used. The intent was to see if the solution possessed the well known long-wavelength (20° to 30° correlation length) property of tide models that have peak power at low global wave numbers.

Figure 20a shows the short distance covariance function for the M_2 corrections (before ocean load was removed) from the independent 1/4 data sets described above in connection with the calibrations. These are consistent and have the long range characteristics expected of a "real" tide correction. Since the most serious nontidal signal in the overlap differences arises from orbit error, and this has been removed empirically, we do not attribute this "tide-like" power decline to anything but tide. Certainly the cycle power

variation with close to 1-year period (fig. 9a) strongly suggests a tidal effect although Geosat data should be taken for another year to confirm it.

The covariance function (in fig. 20a) is computed as a sum of the covariances for the separate harmonic components of the tide among the set of 1,652 station solutions. The tide has both time and space variation (unlike a stationary function on a sphere) but, as shown in appendix B, if I define the spatial covariance for it to be its time average (of averages with respect to the usual fixed distances) then the conventional spatial covariance is obtained by merely averaging the sum of the products of similar harmonic components over all equally spaced data.

By taking the covariance of separate cosine and sine components of my solution, I found (fig. 20b) a significant difference between them, the sine components yielding a smaller covariance function (and smaller correlation length). Figure 20c shows the full function for the complete solution (1,895 stations) and it also displays (at a lower level) behavior typical of functions (like the tide) that are long-wavelength dominated.

In this regard, I also computed the covariance function for the Schwiderski (1983) model evaluated at the same grid points (with sample density shown in fig. 20d). Figure 20e shows the global result with the same long wave past the initial correlation length (of about 25°). Note the rather large fluctuations at both ends of these global covariance functions are undoubtedly due to the sparse sampling for these distances which were computed for multiples of only 1° while the grid spacing here is 4° (equiangular). Thus lags of less than 4° are represented poorly, arising only from the converging grid points at high latitudes.

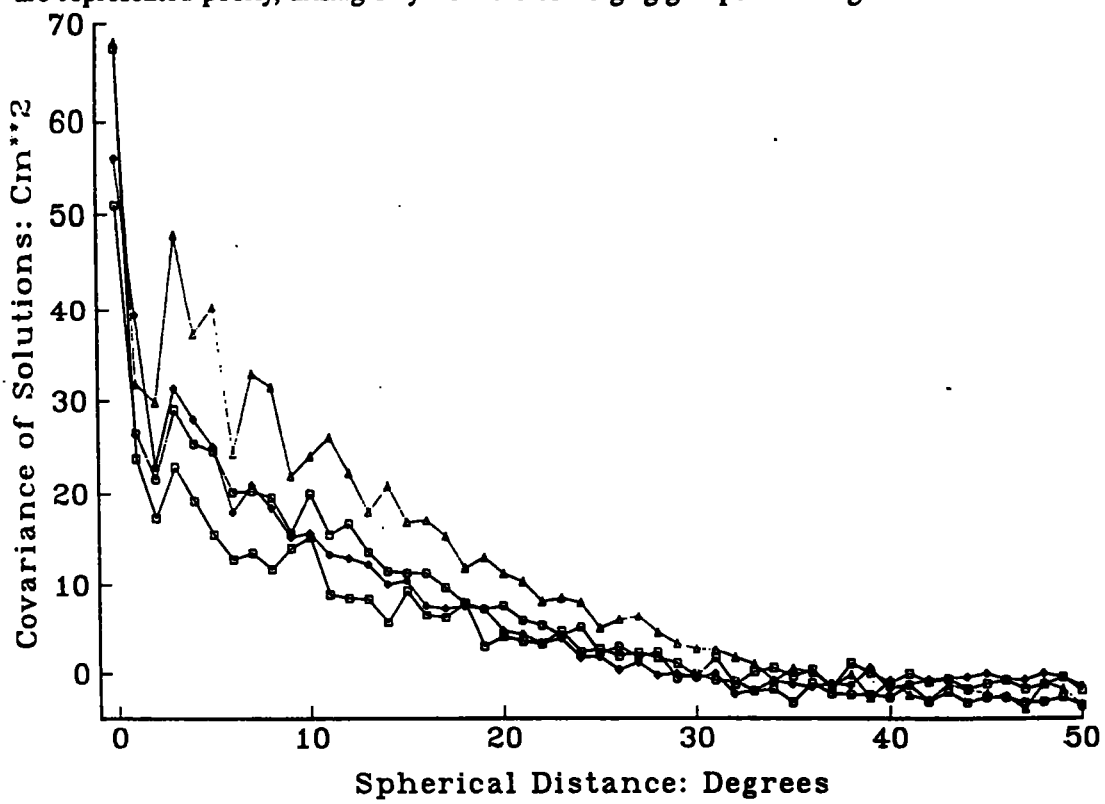

Figure 20a.–Covariance function for M_2 correction solutions: C vs. C plus S vs. S combined. These are the covariance functions for the four independent 1/4 subset M_2 solutions from 4° averaged Geosat altimetry (overlapped differences). Triangles give the function for subset C_1 (using 1,184 stations) octagons for subset C_2 (using 1.245 stations), triangles for subset D_1 (1,105 stations), and boxes for subset D_2 (1,189 stations). Since the data are on a 4° gride (equiangular) the covariance for 1° through 3° are poorly sampled (at high latitudes only). Note the correlation length of these solutions is about 30°.

Once again the similarity in structure of these global functions argues strongly for the tidal origin of my solutions. Most persuasive of all to this argument is the fact that the local covariance function for the Schwiderski model (fig. 20f) also exhibits a similar separation of cosine and sine functions. My solution has evidently made its greatest correction to the Schwiderski model away from the amphidromic areas where the model is most powerful.

There seem to be two phenomena that contribute to the separation of component covariances. Note of course that the definition of C and S is arbitrary, depending only on a fixed epoch for the tide. But the existence of amphidromes in the deep oceans (with the tide circulating around them) strongly suggests that the tide acts resonantly (in concert over at least basin scales) rather than simply passing over the oceans from east to west in simple response to the equilibrium tide under the moon (e.g., Schwiderski 1980). Indeed one of the features of the tide's response is that at the longest periods its spectrum has more and more (relative) power at the lowest wave numbers (Christodoulidis *et al.* 1985) or equivalently more and more correlation at the longest, even global wavelengths. Recall that the M_2 power spectrum peaks at wave numbers 4 to 5 for example. Thus the separation of cosine and sine power appears to be fundamentally due to the global or long wave character of the deep ocean tide and secondarily to the arbitrary definition of the tidal phase. (Thus if another reference time had been chosen for the phase an even greater separation might have been seen or, more likely, less.)

To gain insight into the long wavelength correlation of the M_2 tide, I compare (fig. 21a) the C and S coefficients of the Schwiderski (1983) model evaluated with respect to an epoch at 8.0 November 1986 and for the 1,652 4° grid points of the "best" Geosat solution. The distribution seems to be composed of two sections, an extreme and sparse outer part for which a positive C,S correlation exists and a dense inner part which is characterized by a significantly wider range of C values than S. Both of these features are strong indications that the global M_2 tide is not random. I can illustrate this non-randomness in another way which also shows how the Geosat M_2 correction is "aligned" with its parent model.

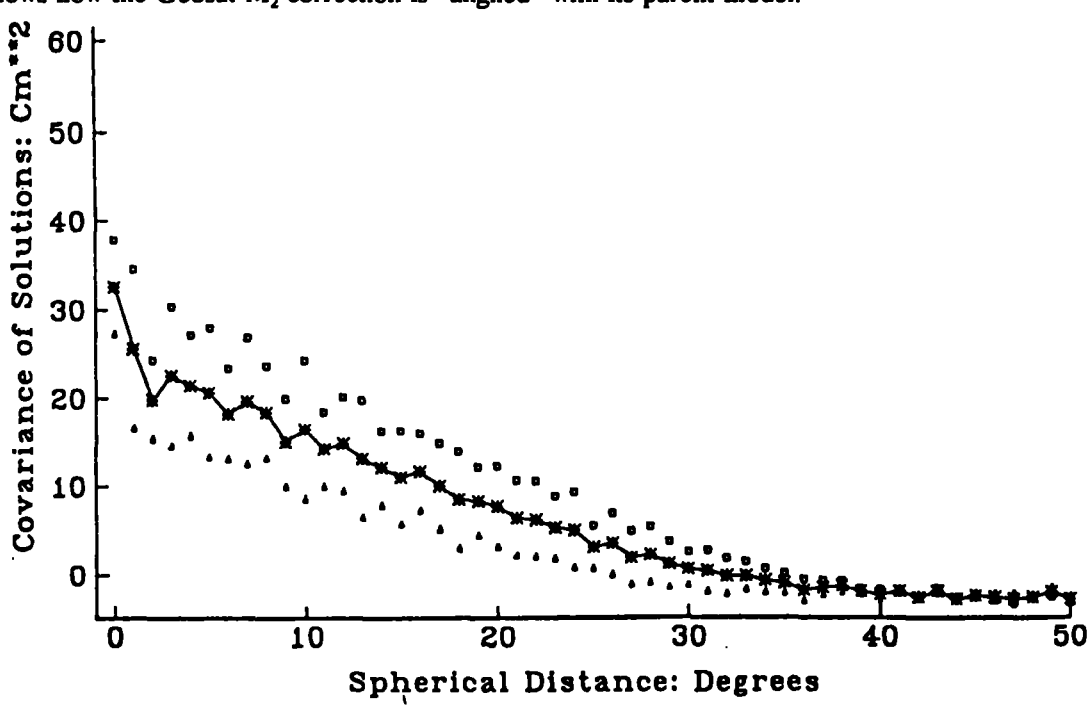

Figure 20b.–Covariance function for M_2 solutions for full 4° data set: C vs. C, S vs. S, and combined. These functions are determined from the 1,652 solutions with calibrated errors less than 5 cm, rms. Boxes give the covariance for C vs. C, triangles give the covariances for S vs. S, and asterisks give the combined result. The separation of C and S is an artifact of the chosen tide epoch.

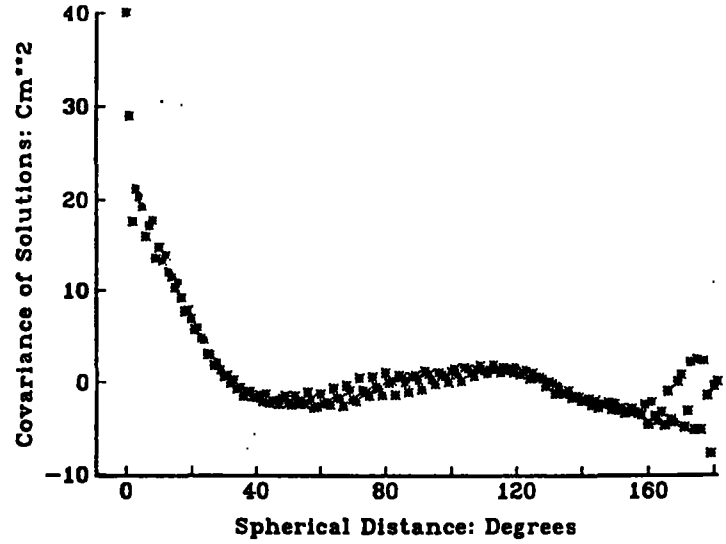

Figure 20c.--Covariance function for all M_2 corrections from 4° Geosat altimetry: C vs. C plus S vs. S. Solutions at 1,895 deep ocean stations were examined for 1,796,400 covariant samples. Instability at largest spherical distances is due to lack of adequate sampling for these separations. Note long oscillatory wave after 40°, another long-wave attribute of deep ocean tide behavior.

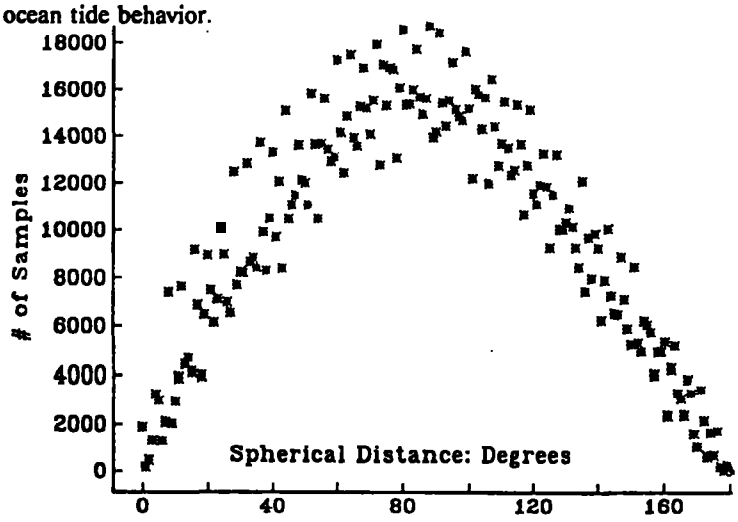

Figure 20d.--Relative strength of full (1895 station) M_2 correction covariance function. Note that at both close and distant separations the covariant sampling is relatively weak.

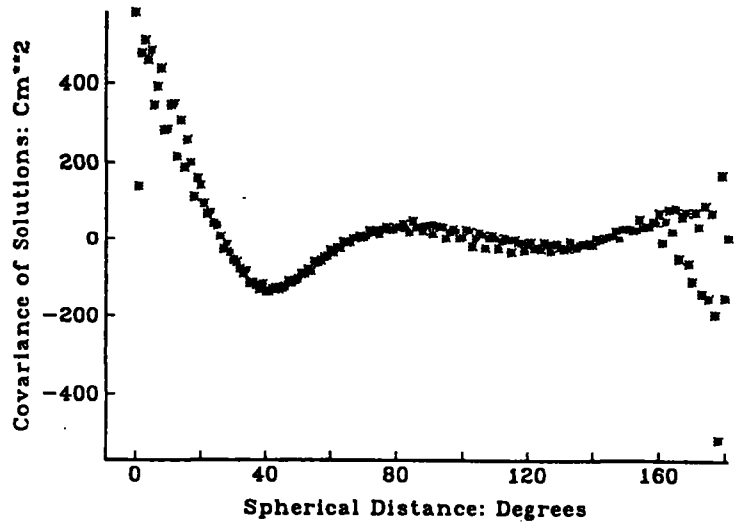

Figure 20e.--Covariance function for the original Schwiderski M_2 model: C vs. C plus S vs. S, evaluated at the same 1,895 deep ocean grid points (4° by 4°) as for the correction solution (fig. 20c). Note similar instabilities at both ends of the distance range. The long wave beginning at the correlation length (about 25°) is, like the correction function (fig. 20c), indicative of a tide with considerable coherence on a global scale.

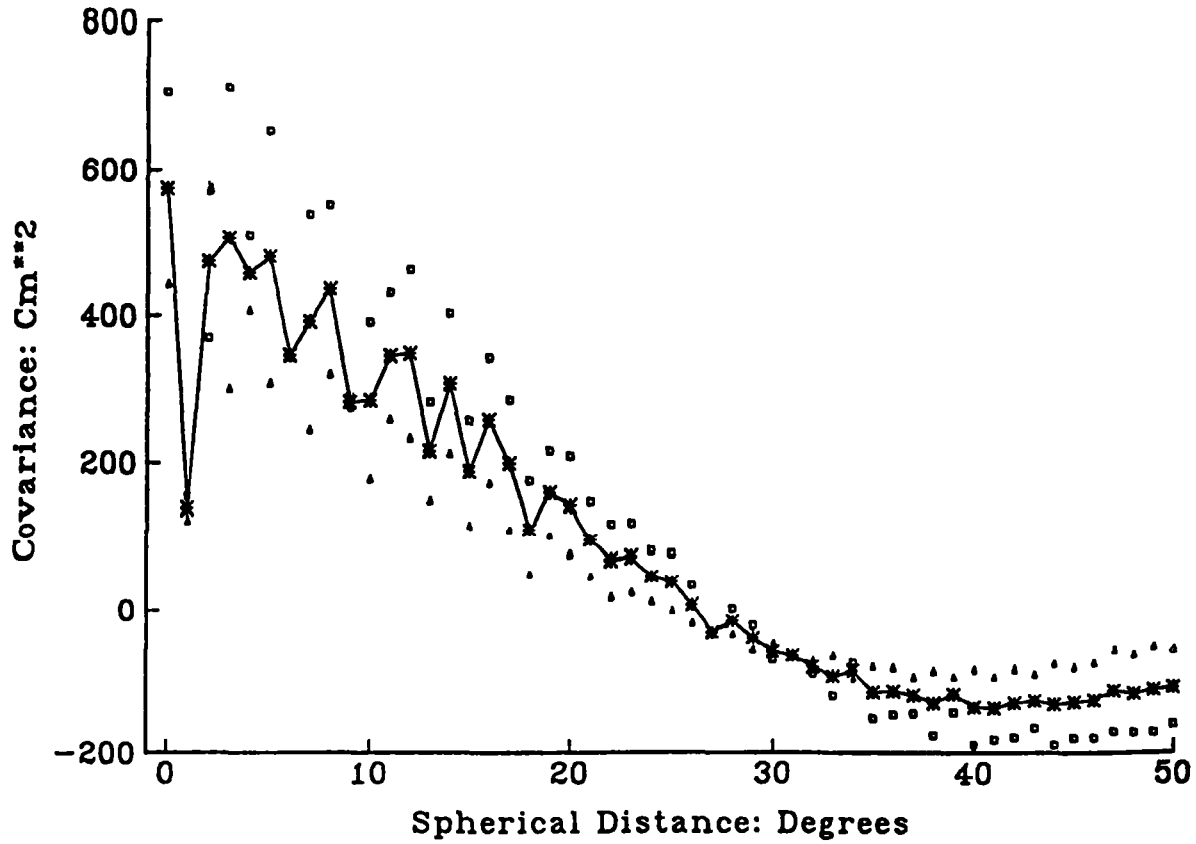

Figure 20f.--Covariance function for Schwiderski 1983 M_2 tide: C vs. C, S vs. S, and combined. Samples are taken over 1,652 stations of the best M_2 corrections from Geosat altimetry. Boxes give covariances for C vs. C, triangles for S vs. S, and asterisks for the full tide. Power (at zero separation) corresponds to variances of 24^2 cm^2. Note same separation of C and S functions as seen for corrections (fig. 20b). The anomalously low value at a separation of 1° is due to poor sampling. (See fig. 20e.)

Figure 21b shows the global power of the harmonic coefficients of these solutions under phase rotations. If the tide had no long-range correlation the global power would be the same for both C and S with any phase definition. The interesting aspect of fig. 21b is that the M_2 correction tends to cohere (in phase as well as amplitude) with the original model. This aspect of the solution is what I would have expected for corrections to a fundamentally valid (long-range) tide model. A direct comparison of the full correction power to the original Schwiderski power for the "best" solutions also shows this tendency, that the largest corrections occur where the original model is most powerful. (See fig. 21c.)

Note also in passing that the M_2 ocean tide correction computed here acts to increase the power of the Schwiderski (1983) model by about 5% (deep ocean average). Since I expect my corrections to be underestimated from a loss of some power to the (uncoupled) orbit solution, this increase may in fact be larger and is certainly a significant finding.

Now I want to examine the global properties of the new Geosat M_2 ocean tide compared to the Schwiderski (1983) model. For this purpose I show only what is known as the co-range of the tide (its full excursion, twice the amplitude) since this parameter brings out the locations of the amphidromes (node points of zero tide) as well. I will show that in spite of the undeniably long-range nature of my tide correction (a realistic feature), there is still a good deal of short range jitter in it, which arises from the significant errors still remaining in the solution. In viewing these comparisons remember that the maximum

calibrated error in the Geosat computed errors for the range should be 10 cm (twice the coefficient error maxima).

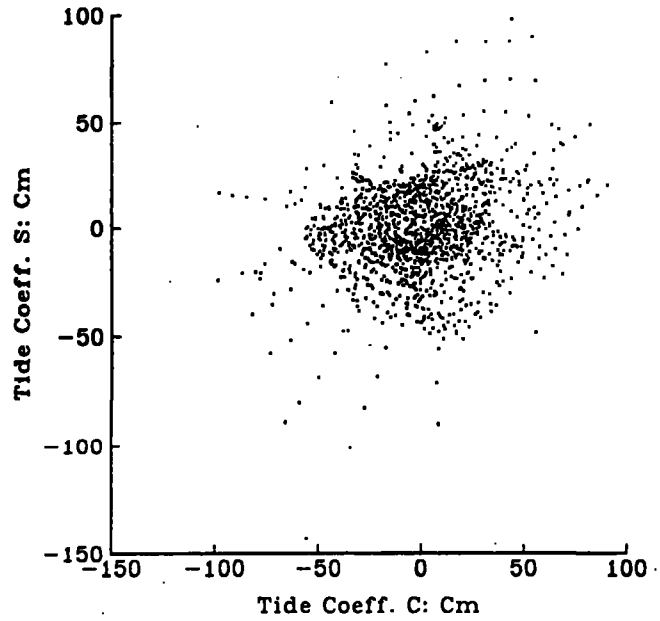

Figure 21a.–Correlation of Schwiderski (1983) M_2 tide model: C vs. S. The epoch for the tide harmonics is the start of the Geosat ERM (8.0 Nov. 1986). The correlation has two dominant aspects. More powerful tides (away from the amphidromes) are generally positively correlated among these phases (defined by the ERM epoch). Tides of generally low amplitude are significantly stronger in their C components (also with a slight positive correlation with respect to S). Both of these aspects are attributed to the long-range nature and coherence of the tides in the deep oceans.

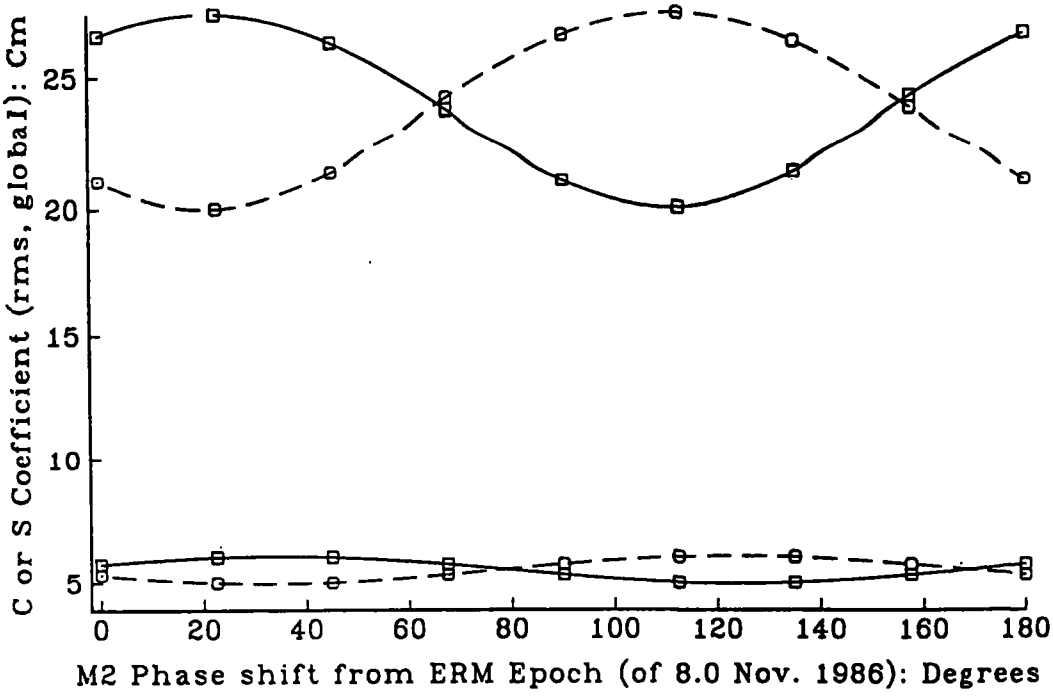

Figure 21b.–M_2 ocean harmonics: Schwiderski (1983) and Geosat corrections. Upper curves give change of global power for cosine term of Schwiderski model (solid) and the sine term (dash) when tide epoch is changed through half an M_2 cycle (6+ hours). Bottom curves give similar power changes for Geosat M_2 corrections. Note how the two sets of curves change in synchronism over these M_2 phase changes. The C corrections are strongest where the C term is strongest and similarly for the S term and its corrections. This in-phase behavior implies thereis little overall change in the tidal phase from the Schwiderski to the Geosat model.

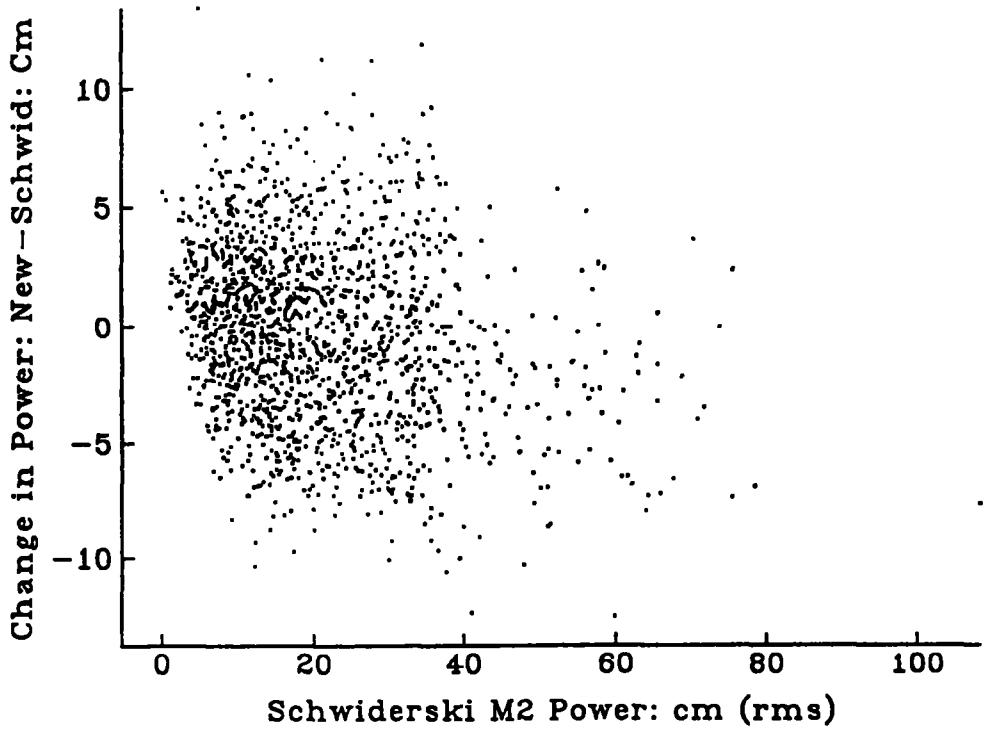

Figure 21c.–Power correlation: change in power vs. Schwiderski power. Data are for 1,652 correction solutions whose calibrated errors are less than 5 cm (rms). Average power change in the new solution is -0.18 cm. The Schwiderski model power for these stations is 23.98 cm, rms. The new solution power is 23.63 cm, rms. Note slight negative correlation of these data overall, the greater the original tide power the greater the tendency for the solution to reduce that power.

CO-RANGE OF M_2 OCEAN TIDE IN THE WORLD'S OCEANS

Figures 22a-c show the co-range for the Schwiderski (1983) model compared to the preliminary 5° by 5° Geosat solution (Wagner 1990) and the current 4° by 4° refinement for the Indian Ocean. The most significant changes to the Schwiderski model appears to be the more powerful high in the middle of this ocean and the elimination of the (weak) amphidrome in its southwest sector. Note in fig. 22b the central Indian Ocean high has increased in power, but the low tide regions remain roughly where they were in the Schwiderski model. Note also the significant jitter of the corrected solution which appears to be compatible with its calibrated errors (maximum: 10 cm). It is interesting that this jitter exists even though the corrections themselves have a long-range correlation. (See figs. 20b,c.) Evidently on the shortest scales (less than 10°) the Schwiderski model covariance function (not well sampled in fig. 20f) is much smoother than the correction solution (also not well sampled as in fig. 20b for the 4° data set). This jitter will only be reduced when more overlaps are analyzed.

No significant features distinguish the Schwiderski and Wagner models in the South Pacific (figs. 23a-c), keeping in mind the Geosat solution is entirely empirical and as such suffers from evident observation jitter.

Figures 24 a-c compare the solutions for the South Atlantic. Aside from an overall decrease in power, there appears to be no significant change in the overall features of the Schwiderski model. The major change from Schwiderski is the reduction in range power over this zone, from 76.7 cm (rms) to 72.7 cm (rms). There is also a hint of a second articulated high tide zone off Africa just south of the equator compared to Schwiderski. Again, in figs. 25a-c the Schwiderski (1983) model remains essentially unchanged in the Geosat solution for the North Atlantic except for an overall reduction in power. Finally, I reach the same conclusions in viewing figs. 26a-c for the North Pacific except that here a small overall increase in power is evident.

DISCUSSION

From many comparisons and extensive analysis, the current Geosat deep ocean M_2 solution appears to be a generally satisfactory correction to hydrodynamical-empirical models based on theory and scattered boundary tide gage data. Since the corrections to these non-altimetric models are so small however (averaging about 20 percent) with the great majority of them less than 10 cm (rms correction) the problem of verification becomes acute. Simulation has shown that a major contribution to error in the current Geosat solution probably arises from the absorption of tidal signal in the (uncoupled) orbit error correction to the difference data prior to the tide solution. This aliasing is an artifact of the long-range nature of the global tide and is not inherent in any given point tide variation determined (as here) empirically. Thus the 12.4206-hour tide period at any ocean point is quite distinct from the 1.67 hour orbit period which carries the principal orbit correction effect.

Unfortunately the proper coupling of the many piecewise orbit corrections for the windows of the ERM examined here would have resulted in a burdensome fairly full matrix reduction which, for the purposes of demonstrating the power of the method, I felt was not worth the programming effort at this stage of the analysis. In particular, I have demonstrated through extensive calibration that the solutions are sufficiently accurate to convey a wealth of important new information. Future solutions will undoubtedly need the proper (simultaneous) elimination of orbit effects because, as figs. 5c,d show, these errors of the solution are distortions of global scale.

Another important technical improvement in the method that promises significant benefits in both reducing the bias in the solution and increasing its signal-to- noise ratio is the inclusion of reference pass bias parameters at each station. Without these the data errors are inherently correlated and, on the average, $\sqrt{2}$ greater than they should be with these parameters.

A third important improvement to the solution should be a further densification so at least the full aliased M_2 tide period of 317 days will be equally represented. The data power-by-cycle analysis (figs. 9a,b) clearly shows the need for an M_2 correction, but its implications should be verified by data in the second year of the ERM as well.

A further needed improvement is the extension of the solution to shallow seas where there are acknowledged deficiencies in the theoretical model (Schwiderski 1983). These areas, such as the Patagonian shelf and the Bering Sea, are important not only because the major part of the M_2 tidal energy is thought to be dissipated there (slowing the Earth's rotation) but also because these tidal errors have had an adverse impact on altimetric determinations of geopotential anomalies in these areas (R. H. Rapp, private communication, 1989).

SUMMARY AND CONCLUSIONS

More than 4,000,000 Geosat altimetric observations of sea height were examined in 1986-87 (mostly) to determine significant corrections to the M_2 ocean tide at 1652 deep ocean 4° by 4° grid points. The solution was calibrated by as many as nine independent subset analyses and by comparisons with tide gage records. The M_2 tide at the 1,652 grid points is estimated (thereby) to be accurate to better than 5 cm.

The correction solution has been adjusted for ocean loading and shows that an earlier theoretical-tide gage empirical model is accurate to 5.5 cm (rms global) in the deep oceans. The results show the features of the theoretical M_2 model are essentially unchanged but that its power should be increased by about 5 percent (deep ocean average).

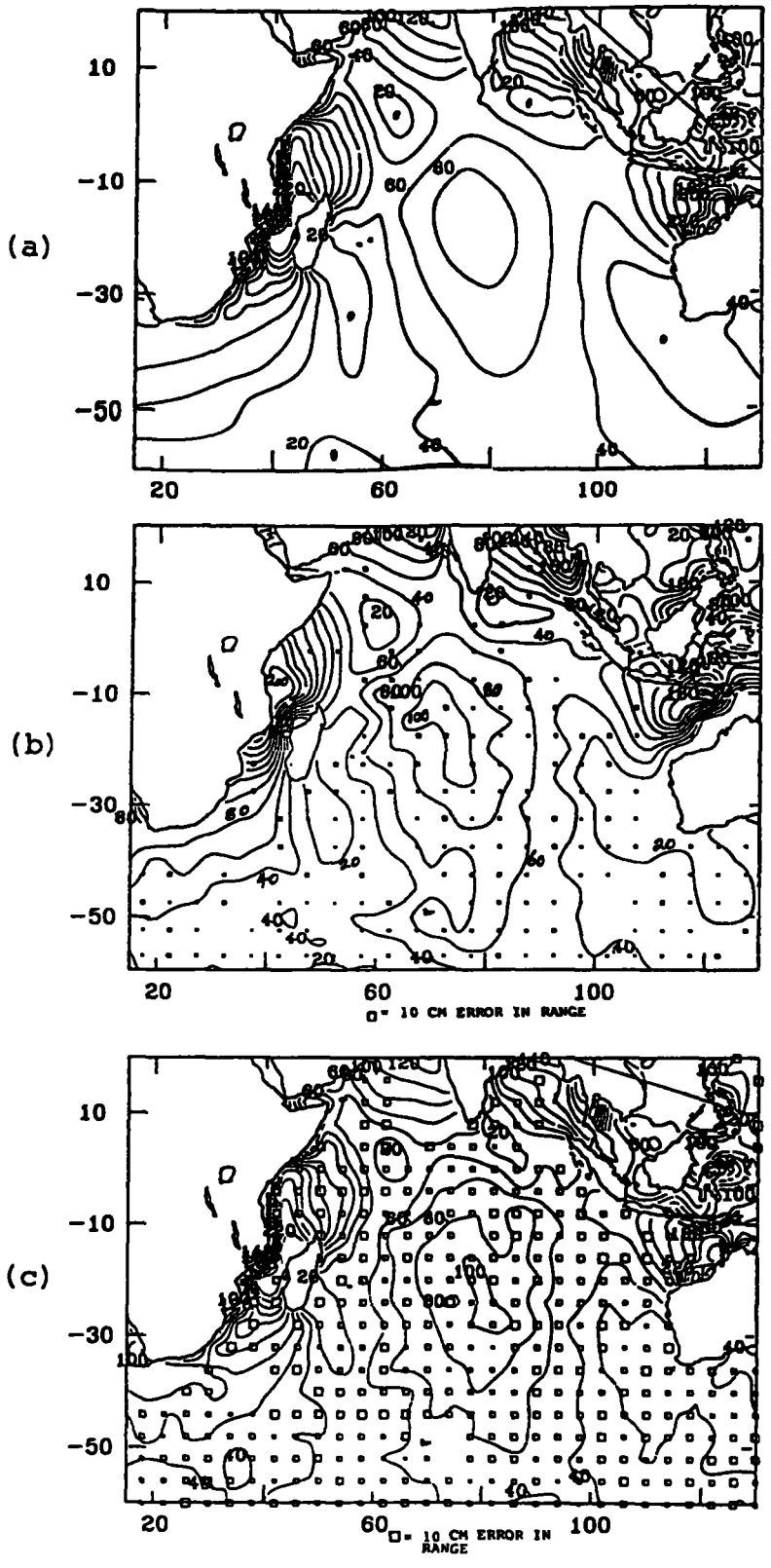

Figure 22.–(a) Schwiderski M_2 tide ranges (in cm) in Indian Ocean. Note single high-tide area in the center of the ocean and the five amphidromic (zero) tide zones rimming the ocean. (b) Geosat-corrected ranges show preliminary solution (in cm) [from Wagner (1989)]. Small boxes show grid points where "best" solutions were obtained (with calibrated errors less than 5 cm, rms). Sizes are scaled to the errors (0.05 in. = 10 cm in range). (c) Geosat-corrected ranges for Indian Ocean show 4° solution in centimeters. This is the result obtained from 1,652 stations with best determined solutions. Enhancement of the central Indian Ocean high remains. Amphidromic area in southwest quadrant has disappeared, but otherwise the overall features of the Schwiderski model are unchanged. The range power in this ocean has been increased from 71.3 (rms) in Schwiderski (1983) to 73.3 cm.

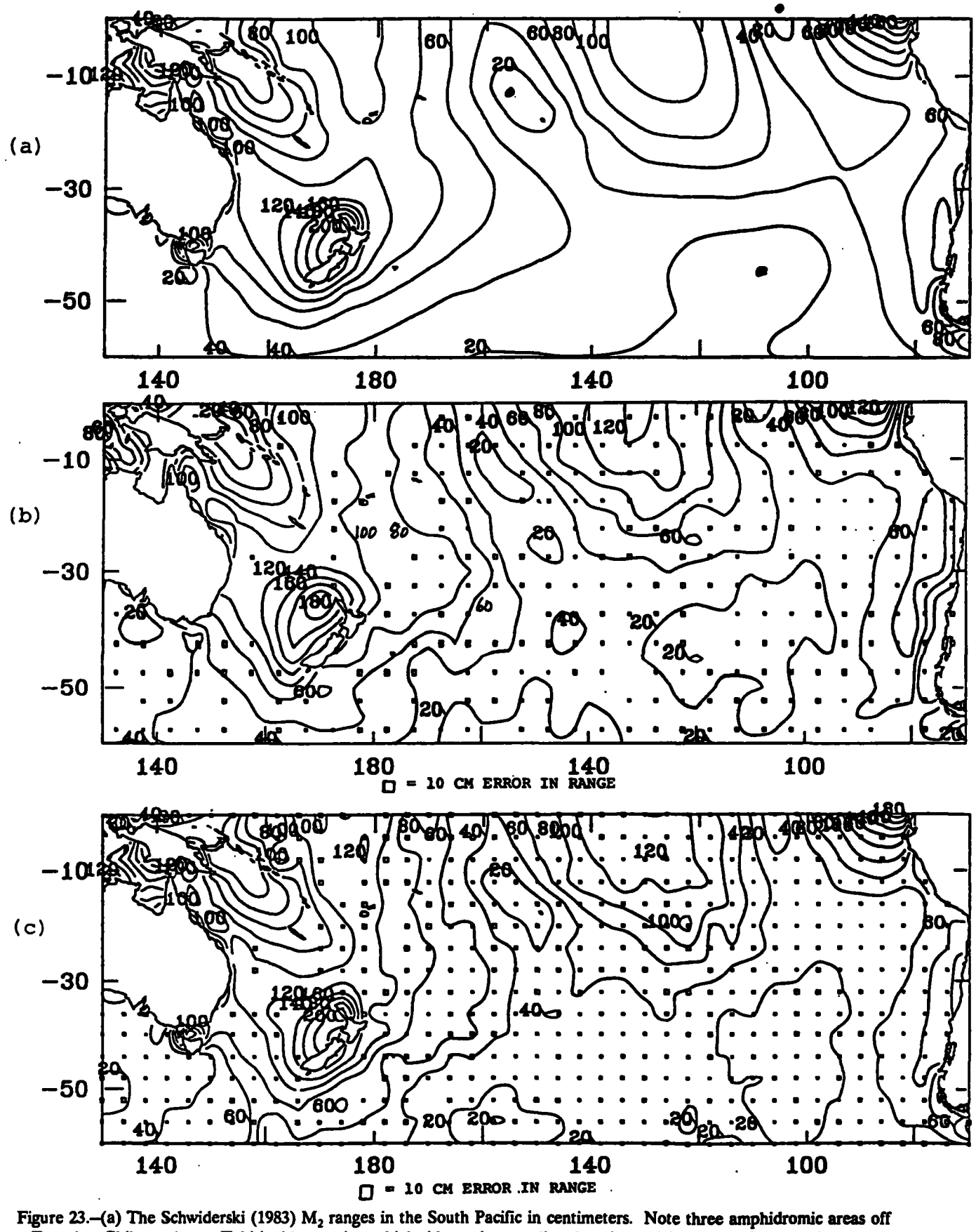

Figure 23.–(a) The Schwiderski (1983) M_2 ranges in the South Pacific in centimeters. Note three amphidromic areas off Equador, Chile, and near Tahiti with prominent high tides at intermediate locations. (b) Geosat M_2 ranges in the preliminary 5° solution (cm) for the South Pacific. (c) Geosat M_2 ranges in the current 4° solution (cm) for the South Pacific. Except for the jitter in this wholly measured tide, the features of the Schwiderski model remain essentially the same.

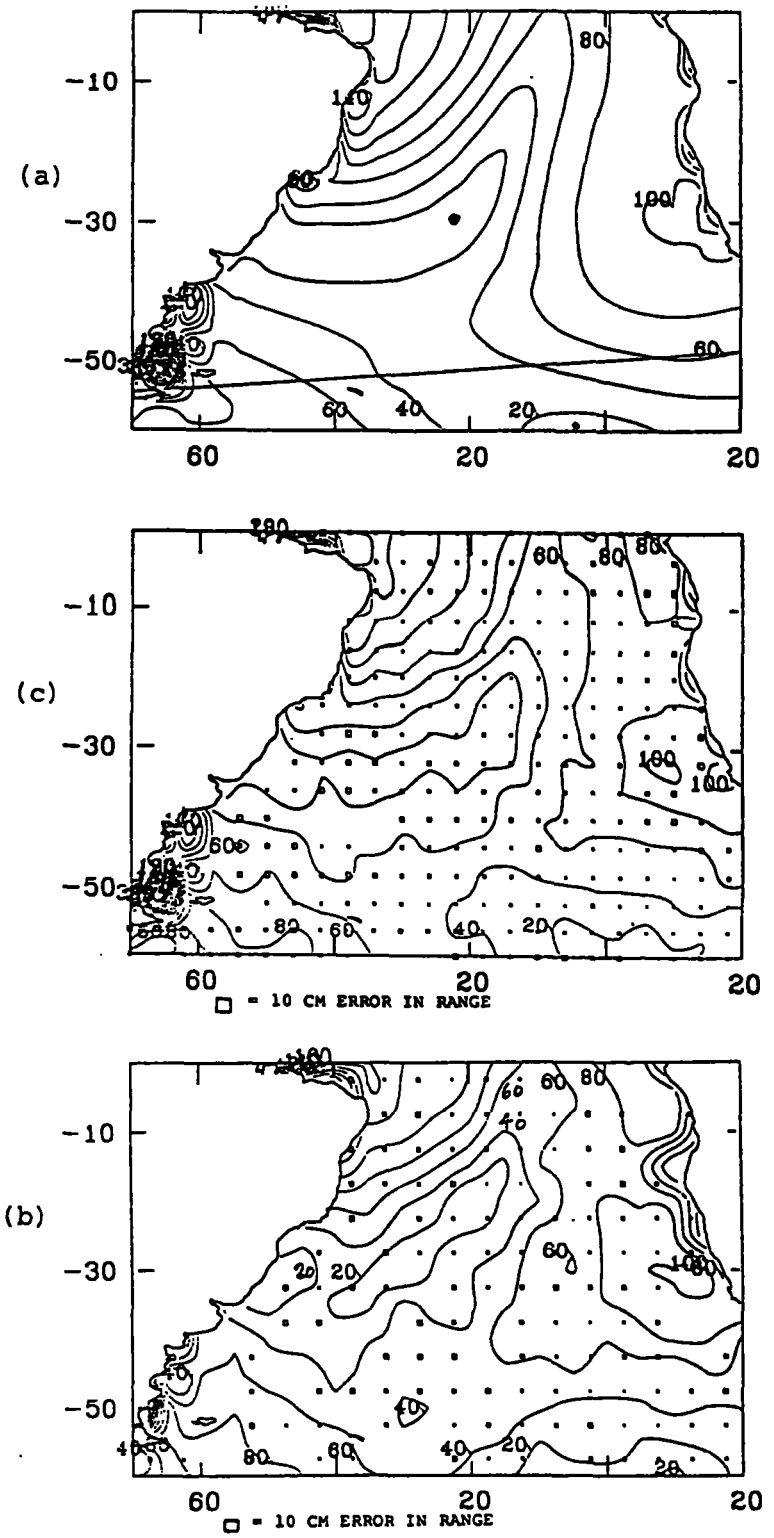

Figure 24.--(a) The Schwiderski (1983) M_2 ranges (in cm) in the South Atlantic. Note two amphidromic areas, one extending far off the coast of Brazil, the other in the southeast corner of this zone. Note also high tide off southwest coast of Africa. (b) The Geosat M^2 ranges for the South Atlantic in the preliminary 5° solution (in cm). Data consist of the Geosat solution at grid points with box symbols (scaled to the calibrated error: maximum size = 10 cm). At blank grid points data are from Schwiderski model. Thus the southwest African high is not well sampled by this preliminary solution but amphidromic areas are and remain about where they were in the Schwiderski model. (c) The Geosat M_2 ranges in the South Atlantic from current 4° solution (in cm). African high tide is now well sampled compared to preliminary solution and agrees well with Schwiderski model.

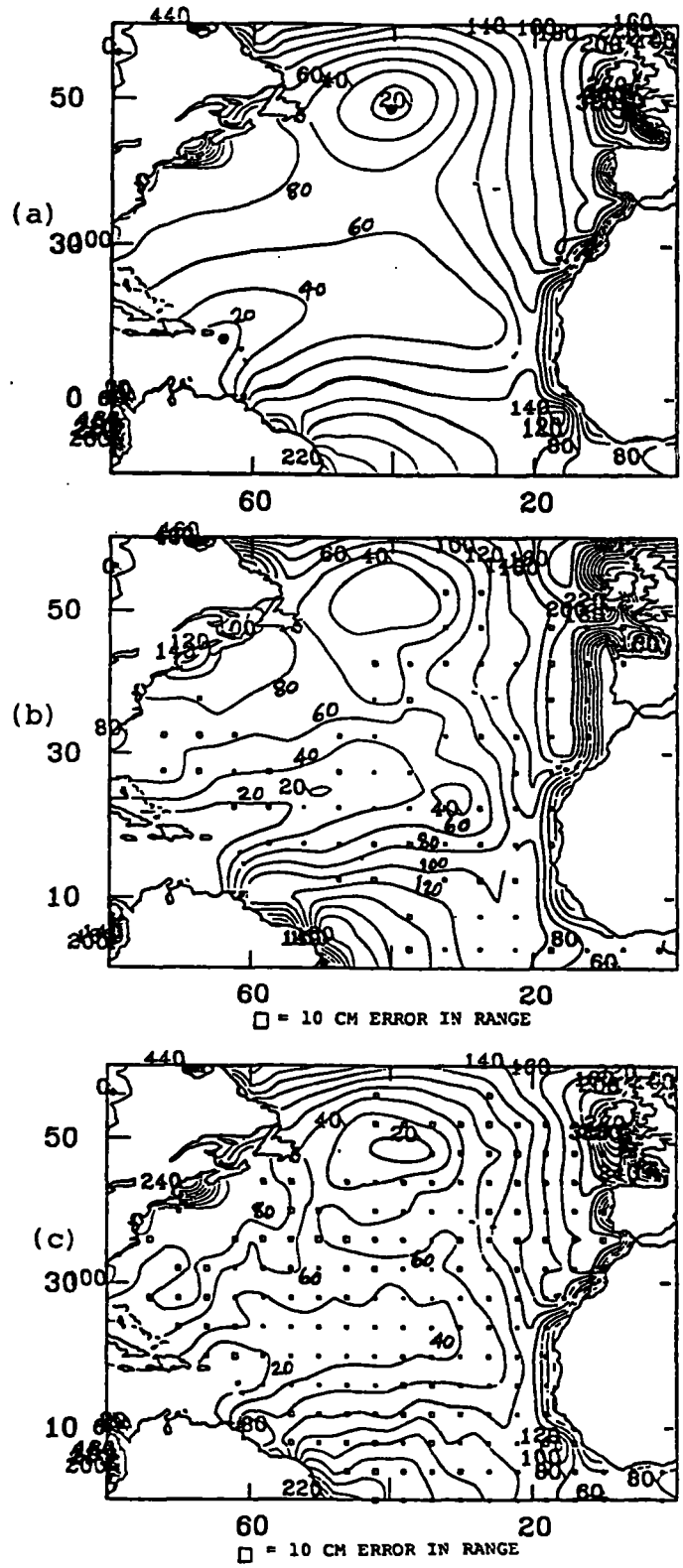

Figure 25.–(a) The Schwiderski (1983) M_2 ranges in the North Atlantic (in cm). Prominent features are the two amphidromic areas, one east of Newfoundland and the other at the edge of the Caribbean Sea. (b). Geosat M_2 ranges in North Atlantic from preliminary 5° solution (in cm). Data here are too sparse to test the two prominent amphidromes, but there is a hint that the Caribbean one extends much farther into the Atlantic. (c) Geosat M_2 ranges in the North Atlantic from current 4° solution (in cm). More Geosat data have restored the locality of the Caribbean amphidrome and confirmed the northern one as well. Again, the power of the North Atlantic ranges here has decreased (from Schwiderski 1983) from 120.7 cm (rms) to 114.8 cm.

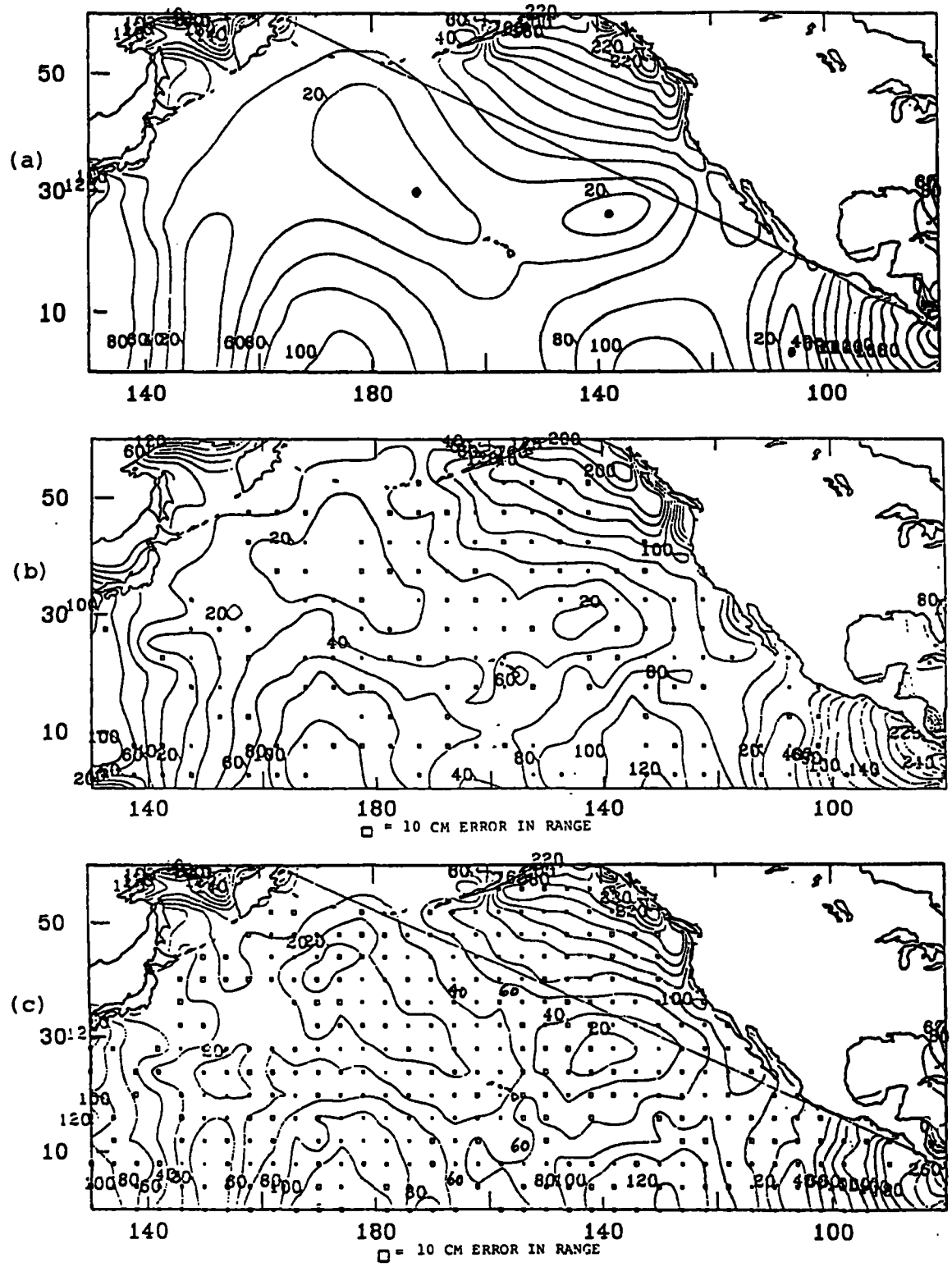

Figure 26.--(a) The Schwiderski (1983) M_2 ranges in the North Pacific (in cm), showing three amphidromic areas in this broad ocean zone. One is near the Equator in the east, another between California and Hawaii, and a third extended one is northwest of Hawaii. (b) Geosat M_2 ranges in North Pacific from preliminary 5° solution (in cm). The overall appearance of the tide is close to Schwiderski's model. In the far southwest corner there is a hint of two separate highs not present in the Schwiderski model. (c) Geosat M_2 ranges in North Pacific from current 4° solution (in cm). Here the two separated highs in the far southwest corner have disappeared but a third seems to be forming on the far western boundary (compared to Schwiderski's). Otherwise the only significant change seemsto be that the two central Pacific amphidromic areas have separated further. In the Schwiderski model they almost seem like one extended feature.

ACKNOWLEDGEMENTS

I thank Laury Miller for the many frustrating hours spent in giving me my first lessons in oceanography. I also deeply appreciate the seemingly untiring efforts of Eleanor Andree in editing this work and of Gloria Williamson in flawlessly preparing the typescript.

REFERENCES

Baker, T. F., 1984: Tidal deformations of the Earth. *Sci. Prof. Oxf. 69*, 197-233.

Brenner, A. C., Koblinsky, C. J., and Beckley, B. D., 1990: A preliminary estimate of geoid induced variations in repeat orbit satellite altimeter observations. *J. Geophs. Res., 95*, 3033-3040.

Brown, R. D., 1983: M_2 ocean tide at Cobb seamount from Seasat altimetry data. *J. Geophys. Res., 88 (C3)*, 1637-1646.

Cartwright, D. E. and Edden, A. C., 1973: Corrected tables of tidal harmonics. *Geophys. Jour. of the Roy. Soc., 23*, 253-264.

Cartwright, D. E. and Ray, R. D., 1990: Oceanic tides from Geosat altimetry. *J. Geophys. Res., 95*, 3069-3090.

Cheney, R. E., Douglas, B. C., and Miller, L., 1989: Evaluation of Geosat altimeter data with application to tropical Pacific sea level variability. *J. Geophys. Res., 94(C4)*, 4737-4747.

Cheney, R. E., Douglas, B. C., Agreen, R. W., Miller, L., and Doyle, N. S., 1988: The NOAA Geosat geophysical data records: Summary of the first year of the exact repeat mission. *NOAA Technical Memorandum NOS NGS-48*. National Geodetic Information Center, Rockville, MD 20852.

Cheney, R. E., Douglas, B. C., Agreen, R. W., Miller, L., and Doyle, N. S., 1987. Geosat altimeter geophysical data record user handbook, *NOAA Technical Memorandum NOS NGS-46*. National Geodetic Information Center, Rockville, MD 20852.

Christodoulidis, D., Williamson, R., Estes, R., and Chinn, D., 1985: Earth and ocean tidal modeling. *NASA Technical Memorandum 86208*, Topex Gravity Model Development Team Activities During Fiscal Year 1984, IF-1 to IF-33.

Colombo, O., 1984: Altimetry, orbits, and tides. *NASA Technical Memorandum 86180*, Goddard Space Flight Center, Greenbelt, MD 20771.

Doyle, N. S., Cheney, R. E., Douglas, B. C., Agreen, R. W., Miller, L., and Timmerman, E. L., 1989: The NOAA Geosat geophysical data records: Summary of the second year of the exact repeat mission. *NOAA Technical Memorandum NOS NGS-49*. National Geodetic Information Center, Rockville, MD 20852.

Francis, O., and Mazzega, P., 1990: Global charts of ocean tide loading effects. *J. Geophys. Res., 95(C7)*, 11,411-11,424.

Goad, C., 1980: Gravimetric tidal loading computed from integrated Green's functions. *J. Geophys. Res., 85(B5)*, 2679-2683.

Haines, B., Born, G., Rosborough, G., Marsh, J., and Williamson, R., 1990: Precise orbit computation for the Geosat exact repeat mission. *J. Geophys. Res., 95*, 2871-2885.

JHU/APL, 1981: The U.S. Navy Navigation Satellite System. The Johns Hopkins University Applied Physics Laboratory Technical Digest 2 (#1).

Lerch, F. J., Marsh, J. G., Klosko, S. M., Pavlis, E. C., Patel, G. B., Chinn, D. S., and Wagner, C. A. 1988: An improved error assessment for the GEM-T1 gravitational model. *NASA Technical Memorandum 100713*, Goddard Space Flight Center, Greenbelt, MD 20771.

Lerch, F. J., Klosko, S. M., Laubscher, R. E., and Wagner, C. A., 1979: Gravity model improvement using Geos 3 (Gem 9 and 10). *J. Geophys. Res., 84(B8)*, 3897-3916.

Marsh, J. G., and Williamson, R. G., 1980: Precision orbit analysis in support of the Seasat altimeter experiment. *J. Astro. Sci., 28(4)*, 345-369.

Marsh, J. G., Lerch, F. J., Putney, B. H., Christodoulidis, D. C., Sanchez, B. V., Felsentreger, T. L., Smith, D. E., Klosko, S. M., Martin, T. V., Pavlis, E. C., Robbins, J. W., Williamson, R. G., Colombo, O. L., Chandler, N. L., Rachlin, K. E., Patel, G. B., Bhati, S., and Chinn, D. S., 1987: A new gravitational model of the Earth from satellite tracking data: GEM-T1. *J. Geophys. Res., 93(B6)*, 6169-6215.

Mazzega, P., 1985: M_2 model of the global ocean tide derived from Seasat altimetry. *Mar. Geod., 9(3)*, 335-363.

Mazzega, P., and Jourdin, F., 1988: Inverting Seasat altimetry for tides in the northeast Atlantic: Preliminary results. *Proceedings of the International Conference on Tidal Hydrodynamics*, Gaithersburg, MD.

Melchior, P., 1978: The tides of the planet Earth. Pergamon Press, New York, p. 27.

Putney, B., 1976: General theory for dynamic satellite geodesy. *NASA sp-365*. The National Geodetic Satellite Program, 319-334.

Rapp, R. H., 1978: A global 1° x 1° anomaly field combining satellite, Geos-3 altimetry and terrestrial anomaly data. *Dept. Geod. Sci. Rep. 278*, Ohio State University, Columbus, OH, September.

Ray, R. D. and Sanchez, B. V., 1989: Radial deformation of the Earth by oceanic tidal loading. *NASA Technical Memorandum 100743*, Goddard Space Flight Center, Greenbelt, MD 20771.

Schwiderski, E. W., 1983: Atlas of ocean tidal charts and caps, part I: the semidiurnal principal lunar tide M_2. *Mar. Geod., 6(3-4), 219-265.*

Schwiderski, E. W., 1980: On charting global ocean tides. *Reviews of Geophysics and Space Physics 18*, 243-268.

Tapley, B. D., Born, G. H., and Parke, M. E., 1982: The Seasat altimeter data and its accuracy assessment. *J. Geophys. Res., 87(C5)*, 3179-3188.

Wagner, C. A., 1989: Summer school lectures on satellite altimetry. *Lecture Notes in Earth Sciences 25*, Edited by F. Sanso and R. Rummel, Springer-Verlag, Berlin, 285-334.

Wagner, C. A., 1990: The M_2 tide from Geosat altimetry. *Manus. Geod., 15*, 283-290.

Wyrtki, K., and Leslie, W. G., 1980: The mean annual variation of sea level in the Pacific Ocean. *Hawaii Inst. of Geophys. Res. Report HIG-80-5*, University of Hawaii, Manoa, HI, 159 pp.

APPENDIX A.--EFFICIENCY OF HARMONIC SOLUTIONS FROM DIRECT OR DIFFERENCED DATA

By efficiency I mean the formal errors of a least squares solution for an harmonic signal disturbed by random (white) noise only. I want to contrast the solution efficiency of direct and difference sampling with two kinds of data: (1) continuous (or ideal), and (2) discrete. For this purpose I will first deal with the ideal case for direct data because it establishes a fundamental standard and results easily carry over to the more interesting problems.

Let:

$$h = C\cos wt + S\sin wt \tag{A-1}$$

be a tide harmonic signal at a point where w is the frequency. Suppose we could make a large uniform sampling N of this tide over its full periodicity. What would be the resulting error in the harmonics C,S determined by a least squares fitting of eq. (A-1) to actual data D according to the condition equation:

$$D = C\cos wt + S\sin wt + e \tag{A-2}$$

where e is assumed here to be a random unit normal deviate (for convenience)? Then the least squares estimates $\hat{C}$, $\hat{S}$ from this fitting have well known errors given from the diagonals of the inverse of the normal matrix derived from (A-2), namely the variance covariance matrix:

$$\sigma^2 = V = \begin{bmatrix} \sum_{n=1}^{N} \cos^2 wt_n & , & \sum_{n=1}^{N} \cos wt_n \sin wt_n \\ \sum_{n=1}^{N} \sin wt_n \cos wt_n & , & \sum_{n=1}^{N} \sin^2 wt_n \end{bmatrix}^{-1} \tag{A-3}$$

The diagonal elements of eq. (A-3) are the variances of C,S and they are evidently:

$$\sigma_{11}^2, \sigma_{22}^2 = \sigma_c^2, \sigma_s^2 = \frac{\sum_{n=1}^{N} \sin^2 wt_n, \sum_{n=1}^{N} \cos^2 wt_n}{\left[\sum_{n=1}^{N} \cos^2 wt_n\right]\left[\sum_{n=1}^{N} \sin^2 wt_n\right] - \left[\sum_{n=1}^{N} \cos wt_n \sin wt_n\right]^2} \tag{A-4}$$

Notice we still have a discrete case here for a large set of points N assumed to be reasonably distributed but otherwise unspecified. I now wish to show how this discrete formulation can be made to pass over to the ideal continuous case with the help of the fundamental definition of the integral in calculus.

For example, suppose I have a function $F(x)$, sampled uniformally over a range of x, say every Δx; thus at $f(x_0 + \Delta x), f(x_o + 2\Delta x),...f(x_0 + N\Delta x)$, where $N\Delta x$ is the fixed sampling interval. Then if I form the sums: $\sum f(x_0 + n\Delta x)$ over the fixed interval and take the limit of these as n goes to infinity while at the same time Δx goes to zero (let the fixed interval be 'a') I have:

$$\lim_{\substack{N\to\infty \\ \Delta\to 0 \\ N\Delta x\to a}} \sum_{n=0}^{N} f(x_0 + n\Delta x) = \int_{x_0}^{x_0+a} f(x)dx \tag{A-5}$$

But we see immediately that we can put the sums in eqs. (A-3) and (A-4) into the form required by eq. (A-5) by pre- and post-multiplying these sums by $(1/\Delta x) = N/a$. Thus I have, for example (over the range $wt_0 \to wt_0 + a$):

$$\sum_{n=0}^{N} \sin^2 wt_n = (1/\Delta wt)\sum \sin^2 wt_n \Delta wt \doteq (N/a)\int_{wt_o}^{wt_o+a} \sin^2 wt\, d(wt) \tag{A-6}$$

$$N > >1$$

Note that N in eq. (A-6) plays the role of a densifier of the discrete sampling since the integral itself is a constant over the fixed interval. Thus there is no limit to the left side of eq. (A-6). As we shall see, the implication is that for a super-dense sampling the formal error of an harmonic determination goes to zero.

Using the familiar orthogonal properties of these periodic functions over $a=2\pi$, I derive for this ideal continuous direct sampling of an harmonic function:

$$\underset{N>>1}{o^2 C,S} = \frac{N/2, N/2}{(N^2/4 - 0)} = 2/N,\ 2/N \tag{A-7}$$

Note especially how with a discrete sample size N I get the familiar result for signals only randomly disturbed: that the harmonic parameter errors (σ) are reduced by $\sqrt{N}$ for repeated (uniform) samplings.

For the simple case above of a uniform large sample, the cosine and sine errors are the same. For more complex cases of sampling they may be different. But in any case a single number which better characterizes the global error of the harmonic determination (over its range) is the average expected signal error from the solution. To finds its value let the harmonics have true error ΔC, ΔS. Then the tide error at any time t is

$$\Delta T = \Delta C \cos wt + \Delta S \sin wt \tag{A-8}$$

or the squared error is

$$\Delta h^2 = \Delta C^2 \cos^2 wt + \Delta S^2 \sin^2 wt + 2\Delta C \Delta S \cos wt \sin wt \tag{A-9}$$

The expected squared error of the signal is then

$$E\,\Delta h^2 = \sigma^2 C \cos^2 wt + \sigma^2 S \sin^2 wt + 2\sigma CS \cos wt \sin wt \tag{A-10}$$

where the covariant quantities on the right side of (A-10) are given by the appropriate terms in V of eq. (A-3) since I have assumed that e_n is an unbiased random normal variate. Equation (A-10) gives the statistical expectation of the squared error at a single time. Averaged over all time (or at least over periodic intervals of the tide), eq. (A-10) yields the well known result:

$$<E\Delta h^2> = (\sigma^2 C + \sigma^2 S)/2 \tag{A-11}$$

again using the orthogonal properties of the harmonic functions.

The rms expected error is then:

$$\sigma_h = \{<E\Delta h^2>\}^{1/2} = \{(\sigma^2 C + \sigma^2 S)/2\}^{1/2} = (2/N)^{1/2} \tag{A-12}$$

It should be pointed out that the units of eq. (A-12) are actually in the units of $\{E\, e_n^2\}^{1/2}$ or the root-mean-square of the expected noise disturbance of the signal. Tacitly I assumed this to be 1.0 in an appropriate unit when I introduced the least squares procedure to evaluate the parameter errors. (In effect our seemingly unweighted least squares result actually assumed a weight of 1.0 to "dimensioned" noise so that the variance-covariance matrix V in eq. (A-3) actually has the dimensions of the square of the dimensions of e.)

Finally, disregarding the $\sqrt{N}$ densifying factor we may say the characteristic error of ideally sampled direct harmonic data is merely $\sqrt{2}$. How does this ideal direct result compare with: (1) an ideal case where sampling of the harmonic function is taken by differences with respect to a base time uniformly (and dense) and, (2) at only discrete times? The latter case is what I am really after, to gain insight into the sampling requirements for effective solutions from differenced altimetry. But in this regard it is also interesting to formulate the case where (3) direct data are sampled at (a limited number of) discrete times.

This last case cannot only be compared to the ideal (continuous) direct sampling but also the actual case of (limited) discrete difference sampling which, because of its complexity I will only carry through for a "simplest" example.

For these discrete cases we shall assume only two observations, the minimum necessary for a complete harmonic solution. As above, I first work out the theoretical efficiency of the solution, but here over all pairs of observation times (with respect to the fundamental period of the harmonic). The errors for this case are given from eq. (A-4) as:

$$\begin{aligned} \sigma^2 C,S &= \frac{\{\sin^2 wt_1 + \sin^2 wt_2\},\{\cos^2 wt_1 + \cos^2 wt_2\}}{\{(\cos^2 wt_1 + \cos^2 wt_2)(\sin^2 wt_1 + \sin^2 wt_2) - (\cos wt_1 \sin wt_1 + \cos wt_2 \sin wt_2)\}} \\ &= \frac{[\sin^2 wt_1 + \sin^2 wt_2],[\cos^2 wt_1 + \cos^2 wt_2]}{\sin^2[wt_1 - wt_2]} \end{aligned} \tag{A-13}$$

Note from eq. (A-13) that the only requirement for finite errors is that the observations be either at distinct times (as we might easily guess) or not 180° apart. Computing the rms expected tide error (over a full period) from eq. (A-11) I have:

$$\sigma_h = |\,[\sin(wt_1 - wt_2)]^{-1}\,| \tag{A-14}$$

Note the minimum of eq. (A-14) occurs when wt_1-wt_2 = nx90 degrees (n, odd) at which point $\sigma_h = 1$. Thus for pair sampling over wide ranges, namely when 45° < $|wt_1$-$wt_2|$ < 135° and 225° < $|wt_1$-$wt_2|$ < 315°, which amounts to half of all possible time pairs, the characteristic error of this simplest discrete sampling is actually smaller than that for the ideal continuous case $\sqrt{2}$. Rather unexpectedly, this result is repeated for harmonic determination from difference data, namely that a large number of discrete

determinations are actually superior (in terms of characteristic error) to the ideal continuous case of uniformly distributed and dense differenced observations (as well as to direct continuous observations).

I also found important distinctions between direct and difference determinations. The most important distinction concerned the differenced cases with respect to a fixed base observation, where the individual parameter errors can depend strongly on the the choice of the base observation with respect to the origin of the tide. Let us now repeat these ideal (continuous) and simplest discrete cases for differenced data to find whether or under what circumstances the difference solution is more powerful than the direct.

Figure A-1 shows the tidal signal for differenced data with respect to a reference time at wt_0. The difference signal itself is given as:

$$\delta h = C[\cos wt - \cos wt_0] + S[\sin wt - \sin wt_0] \tag{A-15}$$

The elements of the variance-covariance matrix of a least squares solution for C and S from such a (unit randomly perturbed) data signal sampled at wt_1, wt_2,...(and differenced with the signal at wt_0) is:

$$\sigma^2 = \begin{bmatrix} B_{11}, B_{12} \\ B_{12}, B_{22} \end{bmatrix}^{-1} \tag{A-16}$$

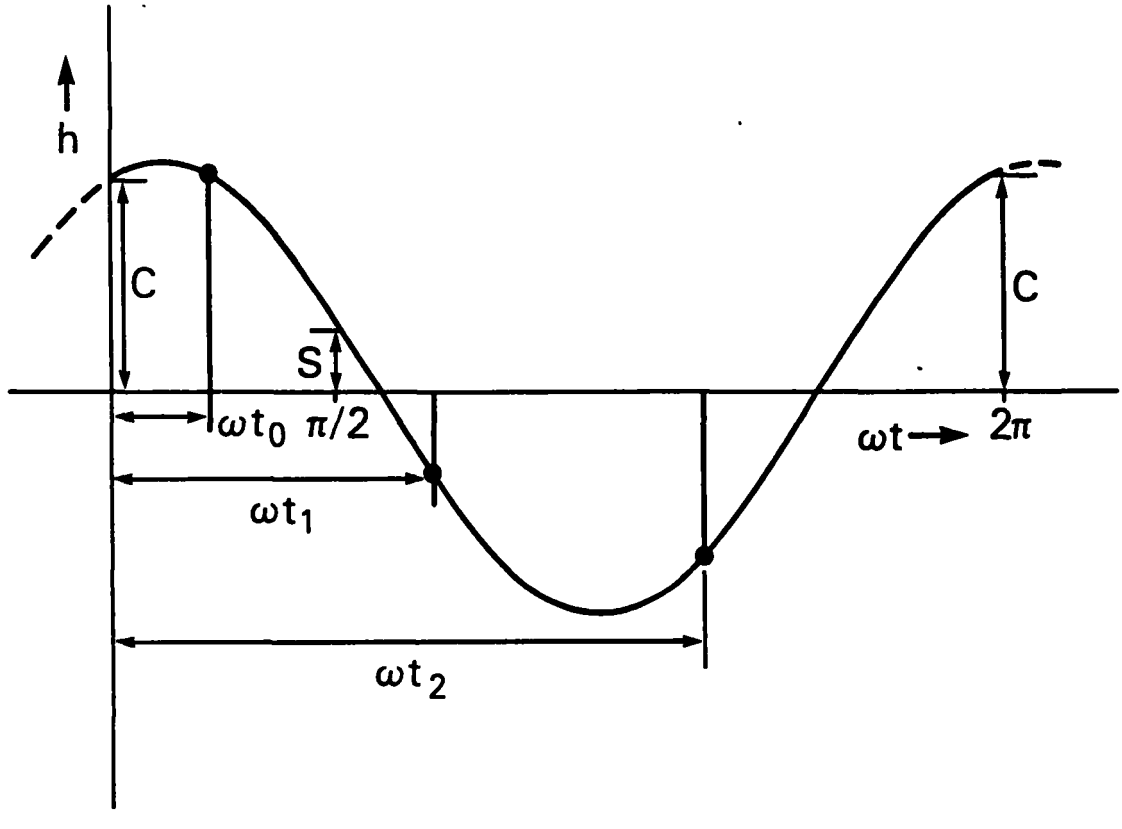

Figure A-1.–Tidal signal with respect to arbitrary reference and sampled times. The harmonic coefficients of the signal (C,S) refer to another arbitrary zero time. The frequency of the signal is w.

where

$$B_{11} = \sum \cos^2 wt_n - 2\cos wt_0 \cos wt_n + \cos^2 wt_0 \tag{A-17}$$

$$B_{12} = \sum \cos wt_n \sin wt_n - \sin wt_0 \cos wt_n - \cos wt_0 \sin wt_n + \cos wt_0 \sin wt_0 \tag{A-18}$$

$$B_{22} = \sum \sin^2 wt_n - 2\sin wt_0 \sin wt_n + \sin^2 wt_0 \tag{A-19}$$

Analogous to the transformation of these finite sums to definite integrals (for dense uniform sampling, the ideal case), using eq. (A-6) I have these results:

$$\sum \cos^2 wt_n \approx (N/2\pi) \int \cos^2 wt \, d(wt) = N/2 \tag{A-20}$$

$$\sum \sin^2 wt_n \approx (N/2\pi) \int \sin^2 wt \, d(wt) = N/2 \tag{A-21}$$

$$\sum [\cos^2 wt_n, \sin^2 wt_n] \approx (N/2\pi) \int [\cos^2 wt, \sin^2 wt] \, d(wt) = N/2 \tag{A-22}$$

$$\sum k(a\ constant) \approx (N/2\pi) \int k \; d(wt) = Nk \tag{A-23}$$

$$\sum k \cos wt_n, k \sin wt_n, k \cos wt_n \sin wt_n \approx 0 \tag{A-24}$$

so that:

$$\sigma^2 = V = (2/3N) \begin{bmatrix} 1 + 2\sin^2 wt_0 & -2\cos wt_0 \sin wt_0 \\ -2\cos^2 wt_0 \sin wt_0 & 1 + 2\cos^2 wt_0 \end{bmatrix} \tag{A-25}$$

Note that in contrast with the case for direct determination, the errors of the individual parameters with differences depend strongly on the choice of reference time. As seen in figure A-1, if wt_0 is zero the base observation (if used directly) would measure the full C value. So it might be expected that differences with respect to this base time would yield the most powerful C determination, as eq. (A-25) indeed shows. A surprise however was the result that even in the ideal case (here) with difference data, there is an inherent correlation between the parameter errors that does not occur with direct data. For example, the correlation coefficient of the parameter errors from eq. (A-25) is

$$cor\ \sigma\, \hat{C}, \hat{S} = \frac{-2\cos wt_0 \sin wt_0}{\{(1 + 2\cos^2 wt_0)\ (1 + 2\sin^2 wt_0)\}^{1/2}} = \frac{-\sin 2wt_0}{[3 + \sin^2 2wt_0]^{1/2}} \tag{A-26}$$

which reaches as much as $\pm 1/2$ when wt_0 = 45°, 135°, 225° and 315°. Thus even with ideal data, differencing generally yields a solution with correlated errors.

But the characteristic error of the differenced solution seen has the desired property of being independent of the reference time. From eqs. (A-25) and (A-11) the range averaged tidal error is

$$\sigma_h = \{(1/3N)(1 + 2\cos^2 wt_0 + 1 + 2\sin^2 wt_0)\}^{1/2} = [4/3N]^{1/2} \tag{A-27}$$

Disregarding the density factor N, the characteristic error is $(4/3)^{1/2}$, which is about 25 percent smaller than that for ideal direct data ($\sqrt{2}$).

An objection which might be made to this favorable result is that since the referenced heights in it are not error-free the characteristic (and other) errors associated with the solutions as computed here should be scaled accordingly. Without further consideration, in fact one might be justified in scaling the differenced errors by $\sqrt{2}$ since the referenced heights presumably have errors of the same unit normal characteristic as the following heights. But the differenced data errors even if they arise from random unit variates are also correlated if they use (as I have assumed in these examples) the reference height repeatedly. The correlated structure of the source error matrix means we must employ a full weight matrix to get the proper least squares solution and to evaluate the error-covariance of that solution with repeated differenced data. The conclusion will be greater harmonic errors than with error-free reference heights, but less error than simply assigning an uncorrelated value of $\sqrt{2}$ to all the height differences.

Rather than working through the correct error variances with a correlated weight matrix, I solved an auxiliary problem which is much easier to implement in practice, is entirely equivalent to it, and promises to yield significantly improved results in future altimetric solutions from differenced data. To introduce this auxiliary problem I merely note that the observation equation corresponding to the resolution of the differenced signal in eq. (A-15) is

$$\delta h = C\{\cos wt - \cos wt_0\} + S\{\sin wt - \sin wt_o\} + e_t - e_0 \tag{A-28}$$

where e_t is the error in the signal at the following time t and e_0 is the error in the signal at the reference time. But for the set of all following height pairs the reference error e_0 is the same. Therefore, rather than accept a least squares solution with a cumbersome fully correlated weight matrix (even in this ideal theoretical case) I can convert the problem to a diagonal case by introducing e_0 as an auxiliary constant parameter to be resolved from the full data set along with the tidal harmonics. This device has profound implications to the solution from actual data: It is a comment on the "datum" problem with differencing. But here I only want to show exactly how much it rightfully degrades the theoretical result we found for differencing with continuous data. Suprisingly, I also find it alters the conclusion that with differencing (ideal data) there is a fundamental correlation between the harmonic errors of the solution. Repeating the calculation of the variance-covariance matrix of the new system of equations with an added constant and now a diagonal (unit) weight matrix, eq. (A-16) as augmented with a solution for e_0 becomes

$$o^2 = (2/N)\begin{bmatrix} 2 & 2\cos wt_0 & 2\sin wt_0 \\ 2\cos wt_0 & 1+2\cos^2 wt_0 & 2\cos wt_0 \sin wt_0 \\ 2\sin wt_0 & 2\cos wt_0 \sin wt_0 & 1+2\sin^2 wt_0 \end{bmatrix}^{-1}$$

$$= (1/N)\begin{bmatrix} 3 & -2\cos wt_0 & -2\sin wt_0 \\ -2\cos wt_0 & 2 & 0 \\ -2\sin wt_0 & 0 & 2 \end{bmatrix} \tag{A-29}$$

First notice with the augmented (constant) solution there is now no correlation between C, and S errors and furthermore no dependence for these errors on the reference time in this continuous data case. Furthermore the averaged tidal error is now:

$$\sigma_h = \{(1/2)(\sigma^2 C + \sigma^2 S)\}^{1/2} = (2/N)^{1/2} \quad . \tag{A-30}$$

The characteristic error is the same as in the case with ideal direct data!

What is the result in the simplest (two observation) case for discrete differenced data? Again I expected to find similar gains in efficiency both with and without consideration of the correlation of the data errors, with differenced data compared to the direct data discrete case [eq. (A-14)]. With only two points, however, it is obviously impossible to derive a unique auxiliary solution for the added constant error of the reference height.

What is the correlated error matrix with differenced data? Suppose I had a large set of height pairs h_n, h_0 forming differences $\delta h_n = h_n - h_0$. Assuming that the errors in these heights are unit normal random variables I have for actual errors Δh_n, Δh_0, $\Delta \delta h_n$:

$$\Delta \delta h_n = \Delta h_n - \Delta h_0 \quad . \tag{A-31}$$

Taking the square of both sides of eq. (A-31) and then the expectation of the result (with the normality assumptions) I have

$$E[\Delta \delta h_n]^2 = \sigma^2 \Delta h_n = \sigma^2 h_n + \sigma^2 h_0 = 2 \quad . \tag{A-32}$$

But the expectation of all cross terms $\Delta h_n \, \Delta h_m$ is not zero (as with direct data) but

$$E[\Delta \delta h_n \Delta \delta h_m] = E[\Delta h_n \Delta h_m - \Delta h_0(\Delta h_n + \Delta h_m) + \Delta h_0^2] \quad . \tag{A-33}$$

The expectations of all terms on the right side of eq. (A-33) are zero except for the last which is 1. Thus, with discrete differenced data, even if I assume (which is also problematical) that the individual height errors at a station are random normal (or at least random from the same probability distribution with zero mean), I must use the following correlated error matrix (scaled to unit variance for a single height):

$$E[ee^T] = \begin{bmatrix} 2,1,.... \\ 2,1,... \\ 2,.. \end{bmatrix} \quad . \tag{A-34}$$

Since the inverse of this matrix is the required weight matrix in a proper weighted least squares procedure we can see the convenience of using the auxiliary problem for a time series with more than a few differences related to the same reference height. There are still disadvantages in using the auxiliary problem, however, if there are not sufficient passes in each distinct time series (related to the same reference height) to separate this "throwaway" base error from the tidal parameters of interest. But this is a question for future investigation. Here for the two-point determination of two tidal harmonics it is obvious I must use the correlated weight matrix approach which, as the inverse of eq. (A-34), is (for the two- point problem):

$$W = [E\,ee^T]^{-1} = \begin{bmatrix} 2 & 1 \\ 1 & 2 \end{bmatrix}^{-1} = (1/3)\begin{bmatrix} 2 & -1 \\ -1 & 2 \end{bmatrix} \quad . \tag{A-35}$$

Treating the 2-point discrete case in these two ways, with and without the correlated weight matrix, yields the following formulas for the characteristic errors:

$$\sigma_h\,(uncor.) = \{2 - [\cos(wt_2 - wt_0) + \cos(wt_1 - wt_0)]\}^{1/2} / D$$

$$\sigma_h\,(corr.) = \{3 - [\cos(wt_2 - wt_1) + \cos(wt_1 - wt_0) + \cos(wt_2 - wt_0)]\}^{1/2} / D$$

where:

$$D = |\{\sin(wt_2 - wt_1) + \sin(wt_1 - wt_o) - \sin(wt_2 - wt_0)\}| \quad \text{(A-36)}$$

It should be noted that the uncorrelated version of this error is what we actually calculated for our solution prior to its error calibration. The solution itself was also computed with an uncorrelated error matrix which undoubtedly introduced a bias in it that (to the extent the bias differed among the arc-dependent time series applicable at each station) I compensated for by the calibration factor. Here, of course, with a two-point determination the solution is unique but the estimated errors for the parameters may be optimistic (as in the continuous case) if the correlated weight matrix is not used.

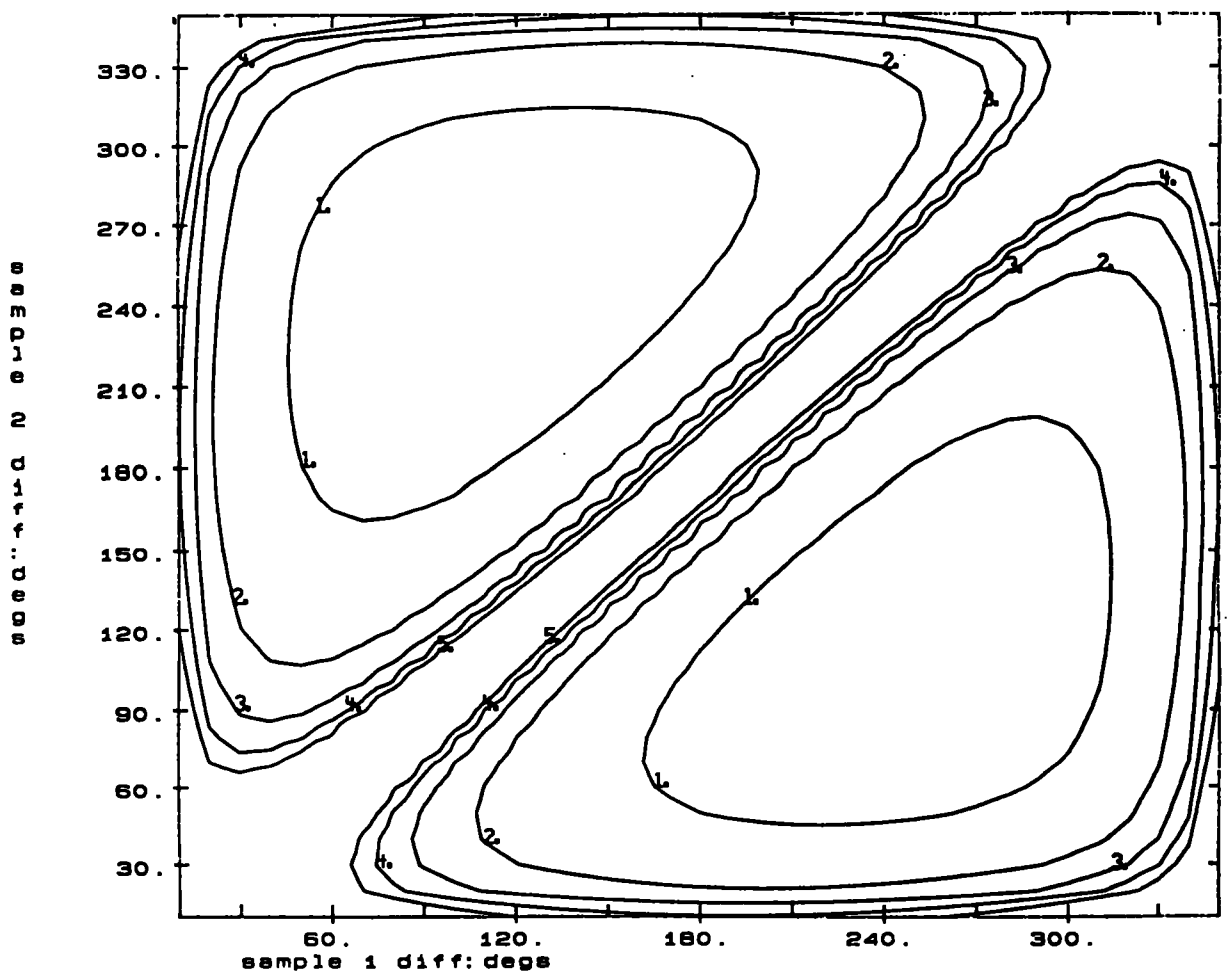

Fig. A-2.--Average harmonic error in minimum difference sample: cm

Figure A-2 shows the evaluation of eq. (A-36) in the uncorrelated case (assuming perfect reference heights). Recalling that in the discrete case the characteristic error was never less than 1, we see there are broad regions where the tide is sampled over large phase differences, in which the characteristic error of the difference solution is significantly less than 1 (minimum = 0.68). In contrast to the continuous case evaluated by the auxiliary (constant) solution however, the characteristic error for the correlated solution is sometimes better and sometimes worse than the uncorrelated solution. Its minimum is actually somewhat smaller, 0.62. The existence of singularities makes a global average of these error functions difficult to compute, but apparently the effect of the strong correlated constraint in a minimum data solution such as this, more than compensates for the degradation arising from the use of $\sqrt{2}$ as the (realistic) error variances with the correlated weight matrix. With large discrete data sets however, the constraint will be less effective and the uncorrelated solution errors should appear more and more optimistic.

APPENDIX B.--COHERENCE AND COMPLIANCE OF TIDE VECTORS

Coherence

The global tide, as distinct from other global functions such as the geopotential, varies in time as well as space (e.g, on a surface). Thus if we wish to know the autocovariance function for a single tide (as the simplest way to gain knowledge of its space structure) or the covariance between two such tide solutions (to gage their relatedness) we must resolve the time as well as the space components of variation.

Extending the concept of covariance as an average of products, I will define the covariance of two functions $x_1(sp,t)$ and $x_2(sp,t)$, where sp refers to space parameters and t to time, as

$$cov\, x_1 x_2 = \langle \langle x_1(sp,t)\, x_2(sp,t) \rangle_t \rangle_{sp} \,, \tag{B-1}$$

meaning I first resolve the covariance of the quantities at a point over time and then find the average of this time averaged product over the space coordinates to get the global covariance. Since the averaging operator is linear it should not matter in which order I take this double averaging. In fact, there may be more than one space coordinate to consider and I am at liberty to take the averages for these in any order I wish according to my convenience. With respect to a well behaved tidal harmonic it is clearly convenient to take the time average first.

Consider two such tide harmonics (with unspecified but temporarily fixed space parameters):

$$\begin{aligned} x_1 &= C_1 \cos wt + S_1 \sin wt \\ x_2 &= C_2 \cos wt + S_2 \sin wt \end{aligned} \tag{B-2}$$

What is the time averaged product and correlation between these two tides? Whether I consider the time to be taken over multiple periods ($T=2\pi/w$) or over a time T' much longer than T, I have

$$\begin{aligned} cov\, x_1 x_2 = \langle x_1 x_2 \rangle t &= \frac{1}{T'} \int x_1 x_2\, dt \,, \qquad T' >> 1 \\ &= \{ C_1 C_2 + S_1 S_2 \}/2 \end{aligned} \tag{B-3}$$

and

$$\begin{aligned} r(corcoeff) x_1 x_2 &= \sum x_1 x_2 / \left\{ \sum x_1^2 \sum x_2^2 \right\} \\ &= \int x_1 x_2\, dt / [\int x_1^2\, dt \int x_2^2\, dt] \\ &= \frac{C_1 C_2 + S_1 S_2}{(C_1^2 + S_1^2)^{1/2} (C_2^2 + S_2^2)^{1/2}} \,. \end{aligned} \tag{B-4}$$

The correlation coefficient or coherence between the two tides can be expressed even more simply by referring to their phase representations:

$$x_1 = A_1 \cos(wt - \gamma_1)$$
$$x_2 = A_2 \cos(wt - \gamma_2) \tag{B-5}$$

where, comparing (B-5) with (B-2),

$$(C_1, C_2) = (A_1, A_2) \cos(\gamma_1, \gamma_2)$$
$$(S_1, S_2) = (A_1, A_2) \sin(\gamma_1, \gamma_2) \quad . \tag{B-6}$$

Writing the coherence r in eq. (B-4) in terms of the ratios of S to C components and using the identification of gamma in terms of these ratios:

$$(\gamma_1, \gamma_2) = \tan^{-1}[(S_1, S_2)/(C_1, C_2)] \tag{B-7}$$

I have

$$r = \frac{1 + \tan\gamma_1 \tan\gamma_2}{\{1 + \tan^2\gamma_1\}^{1/2}\{1 + \tan^2\gamma_2\}^{1/2}}$$
$$= \frac{\cos(\delta\gamma)/[\cos\gamma_1 \cos\gamma_2]}{\sec\gamma_1 \sec\gamma_2} \tag{B-8}$$
$$= \cos(\delta\gamma)$$

where $\delta\gamma$ is the phase difference between the two tides: $[\gamma_1 - \gamma_2]$.

To summarize, the covariance function for tide harmonics is merely the space average of the product of both their corresponding harmonic components. The coherence is the space average of the cosine of their phase differences.

Some authors refer to the coherence as the square of the correlation (e.g., Ray and Sanchez 1989). The coherence in this definition conveys less information than the correlation, wiping out the distinction between positive and negative correlation (where the tides may be out of phase). Also, the coherence in this definition will be deceptively small in well correlated cases (since the square of a small fraction is always a significantly smaller fraction). With experimental data or functions derived from such data it seems wisest to report the coherence as a correlation coefficient, which I do in the body of this report.

Compliance

If two functions (or data) are found to be correlated, it is often useful to express the correlation by a linear regression of one function against the other. This is especially appropriate for the relation between the ocean tide and its load-tide response, which is in large part a simple elastic one. I will call the coefficient expressing this linear relation the compliance coefficient (β). More specifically, I seek a least squares solution to the following relation between two compliant tides:

$$x_1 = \beta x_2 + e \tag{B-9}$$

where the (same period) tides are given by the harmonics C,S (eq. B-2) and e is the discrepancy in the regression at a given time. Taking the average squared discrepancy over the tide period (T) I find this to be

$$E = (1/T)\int e^2 dt = (1/2)\{[C_1 - \beta C_2]^2 + [S_1 - \beta S_2]^2\} \quad . \tag{B-10}$$

Minimizing E with respect to β results in its least squares value of

$$\hat{\beta} = \frac{C_1 C_2 + S_1 S_2}{C_2^2 + S_2^2} \quad . \tag{B-11}$$

Recalling the amplitude-phase definition of the tide (eq. B-5) and the interpretation of any harmonic function as a rotating vector of length A and initial (time zero) phase γ, we see that β in eq. (B-11) represents the ratio of the projection of the vector x_1 (at any time) against x_2, to the length of vector x_2. In amplitude-phase notation,

$$\hat{\beta} = \frac{A_1 \cos\delta\gamma}{A_2} \quad . \tag{B-12}$$

That is, the compliance coefficient is the correlation coefficient scaled by the ratio of the tide amplitudes.

The second useful piece of information from a compliance computation is the error made by assuming perfect compliance ($\delta\gamma = 0$). Using the amplitude-phase representation, this error ($\hat{e}$) is easily seen as the out-of-phase component of the projection of x_1 onto x_2:

$$\hat{e} = A_1 \sin\delta\gamma \quad . \tag{B-13}$$

A single number representing the utility of the linear representation of a compliant tide with respect to its source is this error relative to the compliant component of the tide:

$$\begin{aligned} \eta \text{ (relative error)} &= \hat{e}/(A_2\hat{\beta}) \\ &= \tan\delta\gamma \quad , \end{aligned} \tag{B-14}$$

which is close to $(1 - r^2)^{1/2}$ for coherent vectors.

I have used all these measures of correlation in discussing the M_2 tide solutions in the body of this report.